THE UNIVERSITY OF QUEENSLAND

AUSTRALIA

Optimising intratumoural treatment of head and neck squamous cell carcinoma mouse models with EBC-46

Dr Catherine Margaret Eleanor Barnett

Bachelor of Science
Bachelor of Medicine and Bachelor of Surgery
Master of Science

A thesis submitted for the degree of Master of Philosophy at
The University of Queensland in 2015

School of Medicine

Abstract

The five-year survival rate for patients with head and neck squamous cell carcinoma (HNSCC) has remained at ~50% for the past 30 years despite advances in treatment. EBC-46 is a novel diterpene ester developed by QBiotics Pty Ltd that induces HNSCC cell death *in vitro*.

The aims of this study were to identify a human HNSCC xenograft that responds poorly to intratumoural injection of EBC-46, improve efficacy of EBC-46 treatment by altering different administration parameters, and confirm the molecular mechanism of HNSCC cell death *in vivo* following intratumoural treatment with EBC-46.

Subcutaneous xenografts of HNSCC cell lines were grown in BALB/c *Foxn1*^{nu} and NOD/SCID mice and treated with intratumoural injection of 30 μg EBC-46 or a control solution. A difficult cell line was identified and administration parameters were adjusted in an attempt to overcome treatment resistance. Treated tumours were stained for endothelial cell, macrophage and neutrophil markers. *In vitro* cytotoxic assays were employed to further investigate the mechanism by which EBC-46 works.

A tongue SCC cell line (SCC-15) was identified as the most resistant cell line. A single 30 μg bolus in 40% propylene glycol was the most efficacious administration. Immunohistological staining of treated tumours in BALB/c *Foxn1*^{nu} mice identified tumour vessel disruption, red cell influx, and recruitment of macrophages and neutrophils following treatment with EBC-46. At 24 hr after treatment most of the cells present at the treated site were neutrophils. In contrast, no neutrophil infiltration was present in treated tumours at 24 hr in NOD/SCID mice. EBC-46 at doses comparable to the concentration administered *in vivo* rapidly killed tumour cells by necrosis *in vitro*. Simultaneous treatment with the pan-PKC inhibitor BIS-1 did not completely prevent EBC-46's action. Dual fluorescence labelling observed under the confocal microscope revealed that mitochondrial potential was lost before uptake of propidium iodide.

In conclusion, high dose EBC-46 killed tumour cells *in vitro* by necrosis, associated with loss of mitochondrial potential. The picture is more complex *in vivo*. Disruption of tumour vasculature seen in tissue sections indicated a process of hemorrhagic necrosis. The difference in efficacy between BALB/c *Foxn1*^{nu} and NOD/SCID mouse models indicated a requirement for neutrophils in the host and merits further investigation such as ablation of neutrophils in BALB/c *Foxn1*^{nu}. These results provide new insight into the mechanism of action of EBC-46 and extend the number of HNSCC models further supporting the use of EBC-46 is a suitable agent for progression to human clinical trials in HNSCC.

Declaration by Author

This thesis is composed of my original work, and contains no material previously published or written by another person except where due reference has been made in the text. I have clearly stated the contribution by others to jointly-authored works that I have included in my thesis.

I have clearly stated the contribution of others to my thesis as a whole, including statistical assistance, survey design, data analysis, significant technical procedures, professional editorial advice, and any other original research work used or reported in my thesis. The content of my thesis is the result of work I have carried out since the commencement of my research higher degree candidature and does not include a substantial part of work that has been submitted to qualify for the award of any other degree or diploma in any university or other tertiary institution. I have clearly stated which parts of my thesis, if any, have been submitted to qualify for another award.

I acknowledge that an electronic copy of my thesis must be lodged with the University Library and, subject to the policy and procedures of The University of Queensland, the thesis be made available for research and study in accordance with the Copyright Act 1968 unless a period of embargo has been approved by the Dean of the Graduate School.

I acknowledge that copyright of all material contained in my thesis resides with the copyright holder(s) of that material. Where appropriate I have obtained copyright permission from the copyright holder to reproduce material in this thesis.

Publications during candidature

No publications.

Publications included in this thesis

No publications included.

Contributions by others to this thesis

Dr Jason Cullen provided operational guidance for the real-time tumour cell killing assay in Chapter Five.
Jenny Johns provided extracted and purified EBC-46 from *Fontainea picrosperma*.
Natasa Korica maintained the human SCC cell lines used.
Clay Winterford provided histology services described in Chapter Four.

Statement of parts of the thesis submitted to qualify for the award of another degree

None.

Acknowledgements

I would like to sincerely thank Prof Peter Parsons, A/Prof Ben Panizza and Dr Glen Boyle for the opportunity to work on such an exciting project and for their diligent supervision and generous guidance.

Special thanks goes to Natasa Korica for being so generous with her time, teaching me new techniques and helping me at numerous times throughout my project.

Thanks to Jason Cullen who provided excellent advice and spent time helping me design new assays.

Thank you to the rest of the Parsons crew who were so welcoming and helpful during my time in the lab.

Histology services were kindly provided by Clay Winterford, Microscopy assistance was kindly provided by Nigel Waterhouse.

Finally, thank you to Simon and Emily for their unconditional love and support.

Keywords

Head and neck squamous cell carcinoma, protein kinase c, diterpene ester, ebc-46, intratumoural injection.

Australian and New Zealand Standard Research Classifications (ANZSRC)

ANZSRC code: 111201, Cancer Cell Biology, 33.3%
ANZSRC code: 111204, Cancer Therapy, 33.3%
ANZSRC code: 110315, Otorhinolaryngology, 33.4%

Fields of Research (FoR) Classification

FoR code: 1112, Oncology and Carcinogenesis, 100%

Table of contents

List of Figures

Chapter One

Chapter Three

Chapter Four

Chapter Five

List of Tables

Chapter Two

Chapter Four

List of Abbreviations

ADCC	Antibody-dependent cell-mediated cytotoxicity
aPKC	Atypical PKC
BIS-1	Bisindolylmaleimide-1
CAL 27	Human tongue squamous cell carcinoma cell line
CDK	Cyclin-dependent kinase
cPKC	Conventional PKC
CSC	Cancer stem cells
CT	Computed tomography
DAG	Diacylglycerol
DPI	Diphenylene iodonium
EBC-46	12-Tigloyl-13-(2-methylbutanoyl)-6,7-epoxy-4,5,9,12,13,20-hexahydroxy-1-tigliaen-3-one
EGFR	Endothelial growth factor receptor
ELAM-1	Endothelial-leukocyte adhesion molecule-1
FaDu	Human hypopharyngeal squmaous cell carcinoma cell line
FBS	Foetal bovine serum
Gy	Gray
HNSCC	Head and neck squamous cell carcinoma
HPV	Human papilloma virus
Hr	Hour(s)
ICAM-1	Intracellular adhesion molecule-1
MAPK	Mitogen-activated protein kinase
Min	Minute(s)
MRI	Magnetic resonance imaging
nPKC	Novel PKC
PBS	Phosphate-buffered saline
PET	Positron emission tomography
PG	Propylene glycol
PI	Propidium iodide
PKC	Protein Kinase C
PMN	Polymorphonuclear neutrophils
PS	Phosphatidylserine
QIMRB	Queensland Institute of Medical Research Berghofer

Rb	Retinoblastoma
SCC	Squamous cell carcinoma
SRB	Sulforhodamine B
TMRM	Tetramethylrhodamine methyl ester
TPA	12-O-tetradecanoylphorbol-13-acetate

CHAPTER ONE: General

1.1 Introduction

As the fifth commonest cancer worldwide, there are over 600,000 new patients diagnosed with cancer of the head and neck annually [1]. Head and neck squamous cell carcinoma (HNSCC) is responsible for 90% of all head and neck cancers.

HNSCC is a heterogenous disease, despite the common origin of aerodigestive tract squamous epithelium. There are many factors that contribute to the variation seen clinically. Firstly, the anatomy of the head and neck region is made up of many defined structural subsites that have distinct arterial supply, lymphatic and venous drainage, and inherent microscopic features. Secondly, aetiological risk factors are different for the different subsites, although HNSCC can occur in patients who are young and have no known risk factors. Finally, there is evidence for tumour biological heterogeneity independent of the subsite [2].

Decisions regarding the treatment of a patient with HNSCC involve a large multidisciplinary team of surgeons, radiation and medical oncologists, radiologists, pathologists, speech therapists, dietitians and dentists. Treatment usually includes a combination of surgical resection followed by radiation therapy and/or chemotherapy tailored specifically to the patient's preference, disease characteristics and co-morbidities. Despite sophisticated advances in surgical technique, targeted radiotherapy and drug discovery, the 5 year survival rate has remained low at 50% for the past 30 years [3]. Unfortunately, the median time of survival following loco-regional recurrence or metastatic disease is only six months [4]. Consideration of further surgical resection or radiation therapy following recurrence is precluded at times due to their associated high morbidity on previously treated patients. It has therefore been imperative to investigate novel therapies that can offer increased survival for HNSCC patients with low associated morbidity.

Recently, much focus has been placed on the discovery of diterpene esters, protein kinase C (PKC) activators, which have been shown to induce tumour senescence *in vitro* and *in vivo* [5-9]. Specifically, EBC-46, a novel diterpene ester and PKC activator discovered by QBiotics Pty. Ltd (Queensland, Australia), has recently been found to successfully ablate subcutaneous xenografts of 2 different human HNSCC cell lines in nude mice by

intratumoural injection [10]. This body of work aimed to optimise intratumoural injection of HNSCC mouse models with EBC-46 in conjunction with further investigation into the drug's mechanism of action, to facilitate the progression of EBC-46 into clinical trials.

1.2 HNSCC

1.2.1 Epidemiology and risk factors

As the fifth most common cancer by incidence, and the sixth most common cancer for cancer-related mortality worldwide, head and neck cancer is a significant global health issue [11]. Head and neck cancer includes tumours arising from cutaneous sites, lips, oral cavity, salivary glands, nose, paranasal sinuses, nasopharynx, oropharynx, hypopharynx and larynx. Head and neck cancer includes melanoma, carcinoma, lymphoma and sarcoma. HNSCC comprises approximately 90% of all head and neck tumours [2 12]. Laryngeal cancer is more prevalent in South America, southern and eastern Europe, and western Asia. In comparison, south-central Asia, western and southern Europe, Southern Africa, and Melanesia are high risk regions for oral cavity cancer [1]. Males have an greater incidence (3:1), compared to their female counterparts and the median age at time of diagnosis is within the sixth decade [1 13].

The most salient risk factors identified are excessive alcohol consumption and tobacco use, which appear to increase risk synergistically and have been implicated in 75% of all HNSCC [2 14]. Chewing tobacco or betel nut products is also associated with increased risk of oral cavity cancer [15]. Other less common risk factors for HNSCC include cancer susceptibility syndromes such as Fanconi's anaemia, hereditary non-polyposis colorectal cancer, ataxia telangiectasia and Li-Fraumeni syndrome [16 17]. Within HNSCC, there is a subset lesions which are becoming more prevalent in male patients under 60 years, and are caused by high-risk types of human papillomavirus (HPV), 16 and 18. HPV-16 is found in greater than 90% of HPV-positive oropharyngeal tumours [18]. HPV positivity can be detected with p16 immunohistochemistry and *in situ* hybridisation of tumour tissue, with the strongest association seen with HNSCC of the palatine and lingual tonsils [19]. Patients with HPV-positive tumours generally respond better to chemotherapy and/or radiation therapy and usually have a more favourable outcome [20]. HPV-16 and HPV-18

both encode oncoproteins E6 and E7 which cause alterations in the cell cycle and promote carcinogenesis [21].

In Australia, the incidence of lip, oral cavity, and pharyngeal cancers for males and females has been slowly declining from 1991-2008 at a rate of 1.6% pa and 2.8% pa, respectively [22]. This is postulated to be a consequence of the almost 40% reduction in the prevalence of tobacco smokers over the age of 14, from 24% in 1991 to 15% in 2010 [23]. The overall alcohol consumption per capita in Australia has shown a biphasic trend, with an increase from 9.4 L pa in 1960 to 13.0 L pa in 1980. This rate has declined to 10.1 L in 2009, however it is still reported that 20% of Australians over the age of 14 consume alcohol at a harmful rate [23]. In contrast, tonsil and base of tongue cancer incidence rates have increased 3-4% pa since 1982 and may reflect the increasing prevalence of HPV infection.

1.2.2 Staging

The diagnostic gold standard for HNSCC is a tissue biopsy of the primary lesion or fine needle aspiration of a neck lymph node. In a case where the location of the primary lesion is unknown, an endoscopic examination under general anaesthetic is performed and biopsies from potential sources are taken. There are seven neck lymph node levels that are anatomically catergorized, each one receiving lymph from a known consistent subsite, for example, the anterior tongue lymphatics drain to level I lymph nodes (Figure 1.1). This allows clinicians to treat the respective lymph node level(s) when treating a HNSCC at a specific subsite.

(a)

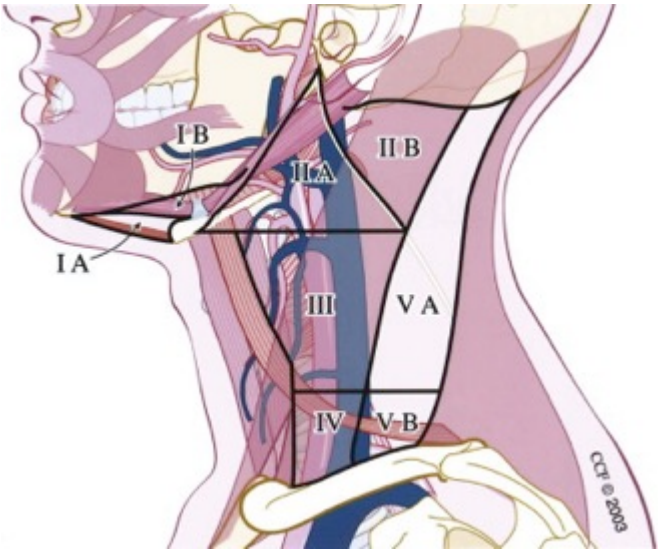

(b)

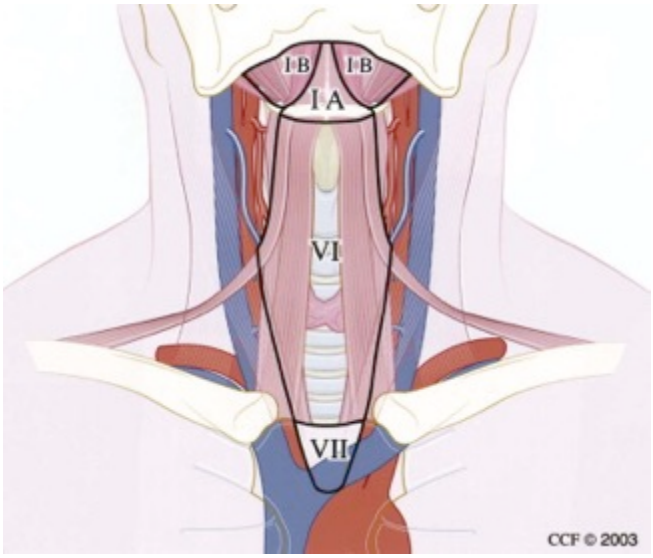

Figure 1.1 Cervical lymph node levels I through V (a). Level II is divided into regions A and B by the accessory nerve (cranial nerve XI). Anterior lymph node levels I, VI, and VII (b) [24].

Clinical examination of the head and neck in combination with computed tomography (CT) and/or magnetic resonance imaging (MRI) determines lymph node involvement. Synchronous second primary tumours are identified in 10-15% of HNSCC patients and can occur in the lungs, thyroid, stomach, colon and pancreas [25]. Positive emission tomography (PET) with fluoro-2-deoxyglucose (FDG) are becoming more widely available and useful in determining the metabolic activity of suspected malignant lesions [26 27].

Staging of HNSCC is determined using the 7th edition of American Joint Committee on Cancer (AJCC) TNM classification [28]. The T classification refers to the characteristics of the primary lesion at the specific site. The N classification refers to the involvement of any lymph nodes. The M classification refers to whether there are any distant metastases present. The resultant stage of a patient's disease then allows the multidisciplinary team of clinicians to determine their subsequent prognosis and treatment regime.

1.2.3 Prognosis

Improvements in surgical technique, targeted radiotherapy, medical management, and reconstruction since the 1970s have resulted in better functional outcomes for patients in areas such as swallowing and speech. However, despite these improvements, the overall survival rate remains approximately 50% [3 12]. Prognosis is also influenced by patient age, smoking status, co-morbidities, tumour size and histology, HPV status, nodal involvement and evidence of perineural spread [29]. Unfortunately, approximately two-thirds of HNSCC patients already have lymph node involvement at the time of diagnosis [30]. For long term survivors, the annual risk of developing a second primary is 4.6% [31]. Furthermore, the median survival following locally recurrent or metastatic disease is only six months [4].

1.3 Treatment

1.3.1 Surgery

Surgical resection has an important role the treatment of HNSCC. An exception is noted for more advanced (> T2, N1) HPV-positive oropharyngeal lesions which are often treated with primary chemoradiation [32]. Surgical resection aims to remove the diseased tissue with clear margins, whilst maintaining head and neck structures that have important functional roles. With the majority of patient's exhibiting cervical nodal involvement at the time of diagnosis, surgical resection frequently also includes nodal clearance.

In 1906, Crile first described a radical neck dissection (RND) where *en bloc* removal of cervical nodal levels I-V were accompanied by the resection of the internal jugular vein, accessory nerve, and sternocleidomastoid muscle [33]. Preservation of any of these additional structures is referred to as a modified radical neck dissection (MRND), and has a superior functional outcome for the patient. A selective neck dissection, where one or more nodal levels are preserved, can be performed based on the known pattern of lymphatic spread from the affected subsite. For patient's with N0 disease, an elective neck dissection is frequently offered if the risk of nodal disease is significant. For example, in oral SCC, the strongest predictor of nodal disease is depth of invasion, with tumours >2mm having a 3.7 fold increased risk [34 35].

Following surgical resection, a team of reconstructive surgeons cover and restore the resected areas in an attempt to preserve form and function. Histological characteristics of the resultant specimen allows the multidisciplinary team of clinicians to further determine prognosis and choose the best post-operative treatment options. Poor histological prognostic factors include: positive margins [36], perineural spread [37], size of nodal deposit(s) and presence of extracapsular spread [38].

1.3.2 Radiation Therapy

Since the 1970s, radiation therapy has played an important role in the treatment of HNSCC. Early stage glottic, tonsil and base of tongue lesions are often treated with definitive radiotherapy alone resulting in high tumour control and cure rates [30].

The schedule for conventional radiation therapy is 2 Gray (Gy) in a single fraction daily, 5 days a week for 7 weeks to give a total of 70 Gy, although this has changed in recent times with hyperfractionated or accelerated radiotherapy schedules [39]. Post-operative radiotherapy is often commenced six weeks postoperatively, allowing for adequate tissue healing, and delivers 60-66 Gy [30]. The advent of intensity-modulated radiation therapy, allows radiation oncologists to deliver radiation in 3 dimensions using CT-planning thus targeting specific sites and avoiding structures at risk such as the optic nerves, brain stem, spinal cord, salivary glands, inner ear, swallowing structures and mandible [40].

Radiotherapy can also be delivered with concurrent chemotherapy with or without prior surgery. A large meta-analysis of data from more than 15,000 participates with HNSCC demonstrated that addition of concurrent chemotherapy to radiotherapy in both definitive and adjuvant postoperative settings led to a 19% reduction in the risk of death, and an 8% improvement in the 5-year survival rate in comparision to treatment with radiotherapy alone [41].

Unfortunately, radiotherapy is not without its adverse effects. Patient's commonly suffer from xerostomia, dysphagia, and hearing loss, whilst osteoradionecrosis of the mandible, radiation-induced nerve palsy, and cerebral radiation necrosis are much less common [40]. Salvage surgery for recurrent disease is also made difficult in a previously irradiated region, secondary to significant fibrosis and loss of normal tissue planes.

1.3.3 Chemotherapy

Chemotherapy alone or in combination with radiotherapy may be given in the treatment of HNSCC. The most commonly used agents are platinum-based, such as cisplatin or carboplatin with 5-flurouracil, with response rates documented between 13-32% [42 43].

A landmark trial published in 1991, demonstrated that in cases of laryngeal SCC, induction cisplatin in combination with radiotherapy resulted in laryngeal preservation and a survival rate comparable to that of laryngectomy with radiotherapy in 64% of the patients [44]. The use of cytotoxic agents, such as cisplatin, is limited by their ototoxicity, nephrotoxicity, haematological toxicity and drug resistance in a subset of HNSCC patients [13 45]. A recent group of researchers have tried to circumvent the toxicity of systemic cisplatin by injecting cisplatin bound to a nanoconjugate directly into mouse models of HNSCC. Their

results demonstrated that the nanoconjugate group had a 40% partial response rate and a 10% complete response rate in comparison to a 10% partial response rate seen in the systemic cisplatin group [13]. The decreased efficacy of systemic chemotherapeutic agents can also be attributed to their relatively poor penetration into the locoregional tumour tissue, resulting in only a small proportion of the agent reaching the tumour tissue or lymph nodes.

1.3.4 Targeted therapy

Recent times have seen much research aimed at more selective, and less systemically toxic therapies for targeting cancer cells. Therapy methods have included monoclonal antibodies (MAbs), gene therapy, tumour vaccines, and small molecule inhibitors [46].

For HNSCC, the most successful agent to date has been Cetuximab (C225, Erbitux® [Bristol-Myers Squibb, New York, NY), a monoclonal antibody that targets the extracellular ligand binding domain of epidermal growth factor receptor (EGFR), a transmembrane cell surface receptor that is integrally involved in cell growth, differentiation and development. Although limited as a monotherapy, a review of recent studies concluded that Cetuximab has improved locoregional control and overall survival when administered in conjuction with definitive radiotherapy in locally recurrent HNSCC [47]. Prolonged survival was also seen when Cetuximab was used in addition to platinum-based chemotherapeutic agents in recurrent or metastatic HNSCC. Unfortunately, a large proportion of patients have intrinsic or acquired resistance to Cetuximab, a phenomenon not predicted by the preclinical research [48]. Several mechanisms of resistance and potential overcoming adjuncts have been purported [49 50]. In Australia, Cetuximab is currently subsidised by the Pharmaceutical Benefits Scheme for initial or continuing treatment of stage III, IVa or IVb SCC of the oropharynx, hypopharynx, or larynx in conjunction with radiotherapy, only in cases where cisplatin was not tolerated or contraindicated.

1.4 Molecular biology of HNSCC

1.4.1 Pathophysiology of HNSCC

The majority of research aimed at identifying the pathogenesis of HNSCC has been performed with oral SCC, likely secondary to their high frequency and ease of sample availability. Oral leukoplakia can be a precursor lesion of oral SCC, with a prevalence of <0.5%, and presents as a mucosal white patch of keratosis that cannot be mechanically scraped off. The malignant transformation rate is estimated to be 1-2% per year [51]. Whilst leukoplakia is a macroscopic indicator of precursor mucosal changes, there is evidence that many other precursor changes are unable to be seen clinically.

Field cancerization is a concept of the presence of one of more mucosal regions that have been exposed to carcinogens and/or have carcinoma-associated genetic alterations which renders them preneoplastic [52 53]. These regions may show histological changes, i.e. leukoplakia, but frequently do not, and are believed to be the source of local recurrences (< 2 cm from primary tumour or occurs within 3 years) or multiple primary lesions (>2 cm from or occurs >3 yrs after the primary tumour) [2]. The preneoplastic regions do not exhibit invasive or metastatic behaviour and require further genetic aberrations to transform into carcinoma.

This accumulation of genetic aberrations over time, leading to the transformation of a normal cell into a cancer cell, forms the basis of the multistep carcinogenesis model that is applied to HNSCC [54 55]. The discovery of patches of mucosal epithelium within the preneoplastic regions or ‘fields’, with TP53 mutations, leading to changes of the tumour suppressor p53, and its function in the cell cycle, has led to the evolution of the hypothetical patch-field-tumour-metastasis model for HNSCC development [2 56]. The model is demonstrated in Figure 1.2.

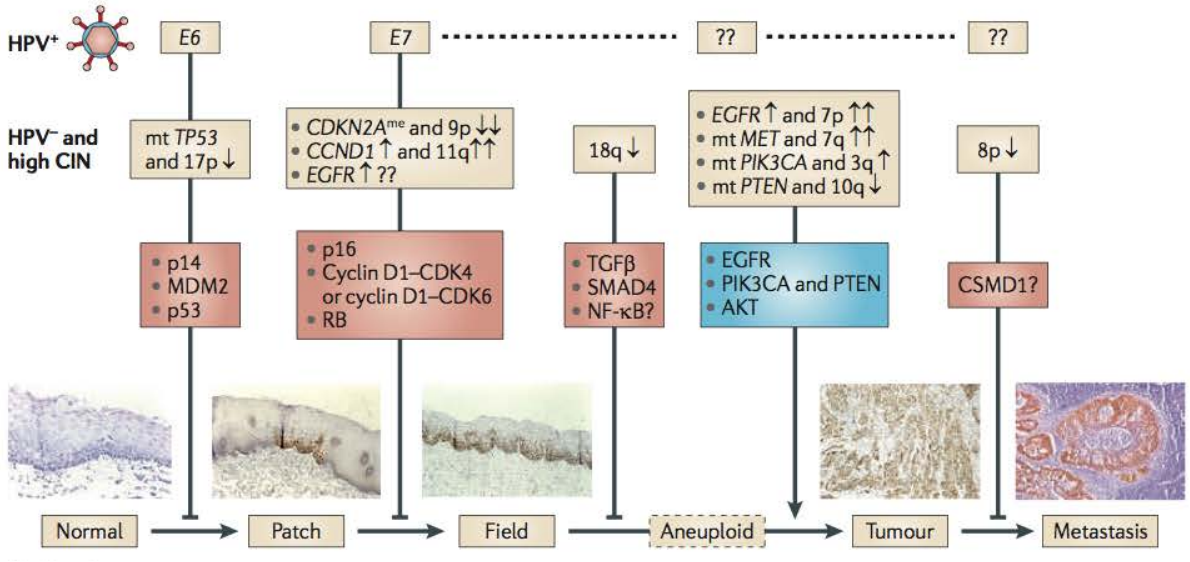

Figure 1.2 An integrated model of head and neck squamous cell carcinoma development in which the genes and pathways involved are depicted. Adapted from Leemans *et al* [2].

The progression of cells through this model is thought to be facilitated by the acquisition of the major cancer-related phenotypes: limitless replicative potential; changes in growth factor signalling; and evasion of apoptosis, invasion and metastasis, and angiogenesis [2].

In order to overcome cellular senescence (permanent cell-cycle arrest) in response to endogenous and exogenous stressors, crucial genes within the p53 and RB pathways are targeted [56]. Inactivation of p53, has been identified in 60-80% of HNSCC cases, caused by somatic mutations in HPV-negative tumours and HPV16 E6 in HPV-induced tumours [2 56]. *In vitro* studies have demonstrated that overexpression of altered p53, telomerase reverse transcriptase (TERT), cyclin D1 or CDK4 resulted in an immortalised oral keratinocyte cell line [57].

Growth factor signalling in epithelial cells involves epidermal growth factor receptor (EGFR), a cell surface tyrosine kinase which activates downstream signals through the Ras-MAPK, Phospholipase C, and PI3K-PTEN-AKT pathways in response to ligand-binding. EGFR can also translocate to the nucleus if bound by EGF and act as a transcription factor of many genes, including CCND1 which encodes cyclin D1, an important player in the regulation of the cell cycle. EGFR is overexpressed in 80-90% of HNSCC cases, [58 59]. Downregulation of transforming growth factor-β (TGFβ), an

inhibitory growth factor which phosphorylate the SMAD family of transcription factors has also been implicated in the development of HNSCC [60 61].

The phosphoinositide 3-kinase, phosphatase and tensin, protein kinase B (PI3K-PTEN-AKT) pathway is involved in the activation of transcription factors, cell cycle inhibitors, and apoptosis inhibitors, that promote cell proliferation and survival. Copy number amplification and mutations of the oncogene *PIK3CA*, the encoding gene for one of the PI3K subunits, have been identified in 31% of oral SCC cases [62].

For invasion and metastasis of HNSCC, cells must change from an epithelial phenotype to a mesenchymal phenotype through a process called epithelial-mesenchymal transition (EMT) [63]. EGF and TGFβ have been implicated in the progress of EMT by regulating a set of transcription factors that directly regulate the genes responsible for cellular adhesion, invasion and migration [63 64]. In a population of HNSCC patients treated with primary chemoradiotherapy, those with NF-kB/p65 nuclear expression confirmed in pretreatment tumour biopsies showed significantly higher rates of lymphatic and haematogenous metastasis, and decreased overall survival [65].

Solid tumours employ angiogenesis to develop new blood vessels that can provide oxygen, anabolites and dispose of catabolites for them. The production of angiogenic factors, such as vascular endothelial growth factor (VEGF) has been linked as a poor prognostic factor in HNSCC [66].

1.4.2 Protein Kinase C

First discovered in 1977, the protein kinase C (PKC) family is a multigene group of phospholipid-dependent protein kinases that phosphorylate serine and threonine residues on a large group of proteins and are therefore involved in numerous cell signaling pathways [67].

There are nine PKC genes, which encode for twelve isozymes divided into three main classifications: classical PKCs, novel PKCs, and atypical PKCs (Figure 1.3).

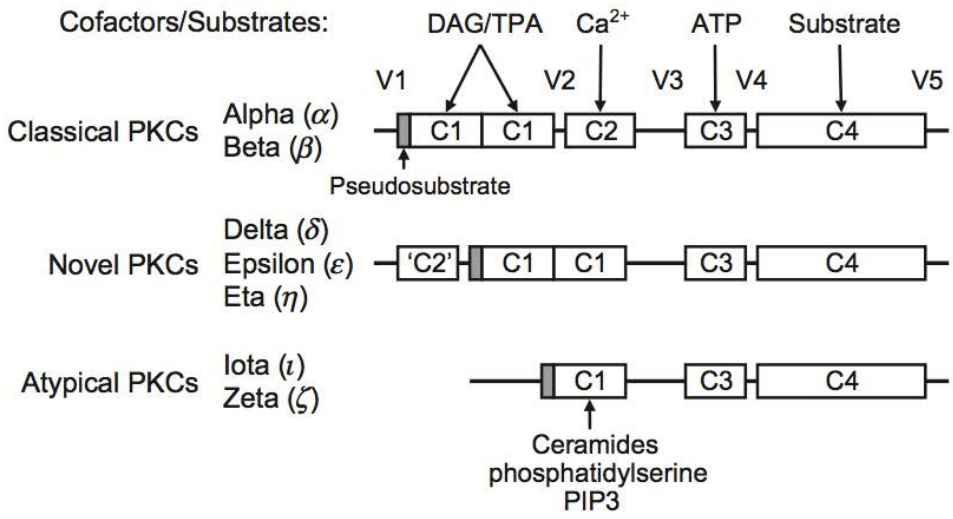

Figure 1.3 A schematic diagram of PKC isozymes. Classical PKC enzymes, exhibit variable 1 (V1) through variable 5 (V5) sequences, an auto- inhibitory pseudosubstrate motif, DAG／TPA-binding C1 domains, a calcium-binding C2 domain, an ATP-binding C3 domain, and a protein substrate interacting C4 domain. All PKC enzymes have the pseudosubstrate, C3, C4 and at least one C1 domain. Adapted from Denning [68].

Classical PKCs (cPKCs: PKCα, PKCβI, PKCβII, and PKCγ) can be activated by calcium and phorbol esters or the lipid diacylglycerol (DAG). Novel PKCs (nPKCs: PKCδ, PKCε, PKC η and PKCθ) can only be activated, independent of calcium, by phorbol esters or DAG. Atypical PKCs (aPKCs: PKCζ and PKCτ) are also calcium independent, and are activated by cis-unsaturated fatty acids [8]. Each PKC isozyme has a catalytic carboxy-terminal region and a regulatory amino-terminal region. When inactive, the conserved regulatory (C1 and C2 domains) region is bound to the catalytic region and prevents activity of the isozyme. An increase in plasma membrane DAG concentration triggers intracellular relocalization and activation of PKC isozymes (Figure 1.4).

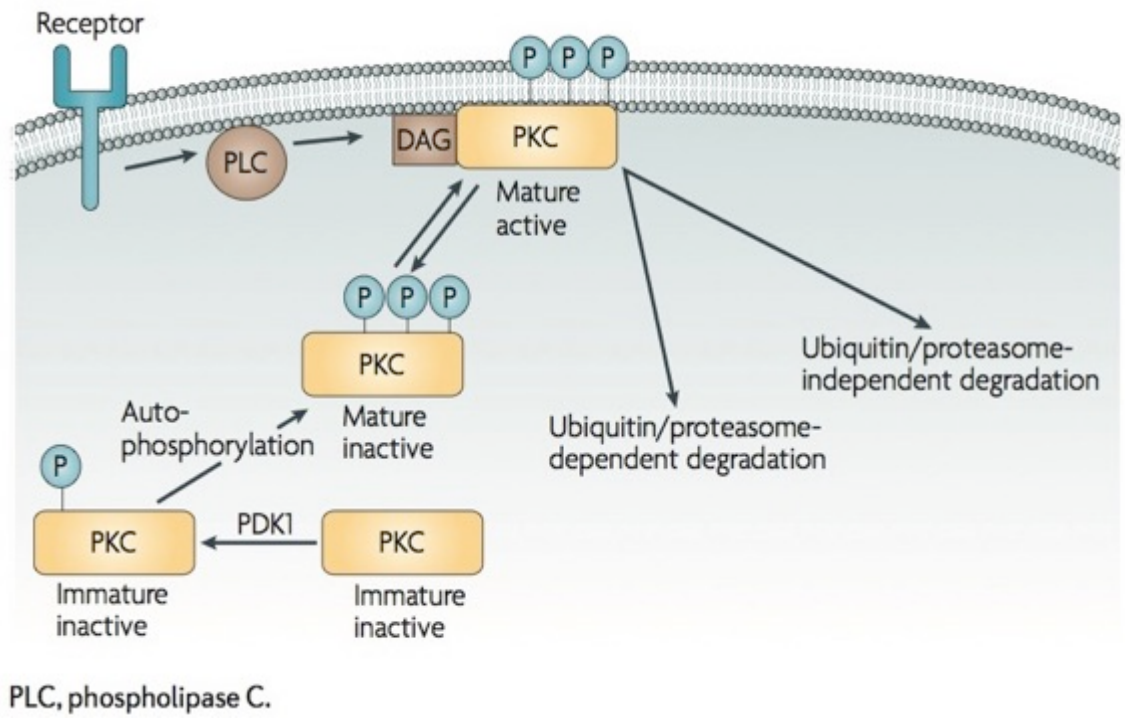

Figure 1.4 Mechanisms of activation and inactivation of protein kinase C [8].

The binding of endogenous ligand DAG results in the capping the hydrophilic cleft in the C1 domain of PKC. This confers hydrophobic properties which then facilitates PKC docking onto membranes and interacting with respective substrates before they are degraded by proteolytic enzymes [8].

The past twenty years has seen a large body of work dedicated to the discovery of the roles and functions of the different PKC isozymes. This goal has been complicated by the discovery that most PKC isozymes are expressed in all tissue types at all stages of development in a ubiquitous fashion [69 70]. However, there is compelling evidence that PKC isozymes have specific and sometimes opposing cell signaling roles in both normal physiological and pathological disease state [71 72]. In particular, PKC isozymes have been found to upregulate gene transcription and translation, regulate cell proliferation and cell death, modify cell morphology and migration [73].

Increased activation of particular PKC isozymes has been implicated in certain types of cancer [8 68], ischaemic heart disease and heart failure [74 75], lung disease [76], diabetes [77], and kidney disease [78].

Considerable cancer research has been focused on identifying PKC isozymes that are involved in tumour cell senescence, with the hypothesis that manipulation of this interaction could eventually be used therapeutically. Cozzi and colleagues [79] demonstrated that activation of a branch of the mitogen activated protein kinase (MAPK) cascade by PKC-activators led to growth inhibition in a melanoma cell line. The MAPK cascade, which involves the kinases Raf, MAPK/ERK kinase (MEK), and ERK/MAPK, links stimuli at the cell surface with alteration of cellular function [80]. Therefore, the cascade plays a central role in regulating cell proliferation, differentiation, survival and apoptosis [81]. Nagpala and colleagues demonstrated that permeability was induced by activation of PKC- β in endothelial cells[82].

1.4.3 Ras guanyl nucleotide releasing proteins (RasGRPs)

Recent research has also discovered other protein families, which also have C1 domains that can be bound and subsequently activated by DAG or DAG analogues [8]. Of note are the RasGRPs, a family of four proteins that are involved in the upstream activation of Ras and other related GTPases that are involved in intracellular signalling. Interestingly, there is also evidence that these proteins can also be activated by PKC phosphorylation [83]. RasGRP1 has been found to be involved in differentiation of immature CD4 and CD8 cells into mature cells in a process called β-selection. RasGRP2 is an activator in platelet aggregation. RasGRP3 is thought to be involved in B cell proliferation and may play a role in macrophage phagocytosis. RasGRP4 is activated by DAG/DAG analogues only, not PKC-mediated phosphorylation, and appears to be mast cell specific [84]. Furthermore, RasGRP1 and RasGRP3 were shown to confer phorbol ester sensitivity in several lymphoma cell lines, leading to growth arrest [85 86].

1.4.4 Diterpene Esters

Diterpene esters are exogenous analogues of the endogenous ligand diacylglycerol (DAG) that activates cPKC and nPKC isozymes by binding to the conserved C1 domain. One such compound is ingenol-3-angelate (I3A, ingenol mebutate), extracted from the sap of *Euphorbia peplus*, a traditional medicine used for many conditions, including skin cancer. Picato® (Leo Pharma Inc, New Jersey, USA) is a topical preparation of I3A (PEP-005) that was recently approved by the Federal Drug Administration (USA) for the treatment of the

SCC precursor, actinic keratosis [87]. In a phase I/II clinical study, a complete clinical response was identified in 50% of SCCs treated topically with Picato® [88]. The compound was also found to be effective in the eradication of subcutaneous xenografts of SCC cell lines LK2 and PAM212 grown in nude mice [5 89]. Challacombe and colleagues [90] identified haemorrhagic necrosis, neutrophil recruitment and antibody-dependent cellular cytotoxicity as the mechanisms of action that provided recurrence-free eradication of their tumour models.

1.5 EBC-46

Derived from the seed of a native Northern Queensland plant, *Fontainea picrosperma*, EBC-46 (12-Tigloyl-13-(2-methylbutanoyl)-6,7-epoxy-4,5,9,12,13,20-hexahydroxy-1-tigliaen-3-one; 562.65 g/mol) is a novel diterpene ester and PKC-activator that has been extracted by collaborators QBiotics Ltd (Queensland, Australia) and the Queensland Institute of Medical Research Berghofer (QIMRB, Queensland, Australia). Veterinary clinical trials, involving over 100 horses, dogs and cats with solid tumours showed very promising results with the majority of tumours eradicated without recurrence by intratumoural injection of EBC-46 (Peter Parsons, pers communication).

This early success led to the hypothesis that this compound could be relevant in human HNSCC. Research demonstrated that EBC-46 did not have the same cytotoxic effects as TPA and Picato® in HNSCC cell lines CAL 27 (tongue) and FaDu (hypopharyngeal), with only a 31.6% and 28.9% reduction in cell survival *in vitro* at concentrations of 10,000 ng/ml, respectively [91]. Following this, CAL 27 and FaDu xenografts were grown in BALB/c *Foxn1*^{nu} mice and subsequently treated with intramural injection of 30 µg of EBC-46. Within 24 hours of intratumoural injection with EBC-46, the xenografts had become haemorrhagic lesions, which progressed to an eschar within 8-10 days. By 21 days, there was scar tissue present at the treatment site only. All of the tumours treated with EBC-46 *in vivo* were eradicated and no recurrence was seen by 90 days. The discrepancy seen between the efficacy of EBC-46 *in vitro* and *in vivo* lead to the hypothesis that the host's own immune system may provide a synergistic effect. Supporting this hypothesis were the findings that human inflammatory cytokines IL-1β and IL-8 were upregulated in FaDu cells, whilst macrophages and neutrophils were recruited to the treatment site following EBC-46 treatment *in vivo*.

A landmark paper on EBC-46 by Boyle et al., (2014) demonstrated that a single intratumoural dose of EBC-46 caused haemorrhagic necrosis and tumour ablation in a melanoma mouse model in addition to the HNSCC models. EBC-46 was also found to induce a respiratory burst from human polymorphonulear cells, and cause increased permeability of human umbilical vein endothelial cells. Furthermore, its action was found to be PKC-dependent, by inhibition with the pan-PKC inhibitor bisindolylmaleimide-1 (BIS-1).

Experiments with EBC-46 so far have used buffered propylene glycol as the standard vehicle for intratumoural injection. Little is known about whether efficacy is improved with alternative suitable excipients, such as γ-cyclodextrin or 2-hydroxypropyl-β-cyclodextrin.

1.6 Project Outline

It has been established that intratumoural injection of the novel PKC-activating drug EBC-46 ablates subcutaneous xenografts of 2 different human HNSCC cell lines in BALB/c *Foxn1*^{nu} mice [10]. Localised hemorrhagic necrosis appeared to be the overt mechanism of action, however the molecular subtleties behind this and the potential to exploit them for enhancing efficacy still need to be investigated. In the aforementioned study, the xenographs were well vascularised and uniform in shape, factors that may confer favourable permanent ablation outcomes. Clinically, however, HNSCC tumours can be irregular in shape and may have variable blood supply, especially post radiotherapy treatment.

1.6.1 Aims and Hypotheses

Therefore, the first aim of this study was to identify a human HNSCC xenograft that responds poorly to intratumoural injection of EBC-46. This would allow identification of tumour characteristics that potentially could predict good or poor outcomes following treatment.

Hypothesis 1:

The efficacy of intratumoural treatment with EBC-46 of different human HNSCC xenografts is variable.

The second aim of this study was to improve efficacy of EBC-46 treatment by altering different administration parameters: dose administration, excipient, volume and with/without prior tumour priming.

Hypothesis 2:

The efficacy of intratumoural treatment with EBC-46 can be altered dependent on its administration.

The third aim of this study was to confirm the molecular mechanism of HNSCC cell death *in vivo* following intratumoural treatment with EBC-46.

Hypothesis 3:

Following treatment with EBC-46, HNSCC cell death *in vivo* occurs by PKC-dependent haemorrhagic necrosis.

CHAPTER TWO: General Materials and Experimental Techniques

2.1 Materials

All chemicals were of analytical quality.

2.1.1 General Reagents and Chemicals

2.1.1.1 Biologicals

Bisindolylmaleimide-1 (BIS-1)	Sigma-Aldrich
DC101 (VEGFR-2 Antibody)	GeneTex
Foetal bovine serum (FBS)	CSL Biosciences
Penicillin	CSL Biosciences
RNase	Sigma-Aldrich
Streptomycin	Invitrogen
Trypsin	Invitrogen

2.1.1.2 Chemicals

EBC-46	QBiotics
Ethanol	Sigma-Aldrich
Formalin	BDH Chemicals
Isopropanol	BDH Chemicals
MilliQ H_2O	Millipore
Propidium iodide	Sigma-Aldrich
Propylene glycol	Sigma-Aldrich
Sodium Chloride	Ajax Finechem
SYTOX® Green	Invitrogen
TMRM	Invitrogen
Trypsin	Sigma-Aldrich

2.1.2 Buffers and Solutions

Cell Lysis Buffer: 20% (w/v) glycerol, 1% (w/v) SDS, 10 mM Tris-HCl (pH 7.4). 2mM PMSF and 1% (w/v) protease inhibitor cocktail added just prior to use.
10x Phosphate Buffered Saline (PBS) Solution: 1.5 M NaCl, 100 mM Na_2HPO_4, 30 mM KH_2PO_4 in MilliQ H_2O
RPMI 1640 media: 10% (v/v) foetal calf serum, 100 μg/ml streptomycin, 60 μg/ml penicillin, 1 mM pyruvate, 0.2 mM nicotinamide, and 3 mM 4-(2-hydroxyethyl)piperazine-1-ethanesulphonic acid)
SRB Solution: 0.4% in 1% acetic acid; 0.8g in 200 ml 1% acetic acid

2.1.3 Sources

Ajax Finechem	Ajax Finechem, Seven Hills, NSW, Australia
BDH Chemicals	BDH Merck Pty, Kilsyth, VIC, Australia
CSL Biosciences	CSL Biosciences Ltd, VIC, Australia
GeneTex	GeneTex Inc, Irvine, CA, USA
Invitrogen	Invitrogen Australia, Mount Waverly, VIC, Australia
Millipore	Millipore Pty Ltd, North Ryde, NSW, Australia
Roche	Roche Diagnostics GmbH, Mannheim, Germany
Sigma-Aldrich	Sigma-Aldrich, St Louis, MO, USA
QBiotics	QBiotics Ltd, Yungaburra, QLD, Australia

2.2 Methods

2.2.1 Human Cell Culture

2.2.1.1 Human Cell Lines

The cell lines used in this project were all of human origin and are listed in Table 2.1.

Table 2.1. Human cell lines used in current study.

Cell Line	Description	Source
SCC-9	Tongue SCC	ATCC No. CRL-1629
SCC-15	Tongue SCC	ATCC No. CRL-1623
SCC-25	Tongue SCC	ATCC No. CRL-1628

2.2.1.2 Cell culture and passaging

All cell lines were cultured in Roswell Park Memorial Institute (RPMI 1640) media containing 10% (v/v) foetal bovine serum (FBS; CSL Biosciences), 100 μg/ml streptomycin (Invitrogen), 60 μg/ml penicillin (CSL Biosciences), 1 mM pyruvate, 0.2 mM nicotinamide, and 3 mM 4-(2-hydroxyethyl)piperazine-1-ethanesulphonic acid). All cell lines were then incubated at 37°C with 5% CO_2 and 95% humidity. Cultured cell lines were passaged biweekly to maintain log phase growth of cells. Once a cell line had reached 80% confluence in the containing flask, media was removed, cells washed with PBS, then detached using trypsin with versene. Cells were then cut 1:10 into new flasks with RPMI 1640.

2.2.1.3 Cryopreservation

Once greater than 80% confluence was achieved, cells could be harvested by removal of media and trypsinized. Cells were then pelleted down by centrifugation for 5 min (1,500 rpm, room temperature). Cell pellets were then resuspended in 1.5 ml of RPMI 1640 and 1.5 ml of 20% dimethyl sulfoxide. Aliquots of 1 ml were added to cryovials, frozen to -80°C, and maintained in liquid nitrogen.

2.2.1.4 Resuscitation from Cryopreservation

Cryovials were transferred from liquid nitrogen to -70°C, followed by immersion in warm tap water to thaw. Cells were then diluted 1:10 with RPMI 1640 at 37°C and then pelleted

by centrifugation for 5 min (1,500 rpm, room temperature). Pellets were then resuspended in 5 ml RPMI 1640 and transferred to a 25 cm^2 flask.

2.2.2 *In vitro* cytotoxicity of EBC-46

2.2.2.1 Sulforhodamine B proliferation assay

The sulforhodamine B (SRB) proliferation assay was used to measure drug–induced cytotoxicity [92]. Initially, 5000 cells/well were seeded in flat-bottomed 96-well microtitre plates and then treated with dose dilutions of a compound for set periods of time. Cell proliferation was then allowed for 5-7 days at 37 °C. The media was then tipped off and cells washed with PBS. Cells were fixed with methylated spirits for at least 5 min.

Following removal of the methylated spirits, cells were washed once gently with tap water and stained with 100 µl/well of 2% SRB solution in 1% acetic acid for 1 hr. The SRB solution was tipped off and cells quickly washed twice with 1% acetic acid. Finally, 100 µl of 10 mM Tris base (unbuffered, pH > 9) was added to each well to release the dye bound to cell protein. The absorbance of the wells was read on an ELISA reader (VERSA max microplate reader; Molecular Devices) at 564 nm with 10 sec prior shaking. Cell survival was plotted as percentage of control well absorbance.

2.2.2.2 Propidium iodide uptake

Using 5 x 10^4 SCC-15 cells/well in a flat-bottomed 96-well microtitre plate, propidium iodide (PI) was added to the RPMI media to give a final concentration of 5 µg/ml. Triplicate wells were treated with EBC-46 in EtOH (50 - 300 µg/ml) for 2 – 60 min alongside negative controls (2 µl EtOH) and positive controls (10 µl of 1% Triton X-100). Imaging was then performed using the AMG EvosFl inverted fluorescence microscope at 10x magnification.

Counting of cells with PI uptake was performed using the OpenCFU software [93]. The percentage of cells with PI uptake at each concentration of EBC-46 compared to the total number of cells present (estimated by positive control) was calculated and plotted and as survival as a function of time.

2.2.2.3 Time-lapse tumour cell killing by EBC-46

Overnight, 1 x 10^5 SCC-15 cells/well were allowed to adhere to a flat-bottomed 8-well plate in 200 μl RPMI media. The following day, 20 μM tetramethylrhodamine methyl ester (TMRM, Invitrogen) and 50 μM SYTOX® Green (Invitrogen) nucleic acid stain was added to fresh 200 μl RPMI media to assess mitochondrial membrane potential (ψm) and cell viability, respectively. The plate was immediately viewed with a Zeiss confocal microscope at 37 °C. Using the associated Zeiss Imaging Software (Zen version 2.0), cell imaging was performed every 30 sec for five minutes prior to the addition of EBC-46. Without moving the plate, 4 μl 20 mg/ml EBC-46 in EtOH was added to the well. Imaging was continued every 30 sec for 30 – 120 min following treatment, depending on continued cell viability.

2.2.3 Subcutaneous inoculation of mice with human cancer cell lines

All experimental work was approved by the QIMRB Animal Ethics Committee (Project number: P345). Five week old BALB/c *Foxn1*^{nu} and NOD/SCID mice were housed under pathogen-free conditions in the QIMRB Animal Facility on a 12 hr light/dark cycle, with freely available water and food. All procedures were performed in with aseptic technique in a laminar flow hood in accordance with institutional standard operating protocols.

In preparation for subcutaneous inoculation, tumour cells from serial passaging of 6-12 T175 flasks were harvested using trypsin/versene in Dulbecco's solution. The number of cells per ml was estimated using a haemocytometer and subsequently facilitated the calculation of the number of cells required for inoculation. The cell lines, cell number per inoculation, and mice used for each experiment are outlined below (Table 2.2).

Following centrifugation at 1,500 rpm for 5 min at 37°C, the resulting cell pellet was resuspended in the pre-calculated volume of RPMI-1640 media with 10% FBS and placed on ice for transportation to the Animal Facility. For experiments using NOD/SCID mice, the fur over their hindquarters was removed with battery-operated clippers (Wahl) prior to inoculation. Inoculation was performed using Terumo® U-100 Insulin 31G x ½" needles to inject 50 μl of the cell suspension just below the dorsal skin of the mouse's hind quarter on the right side, into the subcutaneous space. This was repeated on the left side. The appearance of a translucent bleb following injection confirmed correct placement of the

cells into the subcutaneous space. Mice were ear tagged for future identification and housed in air-filtered cage containing sterile water and food. They were subsequently monitored for tumour size and overall wellbeing.

Table 2.2 Mouse model parameters.

Cell line	Cell density per inoculation site	Mouse strain	No of inoculation sites
SCC-9	2 x 10^6/50 μl	BALB/c *Foxn1*^{nu}	2
SCC-15	2 x 10^5/50 μl and 2 x 10^6/50 μl	BALB/c *Foxn1*^{nu} and NOD/SCID	2
SCC-25	2 x 10^6/50 μl	BALB/c *Foxn1*^{nu}	2

2.2.5 Intratumoural injection with EBC-46

Tumours were monitored until they reached the desired volume of approximately 100 mm^3. Mice in the treated groups received 50-100 µl of 0.3-0.6mg/ml EBC-46 (30 µg; dissolved in 40% propylene glycol or cyclodextrin) to each tumour site using a Terumo® U-100 Insulin syringe with a 29G x ½" needle. Mice in the control groups received 50-100 µl of 40% propylene glycol or cyclodextrin. The mice continued to be regularly monitored for adverse reactions and tumour size.

2.2.6 Infrared temperature analysis

The surface temperature of tumours and surrounding skin was measured using a FLIR E60 handheld infrared camera and FLIR Tools Software (FLIR Systems, Inc, USA). The average surrounding skin temperature was calculated using at least four normal skin regions surrounding each tumour. The difference between the surface tumour temperature and the average surrounding skin temperature was then calculated (tumour °C – normal skin °C).

2.2.7 Mouse monitoring and tumour measurements

Individual tumour dimensions, length (l), width (w) and height (h), were measured biweekly with digital vernier callipers (Kinachrome) and the resulting tumour volume (mm^3) estimated using the formula (l x w x h). Once total tumour burden reached 1000 mm^3 per mouse, mice were euthanized by CO_2 inhalation.

The raw measurement data was recorded and the average volume calculated using Microsoft Excel. The average volume and associated standard deviation (SD) were then plotted against days since treatment. Kaplan-Meier survival curves were prepared in GraphPad Prism 5. Mice were monitored for up to 10 months after tumour treatment.
In addition, digital photographs were taken to document tumour progression. Qualitative measures of tumour characteristics and overall mouse distress were also made.

2.2.8 Immunohistochemistry

Mice were euthanised by CO_2 inhalation at 0 - 24 hr following a single intratumoural injection of EBC-46 or 40% PG to their tumours or normal skin. The treated sites were excised using sterile surgical instruments and fixed in 10% phosphate buffered formalin for 24 hr at 4°C. They were then transferred into 70% ethanol. Tumours were paraffin embedded and stained for haemotoxylin and eosin, neutrophils (LyG6, MPO), macrophages (F4/80), and endothelial cells (CD31) by the QIMRB Histology Facility. Slides were scanned at 40x magnification using the Aperio XT Scanscope.

CHAPTER THREE: Optimising intratumoural treatment of head and neck squamous cell carcinoma mouse models

3.1 Introduction

In the clinical setting, head and neck tumours may exhibit irregular physical characteristics and/or aggressive tumour biology and thus may be more inherently resistant to intratumoural treatment of any therapeutic compounds. It was therefore important to identify a head and neck cancer mouse model that was difficult to ablate and adjust the parameters of treatment with EBC-46 in an attempt to overcome this inherent resistance.

Previous work performed by D'Souza [94] confirmed that 30 μg of EBC-46 (50 μl of 600 μg/ml EBC-46 in 40% propylene glycol) successfully ablated B16-F0 mouse melanoma in C57BL/6J mice in 75-80% of cases compared to 0% of those treated with 10 μg of EBC-46 or propylene glycol alone ($P < 0.0001$). In addition, Adams [91] established human hypopharyngeal (FaDu) and tongue SCC (CAL 27) xenografts using BALB/c *Foxn1*^{nu} mice and was able to successfully ablate tumours with a single intratumoural injection of 30 μg of EBC-46.

The aim of this chapter was to optimize the efficacy of intratumoural injection of EBC-46 in a head and neck cancer mouse model. Therefore, 30 μg of EBC-46 in 40% propylene glycol was used as the standard treatment for the purposes of this project and treatment parameters were then subsequently altered to try to increase the proportion of successfully ablated tumours.

3.2 Results

3.2.1 Identification of a head and neck cancer cell line resistant to intratumoural treatment of EBC-46.

Intratumoural treatment with 30 μg of EBC-46 successfully ablated FaDu and CAL 27 xenografts in BALB/c *Foxn1*^{nu} as previously discussed. In an attempt to identify a cell line that displayed more resistance to EBC-46 treatment, three additional tongue SCC cell lines were obtained from ATCC: SCC-9, SCC-15, and SCC-25. Xenografts of the three cell

lines were established by subcutaneously injecting ten five-week old BALB/c *Foxn1*^{nu} mice for each group with 2 x 10^6 cells at two sites as described in Section 2.2.3. Xenografts took 8 days to reach a treatable size (~100 mm^3) in the SCC-15 group, compared to 17 days for SCC-9 and SCC-25. Of the ten mice in each group, five were treated with 30 μg of EBC-46 (50 μl of 600 mg/ml EBC-46 in 40% propylene glycol) at both tumour sites, whilst the remaining five mice were injected with 50 μl of 40% propylene glycol only (Figure 3.1).

In all three xenograft groups treated with EBC-46, the previously described localized haemorrhagic response and subsequent eschar formation occurred (Figure 3.2). This was not seen in the groups treated with the vehicle control. Average tumour volumes for both groups were calculated and plotted against time (Figure 3.3). Average tumour volumes showed a steady decline following treatment with EBC-46. SCC-15 xenografts were completely ablated by day six post treatment with EBC-46, compared to day 14 post treatment for SCC-9 and SCC-25.

In contrast, the control groups for all three xenografts continued to have tumour growth following intratumoural injection with the vehicle control. Mice were euthanized once total tumour burden had reached approximately 1000 mm^3 per mouse. Figure 3.4 depicts the resulting Kaplan-Meier graphs, which confirmed that EBC-46 treatment led to a statistically significant increase in survival time.

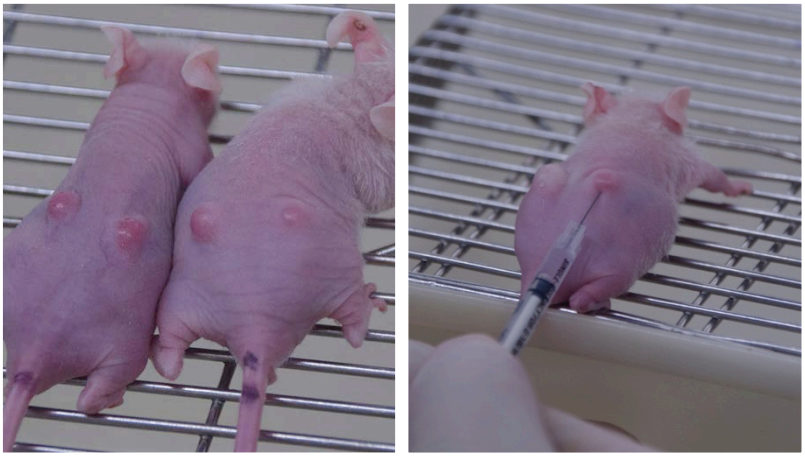

Figure 3.1 SCC-15 subcutaneous xenografts in BALB/c *Foxn1*^{nu} mice and subsequent intratumoural treatment.

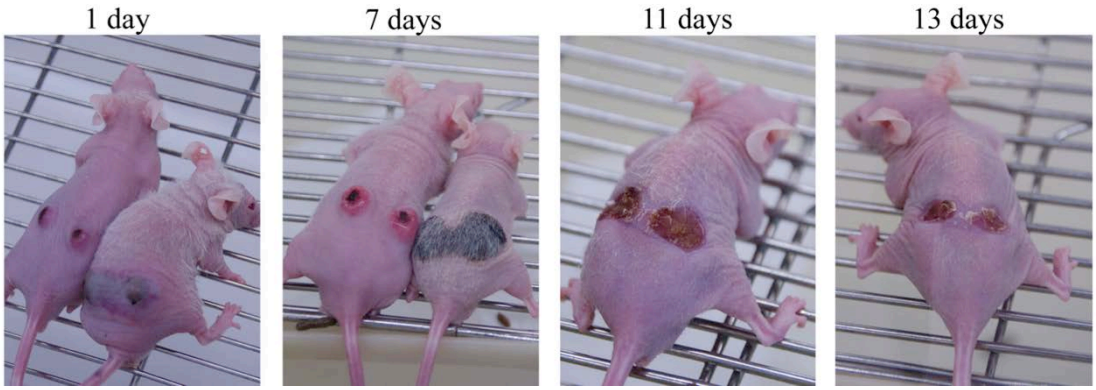

Figure 3.2 Time-lapse SCC-15 subcutaneous xenografts in BALB/c *Foxn1*^{nu} mice following subsequent intratumoural treatment with 40% propylene glycol (left) and 30 μg EBC-46 (right). Maximum tumour burden was reached within two weeks for the mice treated with 40% propylene glycol and therefore they were euthanized and not included in day 11 and 13 photos.

A

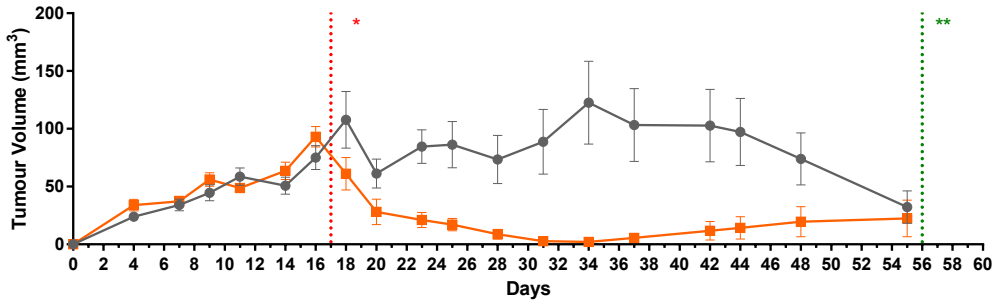

B

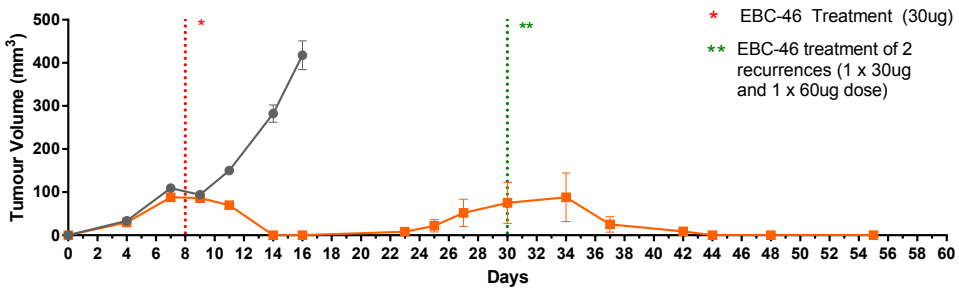

C

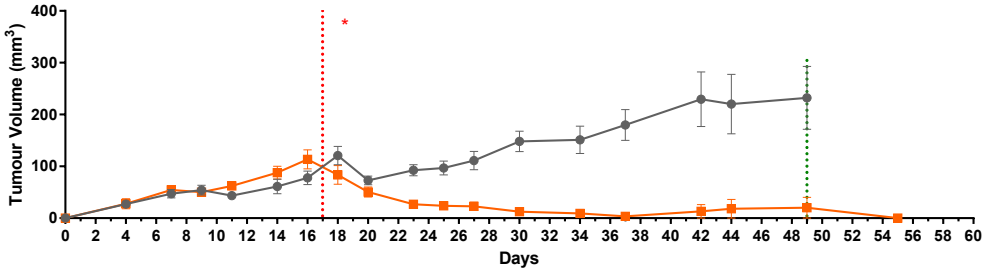

Figure 3.3 Tumour volume of SCC-9 (A), SCC-15 (B) and SCC-25 (C) tumours in BALB/c *Foxn1*^{nu} mice treated with EBC-46 and compared to treatment with 40% PG vehicle control (n = 10 per group). Error bars represent ±SEM.

A

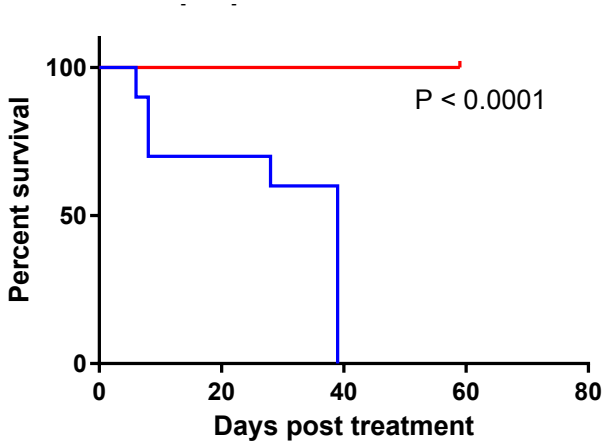

B

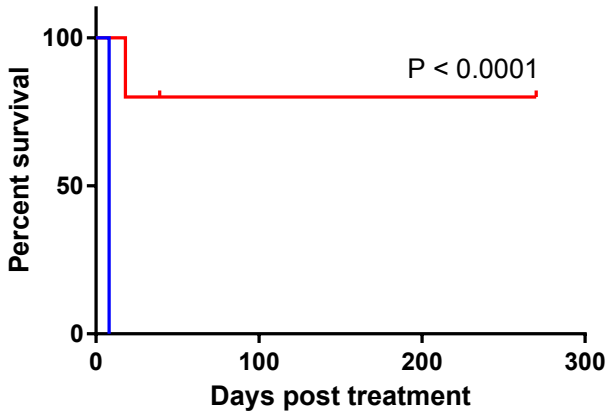

C

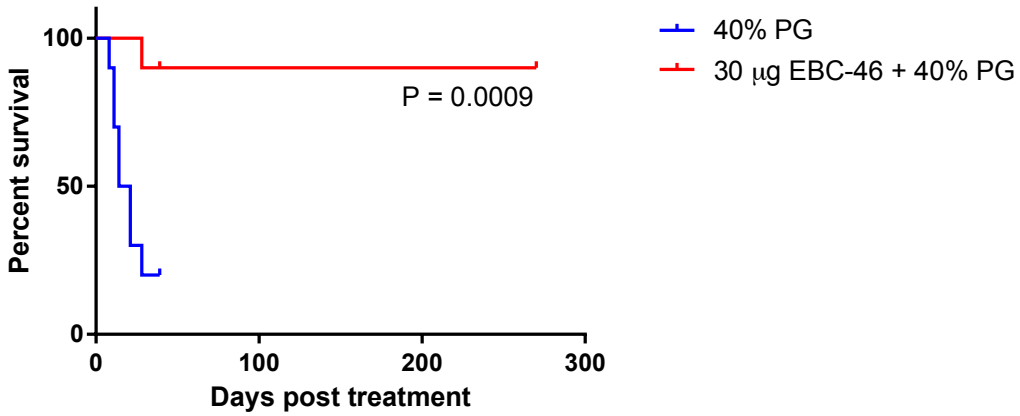

Figure 3.4 Kaplan-Meier plot comparing the differences in survival of BALB/c *Foxn1*^{nu} mice treated for SCC-9 (A), SCC-15 (B), and SCC-25 (C) tumours with EBC-46 or 40% PG vehicle control.

Recurrences was seen at two tumour sites (2/10) for SCC-9 xenografts, and one tumour site (1/10) for SCC-25 xenografts 19 days following treatment with EBC-46. Three recurrences (3/10) in the SCC-15 group were identified day 17 post-initial treatment with EBC-46. Of the total six recurrences seen across the groups, three tumours were re-treated with 30 μg EBC-46 resulting in complete ablation. Mice were monitored for ten months and no further recurrences were seen. Given the greatest proportion of recurrences, SCC-15 was identified as the most resistant cell line to treatment with EBC-46 and therefore selected to be the cell line of utilized for further optimisation of EBC-46 efficacy.

3.2.2 Efficacy of EBC-46 treatment of tongue SCC xenografts in a different mouse model.

The majority of the previous works investigating the efficacy of EBC-46 in the treatment of head and neck cancer mouse models have used BALB/c *Foxn1*^{nu} mice. BALB/c *Foxn1*^{nu} nude mice are athymic and thus cannot produce mature T lymphocytes [95]. This results in the inability of the mice to mount cell-mediated immune responses (CD8+ T cells) as well an antibody formation (CD4+T cells). However, B-cells and natural killer (NK) cells maintain normal function.

In order to see whether the suboptimal efficacy of EBC-46 seen in SCC-15 xenografts were specific to the nude mouse model, xenografts were established in non-obese diabetic severe combined immunodeficient (NOD/SCID) mice for comparison. NOD/SCID mice have impaired development and function of T-cells, B-Cells and NK cells [96].

3.2.2.1 Intratumoural injection of EBC-46 to large tongue SCC xenografts in NOD/SCID mice

Ten five-week old male NOD/SCID mice were subcutaneously inoculated with 2 x 10^6 SCC 15 cells/site as described in Section 2.2.3. Tumour growth occurred very quickly in comparison to the nude mice xenografts, with an average tumour volume of 159 mm^3 (± 65 mm^3 SD) seven days following initial inoculation. On day seven, five mice were intratumourally injected with the previously established treatment of 30 μg EBC-46 and five

mice with 50 μl of the vehicle control 40% PG. Tumour growth and Kaplan Meier survival graphs for both groups are represented in Figures 3.5 and 3.6.

The mice injected with the vehicle control continued to display exponential tumour growth, similar to that seen in the BALB/c *Foxn1*^{nu} mice cohort. In comparison, tumour growth in the group treated with the previously established dosing regimen of 30 μg EBC-46 did not mirror that seen in the nude mice. On average, tumour growth was suppressed by approximately 50%, and no tumours were successfully ablated (0/10). Mice reached maximum tumour burden and were culled at day 14 and day 21, for the control and treated groups, respectively.

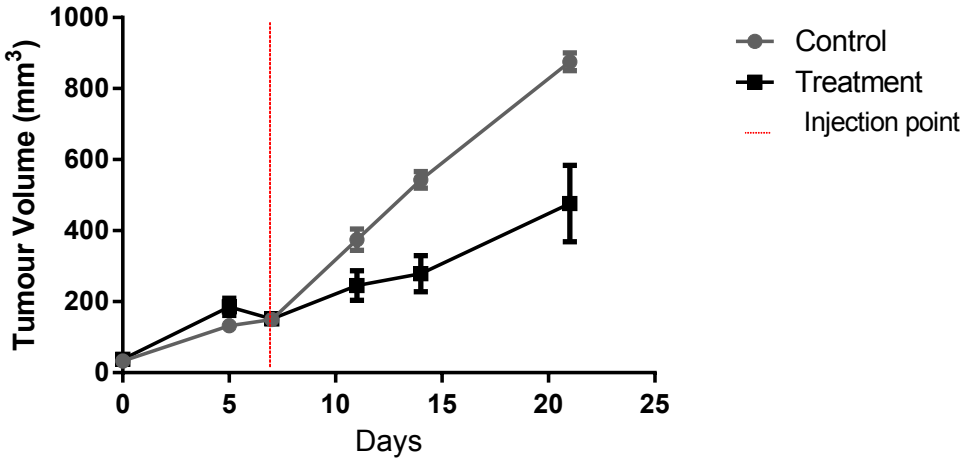

Figure 3.5 Tumour volumes of large (>150 mm^3) SCC-15 tumours in NOD/SCID mice treated with EBC-46 and compared to treatment with 40% PG vehicle control.

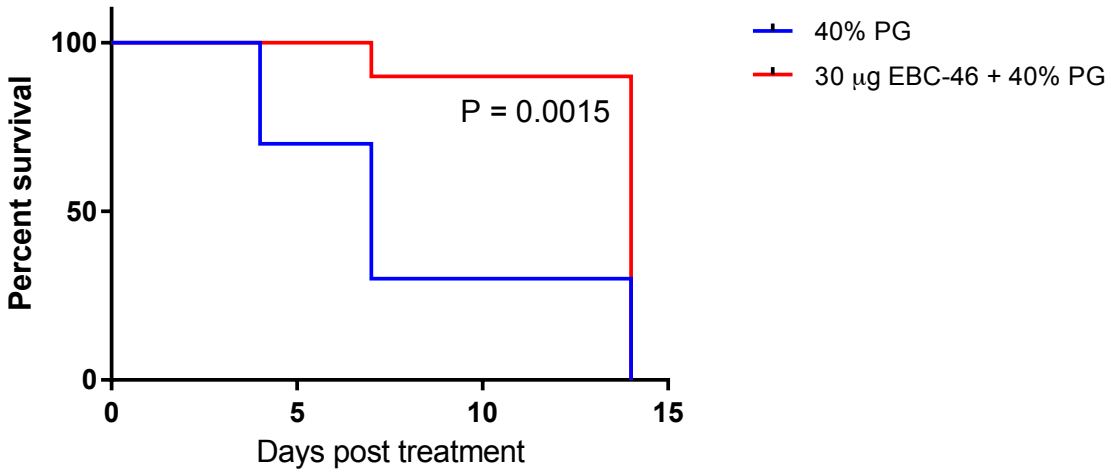

Figure 3.6 Kaplan-Meier plot comparing the differences in survival of NOD/SCID mice treated for large (>150 mm^3) SCC-15 tumours with EBC-46 or 40% PG vehicle control. Five mice per treatment group. Error bars represent ±SEM.

3.2.2.2 Intratumoural injection of EBC-46 to small tongue SCC xenografts in NOD/SCID mice

The reduced efficacy of EBC-46 treatment seen in the larger SCC-15 xenografts in NOD/SCID mice potentially could have been attributed to the larger average tumour size at the time of treatment (159 mm^3 ± 65 mm^3). The dose of EBC-46 may have been inadequate for the number of tumour cells, and/or local spread of tumour cells may have already occurred to a site outside the treatment field.

In an attempt to overcome this reduced efficacy to EBC-46 treatment, 25 NOD/SCID mice were inoculated with 2 x 10^5 cells/site and treated at a reduced mean tumour volume (67 mm^3 ± SD 35 mm^3). Within the group of 25 mice with smaller tumours: five were treated with 50 μl of 40% PG vehicle control and five treated with 30 μg EBC-46 in a single bolus injection (Figures 3.7 and 3.8). Of the five mice treated with EBC-46 with 40% PG, only two mice had successfully ablated tumours. The remaining tumours showed initial clearance but developed local recurrence two weeks following EBC-46 treatment.

3.2.2.3 Single versus divided dose administration of EBC-46.

To investigate whether more tumour cells could be targeted with a dose given in each tumour quadrant, compared to the single dose, five mice were treated with a total 30 μg EBC-46 given in four divided doses (RoD = ring of death). Upon administration of the divided doses, there was a significant amount of leakage of the solution out of the preceding needle puncture sites, thus potentially reducing the overall concentration of EBC-46 in the tumour tissue. Solution leakage was also seen in tumours that appeared to be particularly necrotic. As depicted in Figure 3.8, mice treated with divided doses rather than the single dose of EBC-46 had significantly reduced survival (P = 0.001). No tumours were successfully ablated.

A pilot study using a tattooing apparatus to administer EBC-46 was discontinued because of difficulty in delivering a sufficient, known amount into the tumour.

3.2.2.4 Propylene glycol compared to cyclodextrin as an excipient for EBC-46 administration.

Initial experiments with EBC-46, dissolved the compound into PEG400 for injection into B16-F0 mouse melanoma in C57BL/6 mice. Whilst the tumours were successfully ablated, it was subsequently established that using aqueous propylene glycol (PG) as an excipient displayed similar results and would be more appropriate for clinical intratumoural treatment (D'Souza, 2014).

Cyclodextrins are a family of cyclic oligosaccharides used widely in the food, agricultural, and pharmaceutical industries. The ring-like structure of these compounds provides a hydrophobic inner and a hydrophilic outer region, facilitating the inclusion of hydrophobic/lipophilic compounds and potentially increasing their bioavailability when used as a drug excipient [97]. To compare the efficacy of EBC-46 dissolved in 2-hydroxypropyl-β-cyclodextrin or 40% PG, five of the 25 NOD/SCID mice with smaller tongue SCC-15 tumours were treated with a single dose of 30 μg EBC-46 in 4% 2-hydroxypropyl-β-cyclodextrin. A further five mice were treated with 4% 2-hydroxypropyl-β-cyclodextrin alone as a vehicle control. Overall, EBC-46 in 2-hydroxypropyl-β-cyclodextrin did not significantly improve survival compared to EBC-46 in 40% PG ($p = 0.0293$, Figures 3.7 & 3.8). Two mice had successfully ablated tumour sites. These results confirmed the hypothesis that 2-hydroxypropyl-β-cyclodextrin was no more effective as an excipient as 40% PG.

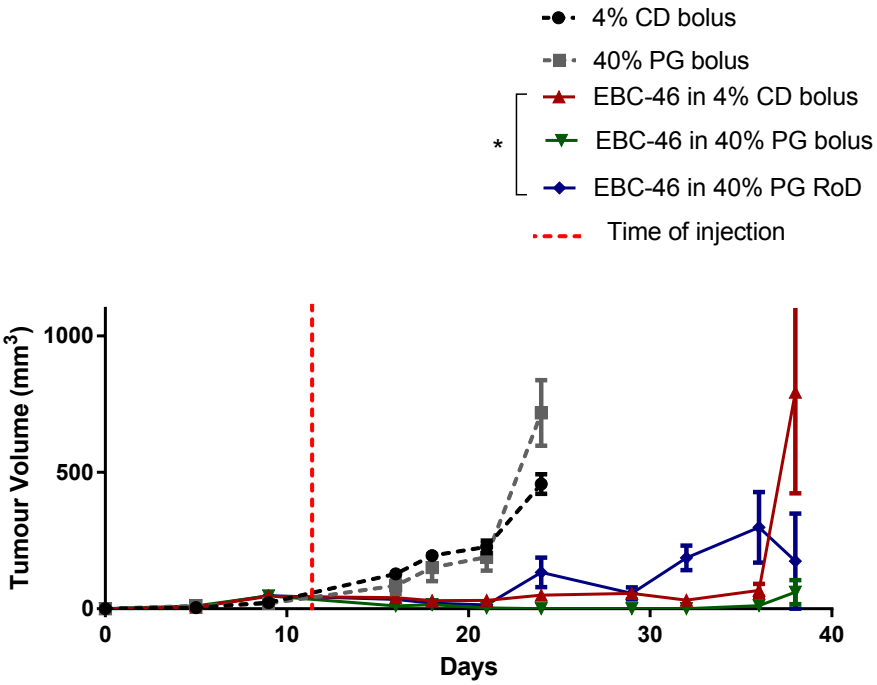

Figure 3.7 Tumour volume of small SCC-15 tumours in NOD/SCID mice treated with single or multiple doses EBC-46 and with 40% PG or 2-hydroxypropyl-β-cyclodextrin as a vehicle control. RoD = ring of death (multiple doses). Error bars represent ±SEM.

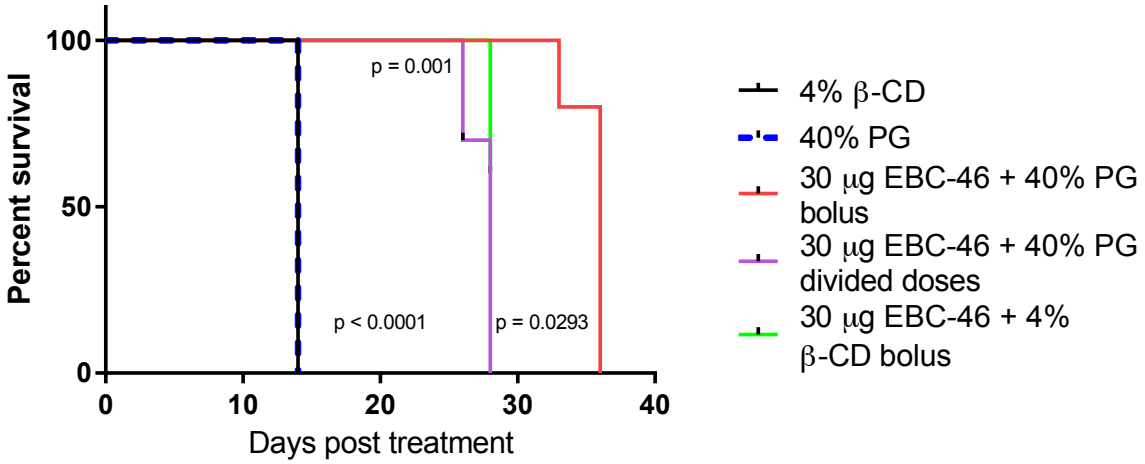

Figure 3.8 Kaplan-Meier plot comparing the differences in survival of NOD/SCID mice with SCC-15 tumours treated with single or multiple doses EBC-46 and with 40% PG or 2-hydroxypropyl-β-cyclodextrin as a vehicle control.

3.2.2.5 Efficacy of EBC-46 with tumour priming

Challacombe and colleagues [90] showed that topical treatment with a related diterpene ester, Picato ® (PEP005, ingenol-3-angelate) was associated with a significant neutrophil infiltration in BALB/c *Foxn1*^{nu} mice with skin tumours, indicating an acute T-cell independent inflammatory response. A reactive neutrophil infiltration was also seen following intratumoural injection of EBC-46 in a melanoma mouse model (D'Souza, 2014). Furthermore, depletion of peripheral neutrophils with the neutrophil-neutralizing monoclonal antibody anti-Ly6G resulted in tumour relapse in approximately ~40% of sites.

The role of neutrophil extracellular traps (NETs) in cancer progression is currently controversial and incompletely understood. In response to cytokines, such as interleukin 8 (IL-8) and tumour necrosis factor-α (TNF-α) neutrophils extrude their nuclear DNA, which then binds proteins and peptides [98]. Initially, these were known to have antimicrobial effects but NETs are now proposed to facilitate either a pro or anti-tumourigenic microenvironment. Interestingly, NET production (NETosis) can also be induced by phorbol esters, such as PMA [99].

It was therefore hypothesized that priming tumour infiltrated neutrophils with a small dose of EBC-46 may increase the tumour concentration of NETs and subsequently influence tumour growth. Twenty 5-week old NOD/SCID mice were utilized to establish SCC-15 xenografts with 2 x 10^5 cells/site as previously described (Section 2.2.3). Tumours were treated at an average volume of 75 mm^3. Five mice were treated with a 6 μg bolus of EBC-46 24 hours prior to the previously established treatment regimen of 30 μg. Another five mice received the priming dose 4 hours prior to standard treatment. For comparison, five mice were treated with no priming dose prior to 30 μg EBC-46 and five received 40% PG as a vehicle control.

Of those mice treated with a 6 μg bolus 24 hours prior to a 30 μg bolus, one mouse demonstrated complete ablation at both tumour sites 34 days following treatment (Figure 3.9). Comparatively, tumour ablation occurred in three mice treated with 30 μg bolus only. Overall survival was not significantly different between the two groups (P = 0.4902). All mice treated with a 6 μg priming dose 4 hours prior to standard treatment showed continued tumour growth, no successful ablations, and significantly reduced survival (P = 0.0048).

Thirty-four days following initial treatment with EBC-46, the four mice that had primary tumour clearance, were noted to have bilateral inguinal lymphadenopathy approximately 10-15 mm in diameter, requiring euthanasia (Figure 3.10). A representative mouse was dissected to display the lymph nodes in question and specimens were sent to histology to confirm metastatic SCC (Figure 3.11).

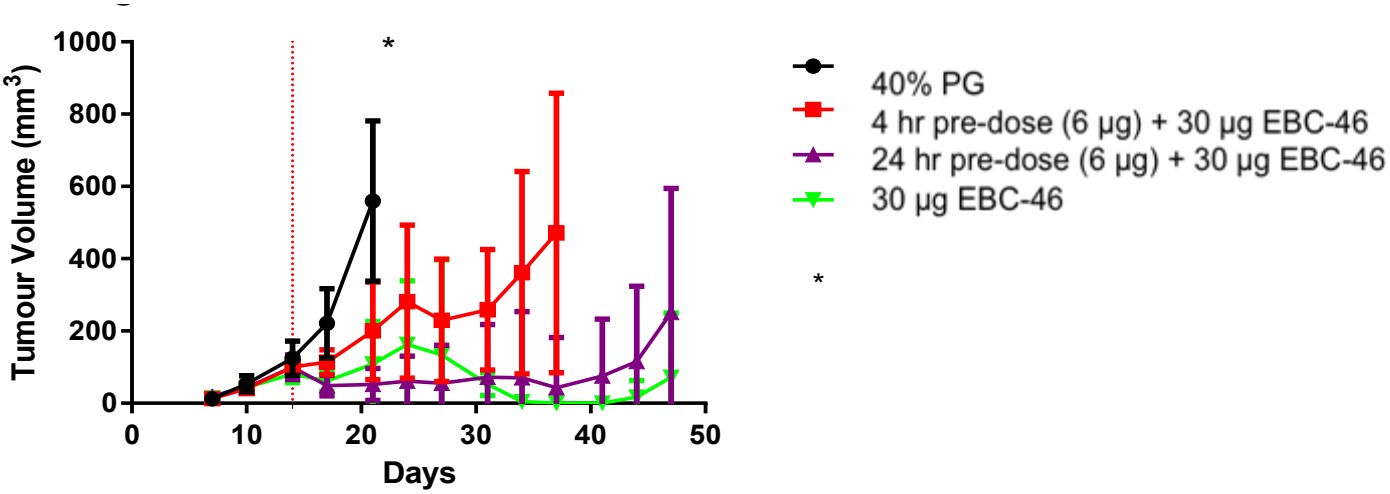

Figure 3.9 Tumour volume of SCC-15 tumours in NOD/SCID mice treated (*) with 6 µg pre-dose of EBC-46 4 hours or 24 hours prior to 30 µg bolus compared to standard 30 µg bolus of EBC-46 alone.

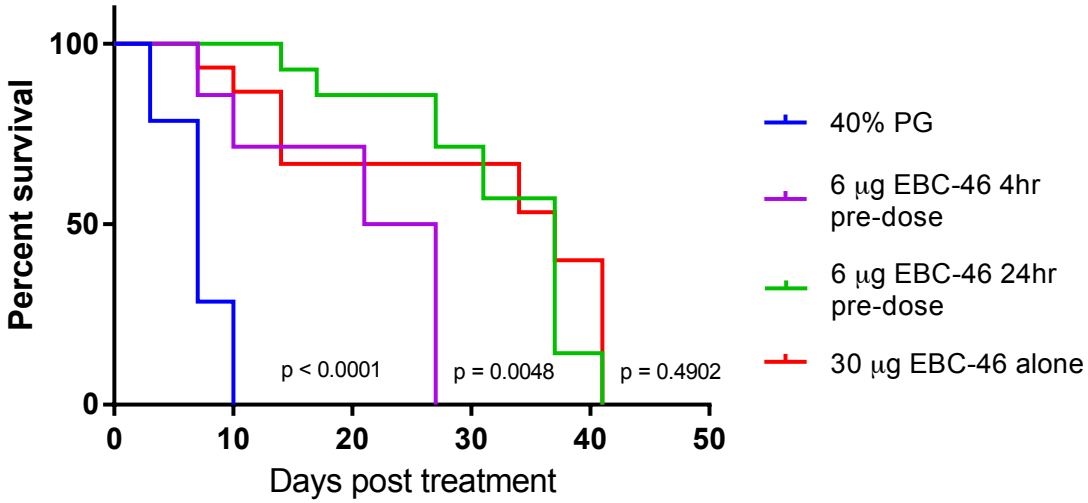

Figure 3.10 Kaplan-Meier plot comparing the differences in survival of NOD/SCID mice with SCC-15 tumours treated with 6 µg pre-dose of EBC-46 4 hours or 24 hours prior to 30 µg bolus compared to standard 30 µg bolus of EBC-46 alone.

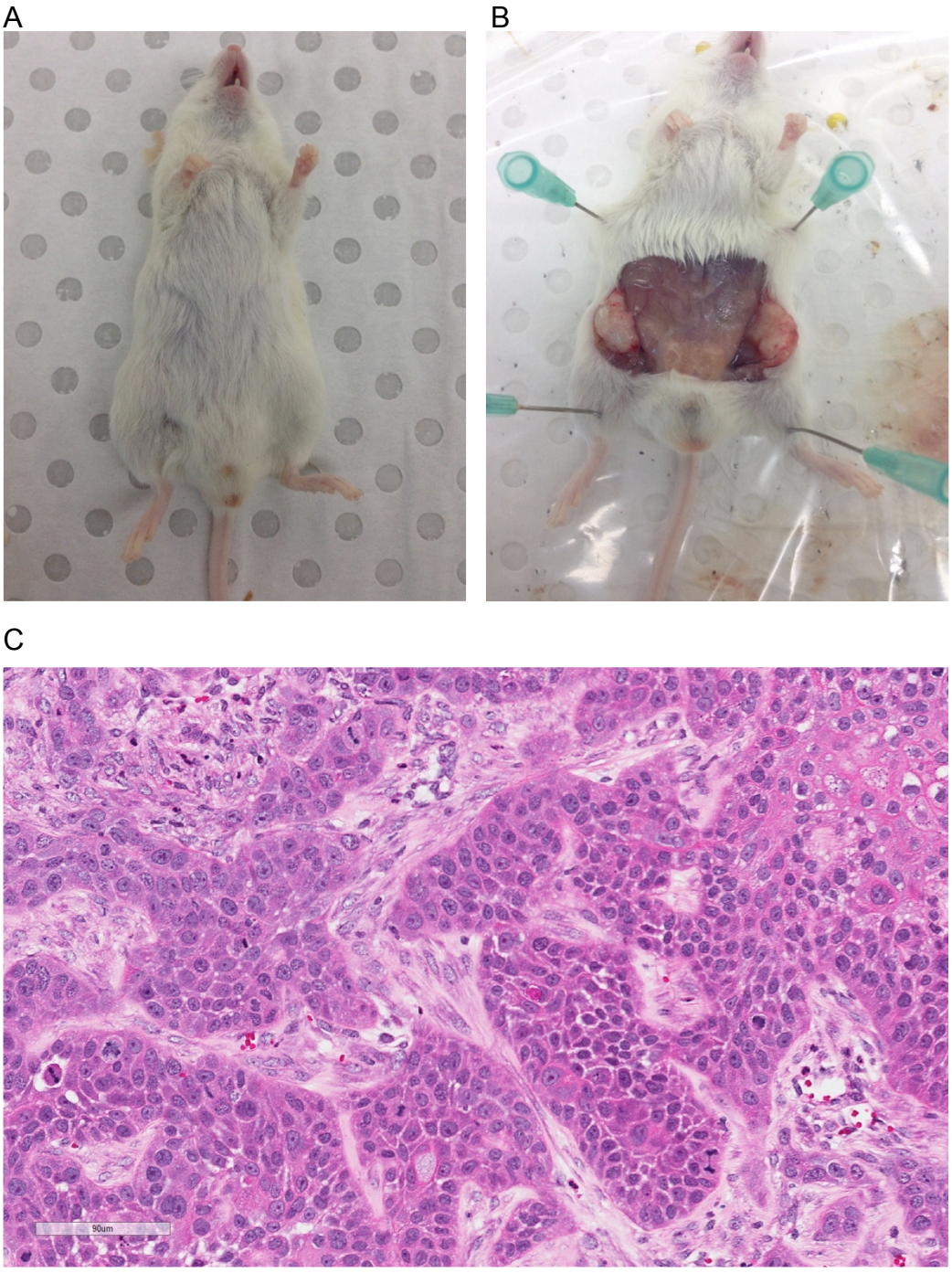

Figure 3.11 Inguinal lymph node metastases before (A) and during (B) dissection. H&E staining confirmed the presence of metastatic SCC (C).

3.2.2.6 Efficacy of EBC-46 delivered in larger volume

As previously mentioned, during administration of 30 μg of EBC-46 in 50 μl of vehicle to some xenografts in NOD/SCID mice, significant leakage of the solution from necrotic areas of the tumour occurred and subsequent reduced tumour infiltration was noted. Those particular tumours often were not successfully ablated likely due to the overall reduced concentration of EBC-46 at the tumour site or reduced treatment field area.

It was therefore proposed that increasing the solution volume, with the same dose (30 μg) could potentially minimize dose wastage from leaking and improve tumour infiltration. SCC-15 xenografts were established in NOD/SCID mice (Section 2.2.3) and treated with 40% PG alone (5), 30 μg EBC-46 in 50 μl with 40% PG (5), or 30 μg EBC-46 in 100 μl with 40% PG (5). Following EBC-46 treatment, the resulting haemorrhagic region surrounding the tumour appeared moderately more extensive for those treated with 30 μg EBC-46 in 100 μl with 40% PG (Figure 3.12). No additional adverse effects were noted during routine mouse and tumour monitoring.

No significant difference in tumour growth or survival was apparent between the two EBC-46 treated groups Figures 3.13 and 3.14).

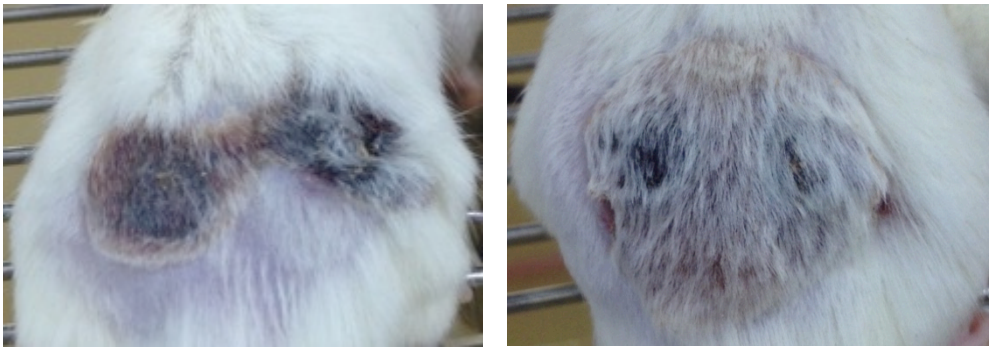

Figure 3.12 Photographs of NOD/SCID SCC-15 xenografts seven days following treatment with 30 μg bolus EBC-46 in 100 μl of 40% PG vehicle control (right) compared to 30 μg bolus EBC-46 in 50 μl of 40% PG (left).

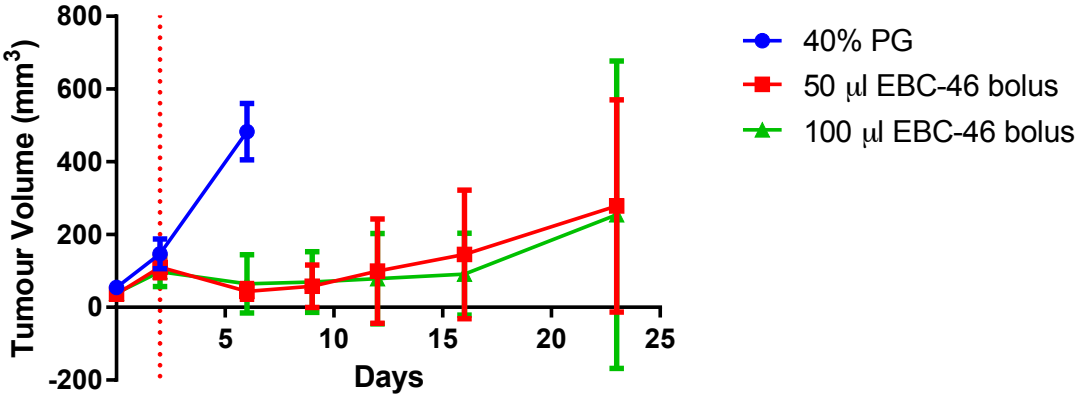

Figure 3.13 Tumour volume of SCC-15 tumours in NOD/SCID mice treated with 30 µg bolus EBC-46 in 100 µl of 40% PG vehicle control compared to 30 µg bolus EBC-46 in 50 µl of 40% PG.

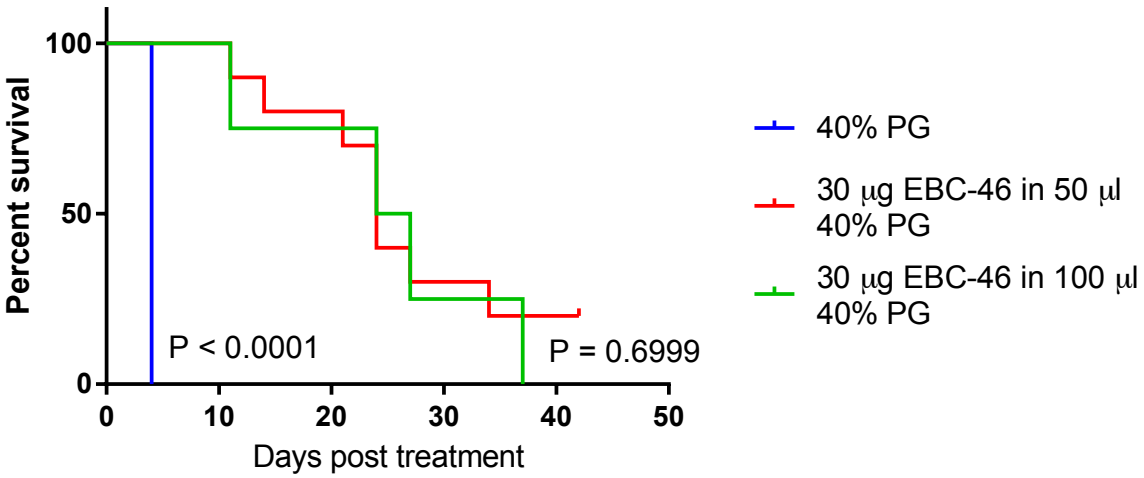

Figure 3.14 Kaplan-Meier plot comparing the differences in survival of NOD/SCID mice with SCC-15 tumours treated with 30 µg bolus EBC-46 in 100 µl of 40% PG vehicle control compared to 30 µg bolus EBC-46 in 50 µl of 40% PG.

3.3 Discussion

The aim of this chapter was to identify a head and neck SCC mouse model that was inherently difficult to treat with EBC-46 and try to overcome this resistance using variations of dose administration, excipient, volume and tumour priming.

SCC-15, a tongue SCC cell line, demonstrated the most resistance to intratumoural EBC-46 treatment with ~30% relapse rate in BALB/c *Foxn1*^{nu} mice, however repeated dosing with EBC-46 led to cure with no sign of recurrence ten months later. Greater tumour resistance was seen in SCC-15 xenografts grown on NOD/SCID mice, which indicated involvement of the host's innate immune system in EBC-46's mechanism of action. BALB/c *Foxn1*^{nu} mice are more immunocompetent than their NOD/SCID mice counterparts. Whilst both strains have impaired B-cell and T-cell lymphocyte development, NOD/SCID mice have an additional impairment of their macrophages, natural killer (NK) cells and complement components [96].

Using the difficult tongue SCC mouse model, EBC-46 administration parameters were then adjusted in an attempt to overcome this inherent resistance. It was shown that a single bolus dose of 30 μg EBC-46 in 50 μl 40% PG, to a tumour site led to a greater ablation rate compared to divided doses of the novel drug. Potentially this was due to additional leakage of the solution out of preceding needle holes in a relatively small tumour volume, thus reducing the overall concentration of the drug at the tumour site. In a clinical scenario, a tumour may be large and/or irregularly shaped, thus requiring more than a single intratumoural dose of EBC-46.

Despite the hypothesis that 2-hydroxypropyl-β-cyclodextrin could potentially carry EBC-46 in its hydrophobic centre and remain at the tumour site for an extended period of time, the use of this compound as an excipient yielded no improved survival or further reduction in tumour growth. This study confirmed that 50 μl 40% PG as an excipient for EBC-46 appeared to be the most efficacious, however, with the gaining popularity of other excipients, such as nanoparticles, it may be prudent to investigate these compounds in future experiments.

Tumour priming with a small dose of EBC-46 was hypothesized to potentially cause a release of pro-inflammatory cytokines and chemokines at the tumour site, thus recruiting

more host macrophages and neutrophils. It was theorized that the amplification of the host's innate immune response would then facilitate cell death of a larger proportion of tumour cells following treatment with EBC-46. However, no significant improvement in survival or tumour ablation was found in the present study.

Overall, this chapter confirmed that 30 μg EBC-46 in 50 μl 40% PG given intratumourally as a single bolus dose without prior priming was the most efficacious treatment for a tongue SCC mouse model. The greater efficacy of EBC-46 treatment in the BALB/c *Foxn1*^{nu} mice potentially indicates the additional role of the host's innate immune system. The following chapters focused on characterization of the host's innate immune response to EBC-46 treatment, using salient immunohistochemical markers, and further investigation of the mechanism by which EBC-46 caused tumour cell death.

CHAPTER FOUR: Histological analysis of SCC-15 xenografts following intratumoural treatment with EBC-46

4.1 Introduction

Boyle *et al* (2014) observed that intratumoural treatment of hypopharyngeal SCC (FaDu) xenografts with EBC-46 in BALB/c *Foxn1*^{nu} mice led to a loss of tumour vasculature integrity and red blood cell extravasation within 2- 4 hours. Notably, these effects were not seen in normal skin of BALB/c *Foxn1*^{nu} mice treated with PG or EBC-46.

Tumour blood vessel disruption was also seen following topical treatment with PEP005 (now known as Picato®), a related diterpene ester [90]. In addition, there was an associated infiltration of neutrophils in BALB/c *Foxn1*^{nu} mice with skin tumours, indicating an acute T-cell independent inflammatory response. In a melanoma mouse model, a reactive macrophage and neutrophil infiltration was seen 4 hr following intratumoural injection of 30 µg EBC-46. A moderate increase of neutrophils was noted at 8 hr and they continued to be present 48 hr following treatment (D'Souza, 2014). Interestingly, tumour relapse in approximately 40% of sites occurred when peripheral neutrophils were depleted with the neutrophil-neutralizing monoclonal antibody anti-Ly6G.

To investigate whether a similar response occurred following treatment of SCC-15 xenografts in both BALB/c *Foxn1*^{nu} and NOD/SCID mice, and whether a recruitment of macrophages and/or neutrophils also occurred, immunohistochemistry was performed for general morphology and salient markers following EBC-46 treatment.

4.2 Results

4.2.1 Immunohistochemistry of BALB/c *Foxn1*^{nu} SCC-15 xenografts

Twenty BALB/c *Foxn1*^{nu} mice were inoculated with 2 x 10^5 SCC-15 cells and tumours grown to approximately 100 mm^3 prior to intratumoural treatment with 30 µg EBC-46 or 50 µL 40% PG. A control mouse was left untreated to represent the 0 hr time point. Mice were culled 2, 4, 8 and 24 hr following treatment, tumours excised and placed in PBS or formalin for 24 hr at 4 °C. Specimens in PBS were processed into single-cell suspensions

with 100 μl collagenase A for 30 min at 37 °C, spun at 13,200 rpm for 5 min at room temperature and the supernatant collected for haemoglobin concentration estimation (Section 4.2.3). Establishment of an *ex vivo* culture was attempted however; the plating efficiency of the controls was too low and variable to obtain reproducible results.

Tumour specimens were then transferred from formalin into 70% ethanol and transported to the QIMRB Histology Department for paraffin processing and immunohistochemical analysis. Staining for haematoxylin and eosin (H & E), endothelial cells (CD31), macrophages (F4/80) and neutrophils (LyG6, MPO) was performed.

4.2.1.1 General histology

Two hours following intratumoural injection of 30 μg EBC-46, a change of vasculature integrity and a small influx of red blood cells were demonstrated (Figure 4.1). These features continued to be amplified as time progressed, with almost complete destruction of general tissue morphology and significant extravasation of red blood cells by 24 hr post treatment. No significant change to tissue morphology, tumour vasculature or red blood cell presence was noted in tumour tissue treated with 40% PG alone.

4.2.1.2 Endothelial cells

Immunohistochemical staining for endothelial cells with CD31 (platelet endothelial cell adhesion molecule, Figure 4.2) showed dilatation of the vessels (66.0 ± 32.9 μm) after 2 hours following EBC-46 administration, compared to 40% PG (32.0 ± 38.9 μm). Disruption of the endothelial cells' integrity was also apparent, with incomplete vascular walls and complete destruction by 24 hours. No vasculature damage was seen in the specimens treated with 40% PG.

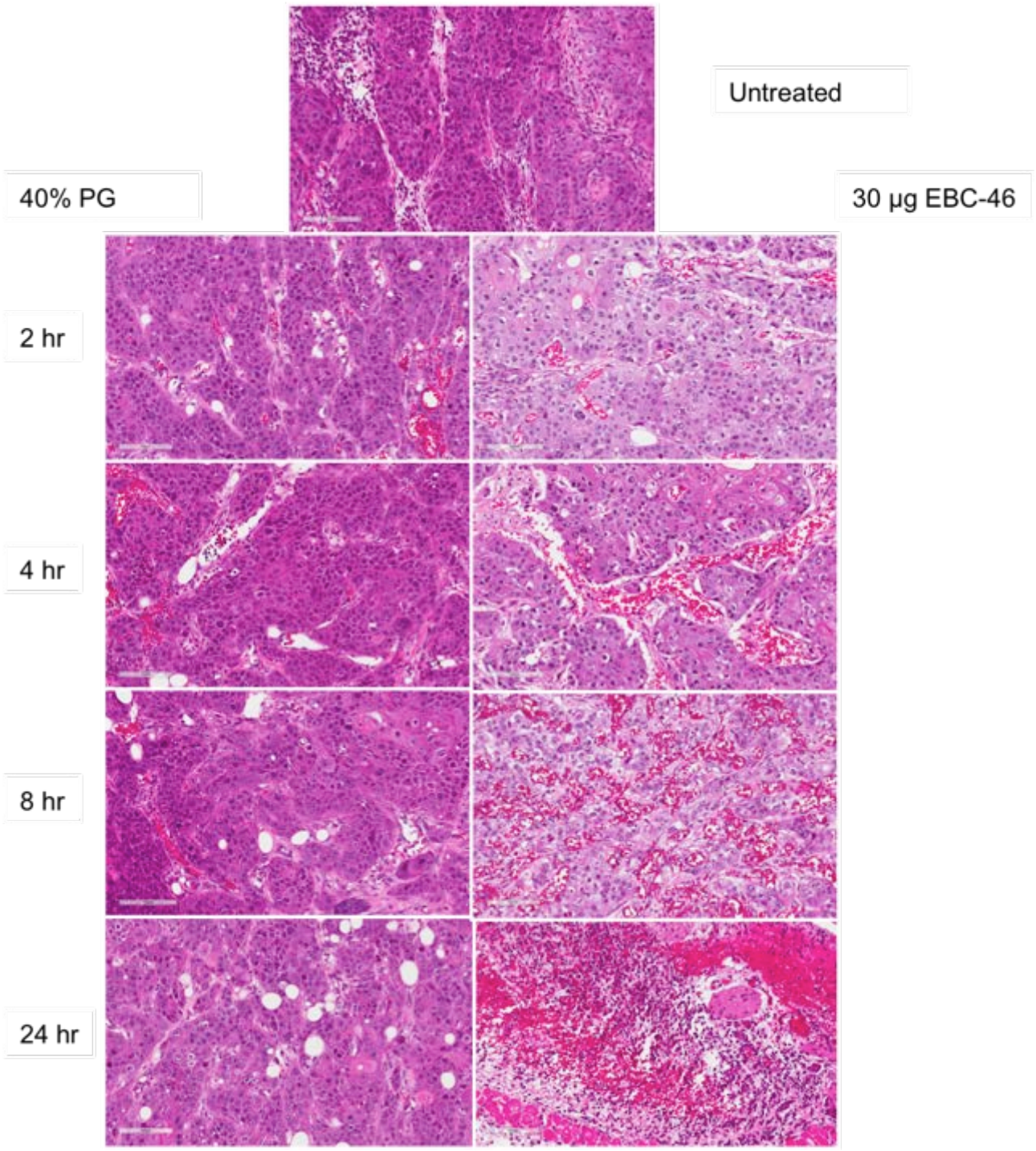

Figure 4.1 Photomicrographs of SCC-15 tumour sections in BALB/c *Foxn1*^{nu} mice stained for haematoxylin and eosin following single intratumoural injection of 30 µg EBC-46 per tumour or 50 µL 40% PG vehicle control from 0 hr to 24 hr. Destruction of general tissue morphology and significant extravasation of red blood cells was seen by 24 hr post treatment with EBC-46.

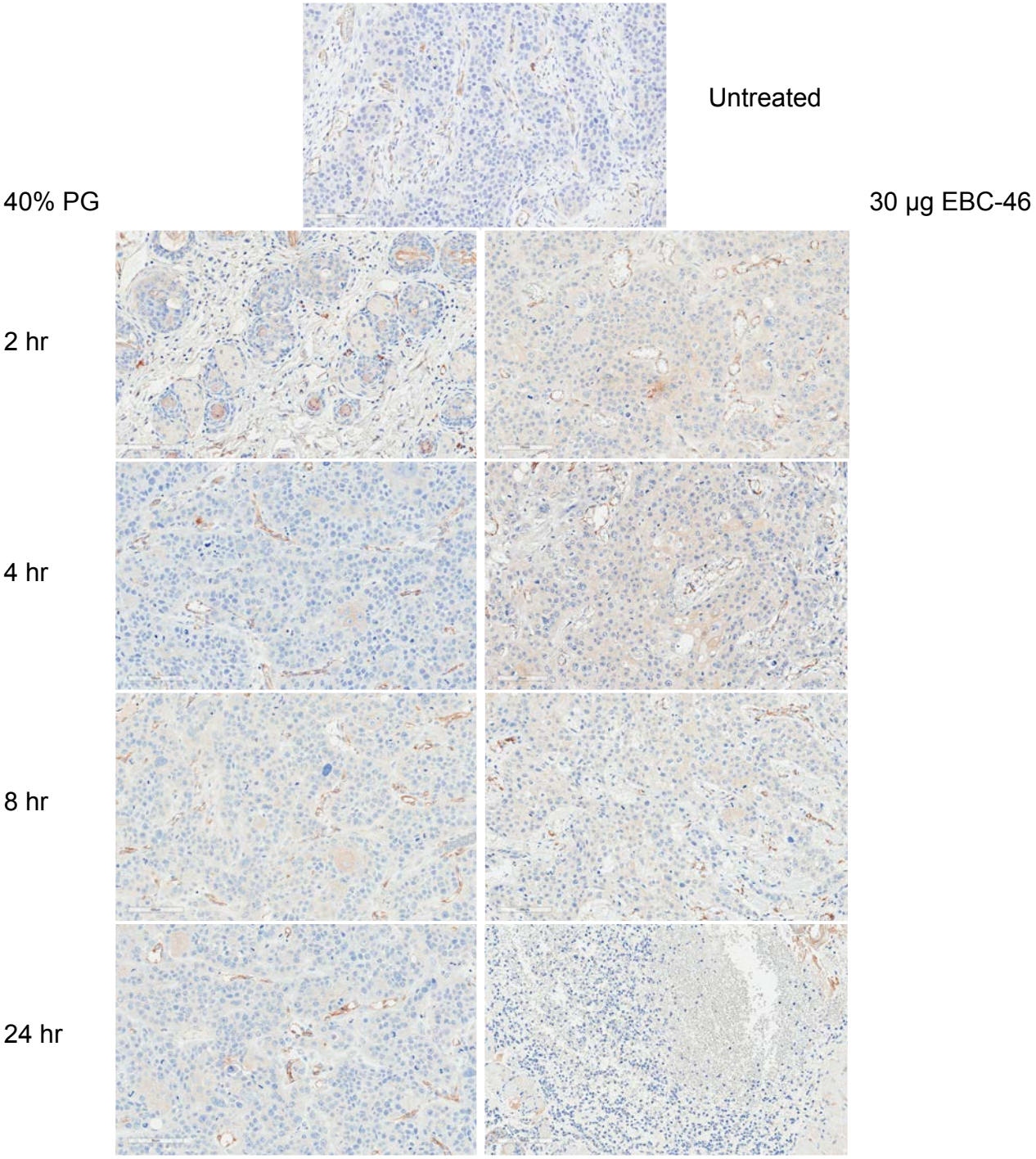

Figure 4.2 Photomicrographs of SCC-15 tumour sections in BALB/c *Foxn1*^{nu} mice stained for endothelial cells (CD31) following single intratumoural injection of 30 µg EBC-46 per tumour or 50 µL 40% PG vehicle control from 0 hr to 24 hr. Following EBC-46 administration, dilatation of blood vessels, disruption of the endothelial cells' integrity was apparent from 2 hours. Scale bar = 90 µm.

4.2.1.3 Macrophages

Staining for murine macrophage-expressed glycoprotein F4/80, was consistent amongst tumours treated with 40% PG and comparable to that of the untreated tumour (Figure 4.3). Tumours that were treated with 30 µg EBC-46 demonstrated a peak in the number of macrophages 4 hr following intratumoural injection with a resolution by 8 hr. No appreciable change in macrophage presence was seen in specimens injected with 40% PG.

4.2.1.4 Neutrophils

Immunohistochemical staining was performed for LyG6, a myeloid differentiation antigen present on peripheral neutrophils in addition to myeloperoxidase (MPO), a lysosomal protein expressed in neutrophil granules. Both stains identified the presence of neutrophils in the tumour; however, MPO could also potentially identify sites of recent neutrophil degranulation.

A substantial infiltration of neutrophils into tumour tissue was apparent 24 hr after intratumoural treatment with EBC-46 (Figure 4.4). Evidence of this infiltration was supported with a similar response seen in MPO staining at 24 hr (Figure 4.5).
No neutrophil infiltrations or areas of degranulation were demonstrated in tumour tissue treated with 40% PG.

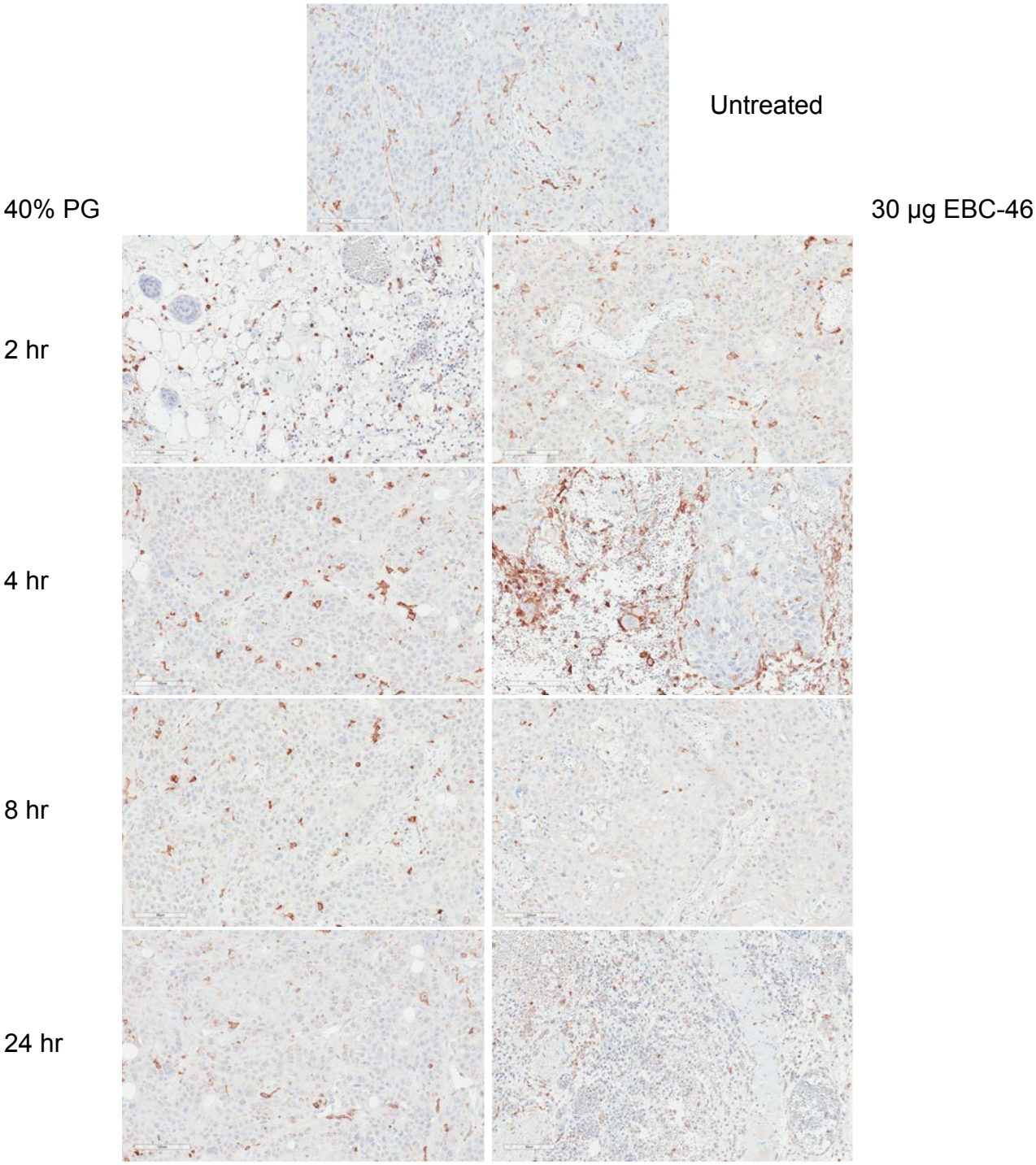

Figure 4.3 Photomicrographs of SCC-15 tumour sections in BALB/c *Foxn1*^{nu} mice stained for macrophages (F4/80) following single intratumoural injection of 30 µg EBC-46 per tumour or 50 µL 40% PG vehicle control from 0 hr to 24 hr. An infiltration of macrophages were seen 4 hours following EBC-46 treatment. Scale bar = 90 µm.

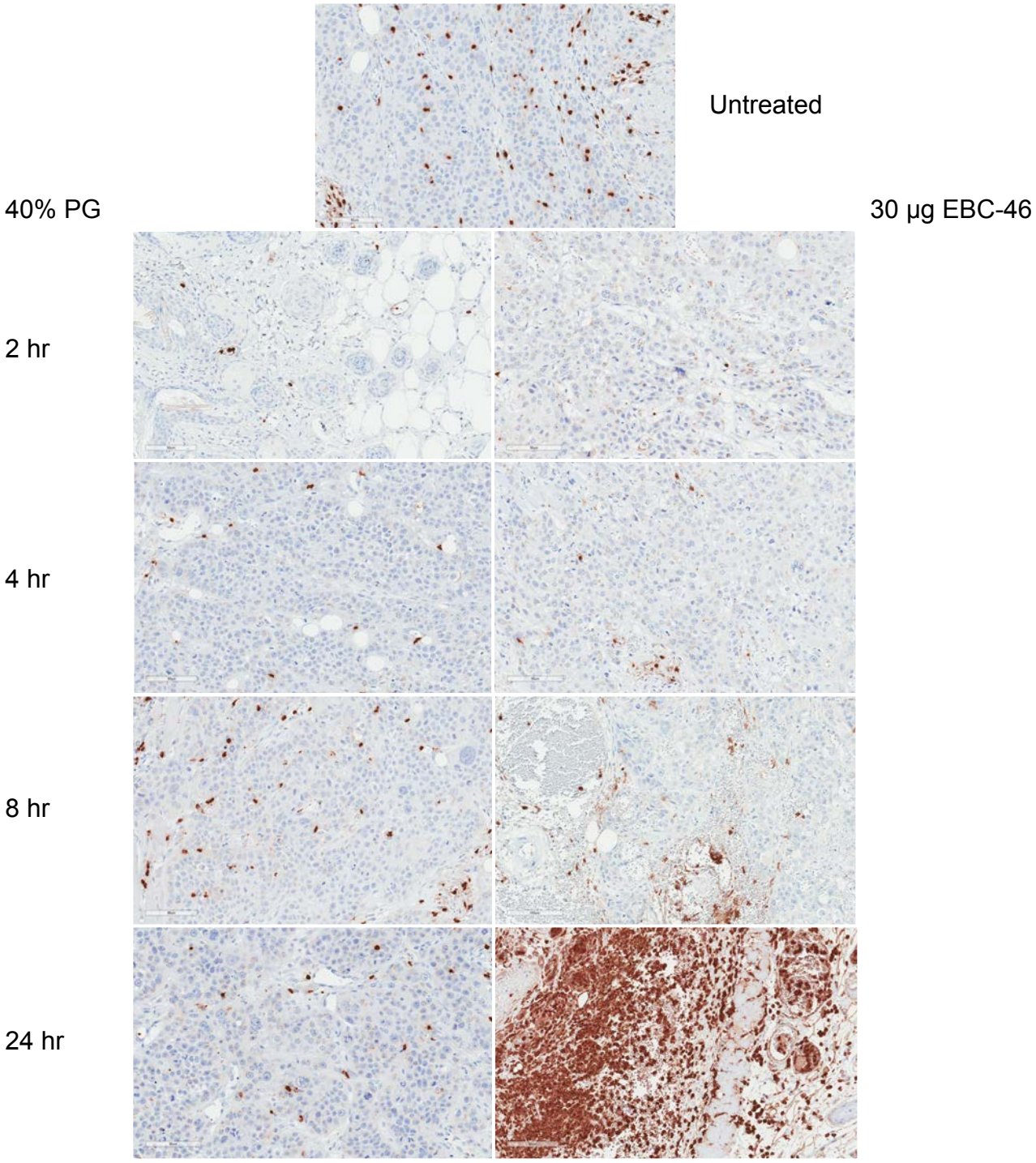

Figure 4.4 Photomicrographs of SCC-15 tumour sections in BALB/c *Foxn1*^{nu} mice stained for neutrophils (LyG6) following single intratumoural injection of 30 µg EBC-46 per tumour or 50 µL 40% PG vehicle control from 0 hr to 24 hr. A large infiltration of neutrophils occurred 24 hours after EBC-46 treatment. Scale bar = 90 µm.

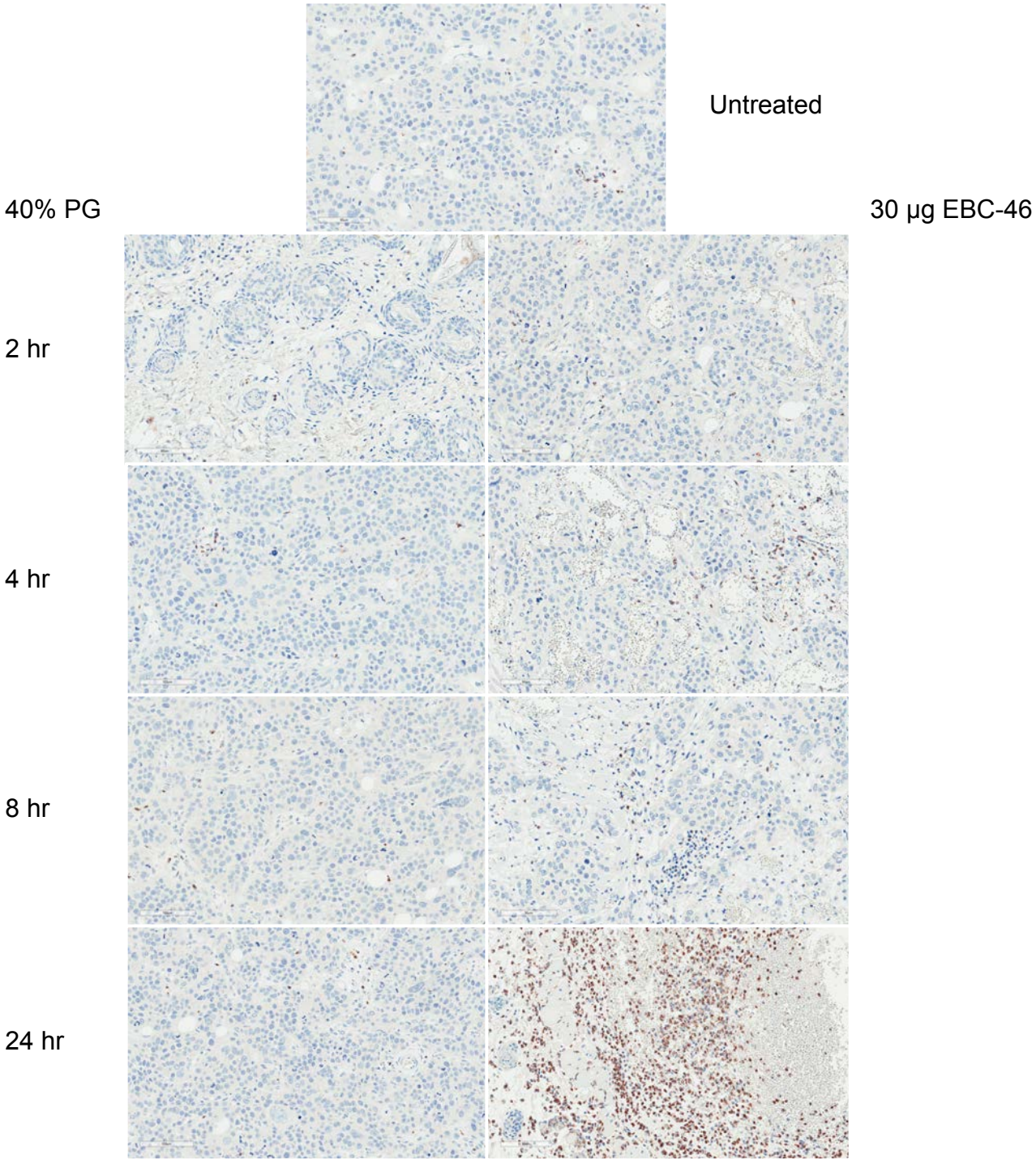

Figure 4.5 Photomicrographs of SCC-15 tumour sections in BALB/c *Foxn1*^{nu} mice stained for neutrophils (MPO) following single intratumoural injection of 30 µg EBC-46 per tumour or 50 µL 40% PG vehicle control from 0 hr to 24 hr. An infiltration of neutrophils 24 hours after EBC-46 treatment was seen. Scale bar = 90 µm.

4.2.2 Immunohistochemistry of NOD/SCID SCC-15 xenografts

To identify any histological differences following EBC-46 treatment between BALB/c *Foxn1*^{nu} and NOD/SCID mice with xenografts, the experiment described in Section 4.2.1 was replicated with NOD/SCID mice. However, given that the administration of 40% PG alone did not yield any appreciable histological change in the BALB/c *Foxn1*^{nu} specimens, this control arm was omitted from the current experiment for ethical reasons.

4.2.1.1 General histology

Similar to the pattern seen in BALB/c *Foxn1*^{nu} mice, there was apparent loss of vasculature integrity and significant extravasation of red blood cells into the tumour progressively from 2 hr onwards (Figure 4.6). Significant disruption to general tissue morphology was present at 24 hr.

4.2.1.2 Endothelial cells

Staining for CD31 demonstrated that tumour vasculature diameter was on average 13 ± 4.5 μm in unstained tumour tissue (Figure 4.7). Following EBC-46 treatment, the average diameter progressively increased to 62 ± 27.7 μm (2 hr), 68 ± 30.3 μm (4 hr), and 160 ± 191.7 μm (8 hr) with an associated loss of endothelial cell integrity. Twenty-four hours after treatment, tumour tissue integrity was so disrupted that blood vessel diameters could not be measured.

4.2.1.3 Macrophages

A moderate infiltration of macrophages into the tumour tissue presented 4 hr following treatment with EBC-46 (Figure 4.8). Evidence of this infiltration was still present at 8 hr but demonstrated resolution by 24 hr.

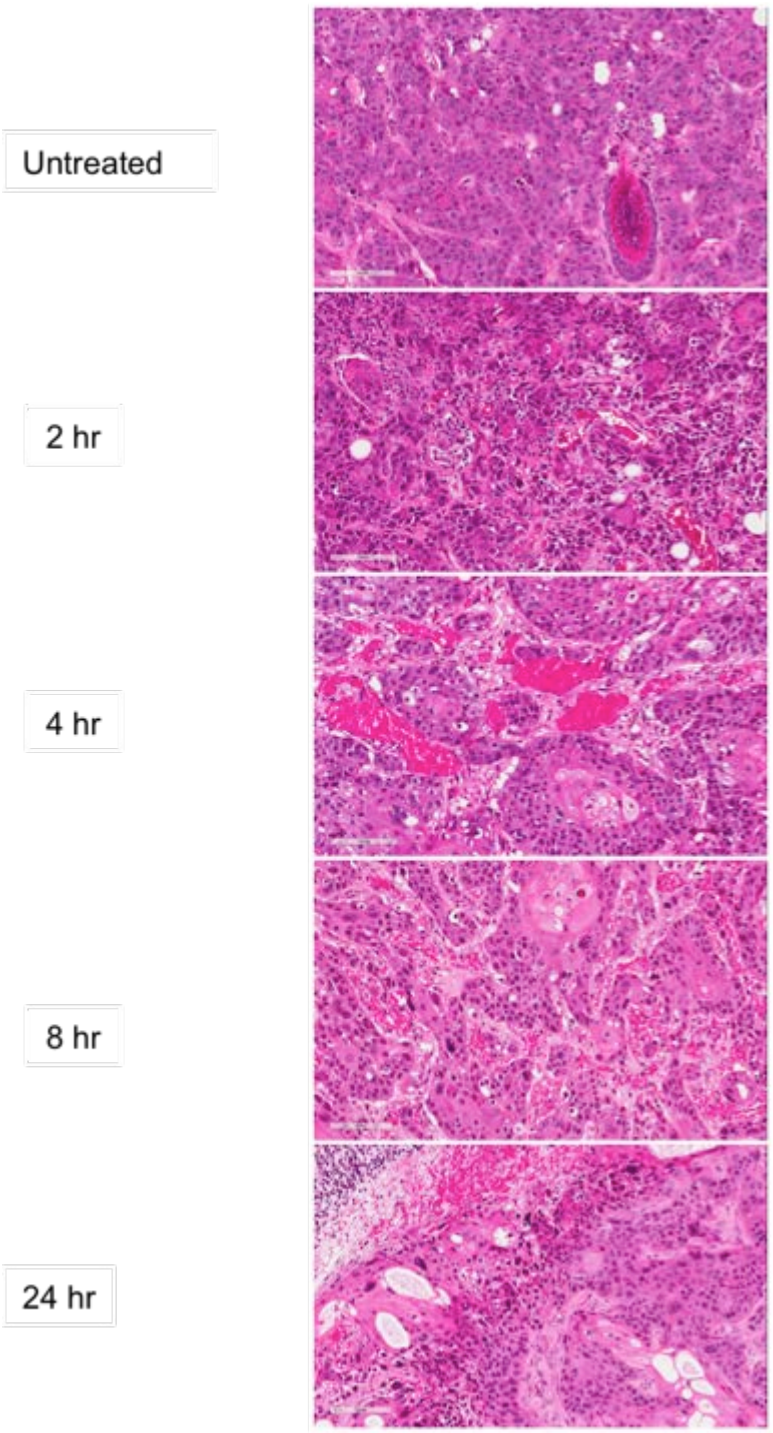

Figure 4.6 Photomicrographs of SCC-15 tumour sections in NOD/SCID mice stained for haematoxylin and eosin following single intratumoural injection of 30 µg EBC-46 per tumour or 50 µL 40% PG vehicle control from 0 hr to 24 hr. Vasculature disruption and red blood cell infiltration was noted from 2 hours post treatment. Scale bar = 90 µm.

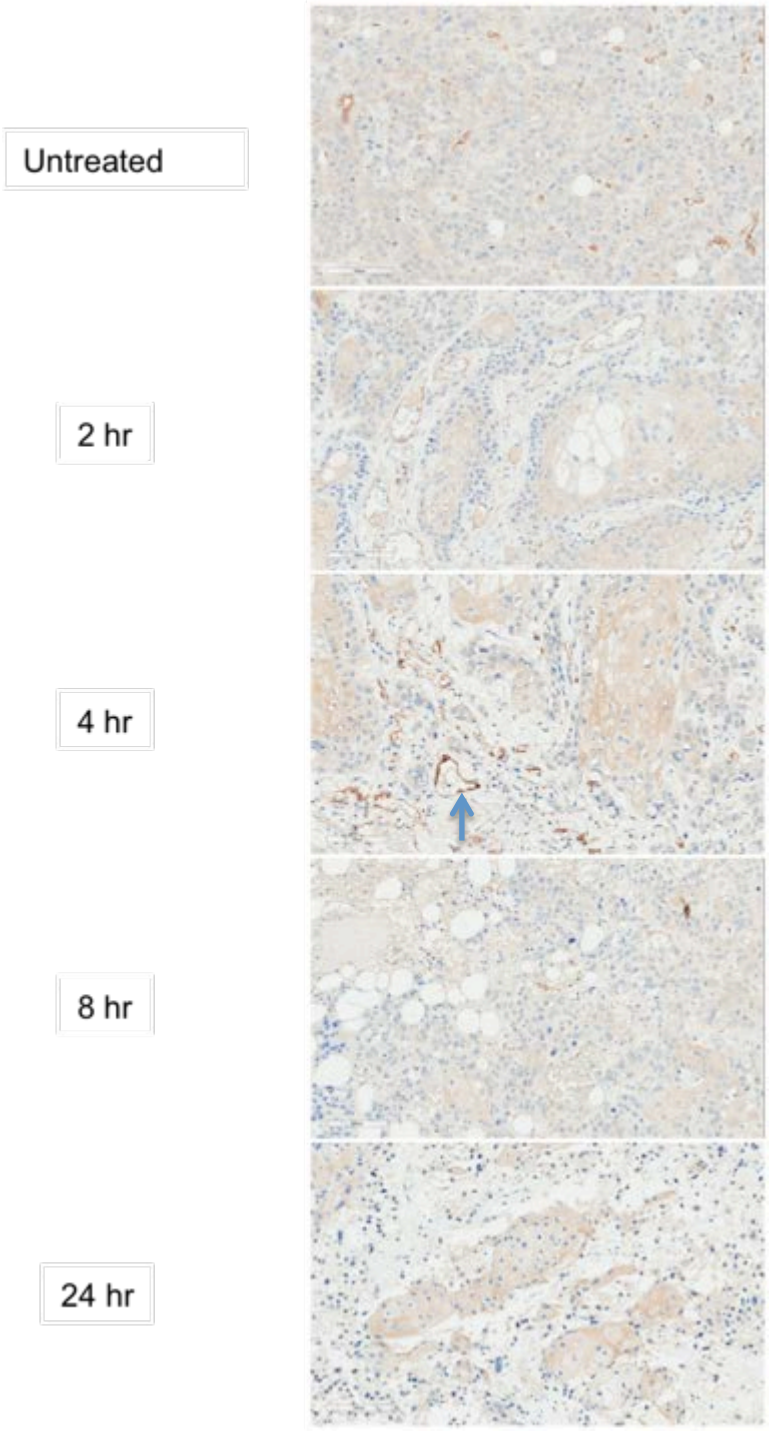

Figure 4.7 Photomicrographs of SCC-15 tumour sections in NOD/SCID mice stained for endothelial cells (CD31) following single intratumoural injection of 30 µg EBC-46 per tumour or 50 µL 40% PG vehicle control from 0 hr to 24 hr. Progressive blood vessel dilatation is demonstrated (arrow). Scale bar = 90 µm.

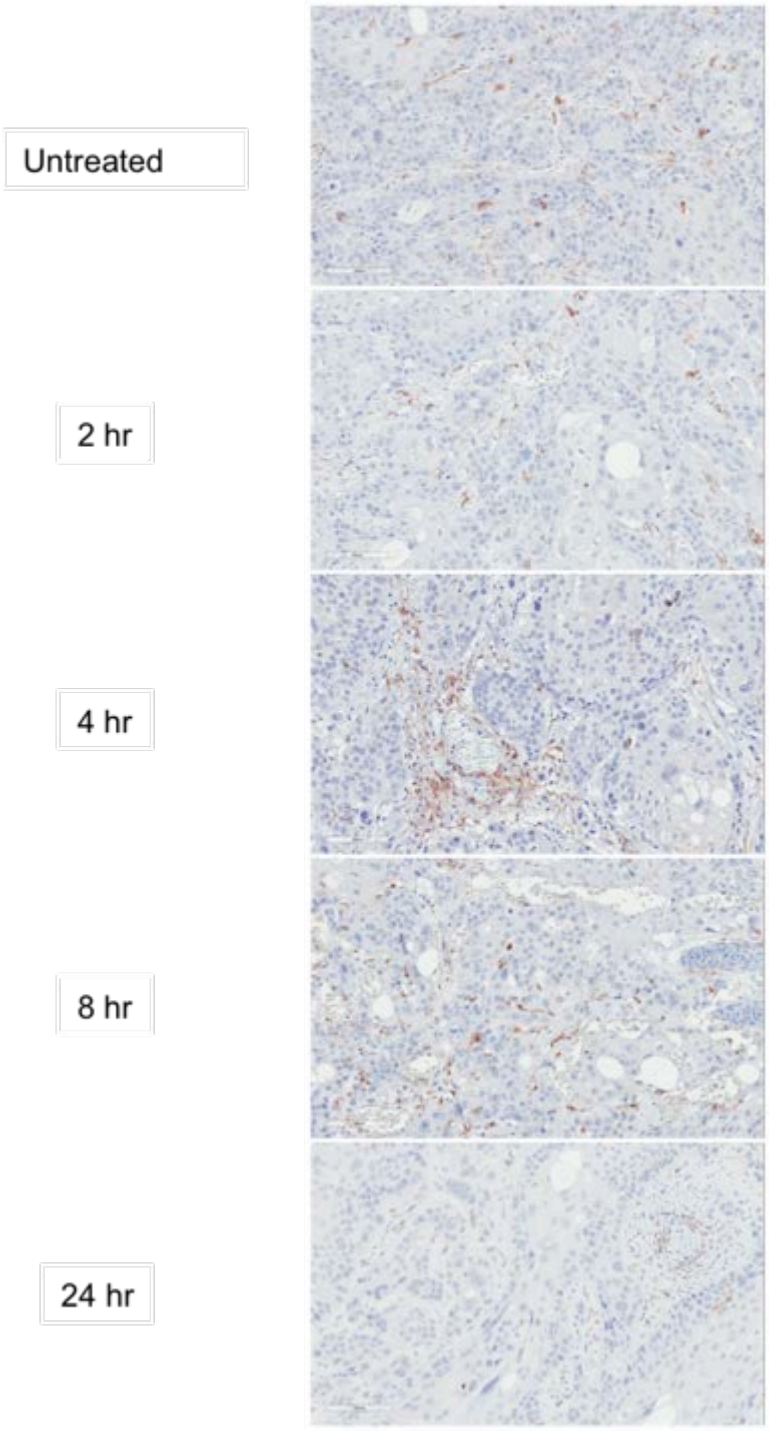

Figure 4.8 Photomicrographs of SCC-15 tumour sections in NOD/SCID mice stained for macrophages (F4/80) following single intratumoural injection of 30 µg EBC-46 per tumour or 50 µL 40% PG vehicle control from 0 hr to 24 hr. A macrophage infiltration was seen 4 hours following treatment. Scale bar = 90 µm.

4.2.1.4 Neutrophils

Although present in BALB/c *Foxn1*^{nu} mice, no infiltration of neutrophils or evidence of increased sites of neutrophil degranulation were identified following treatment with EBC-46 (Figures 4.9 and 4.10). LyG6 and MPO staining across all time points were similar to that seen in the untreated tumour tissue.

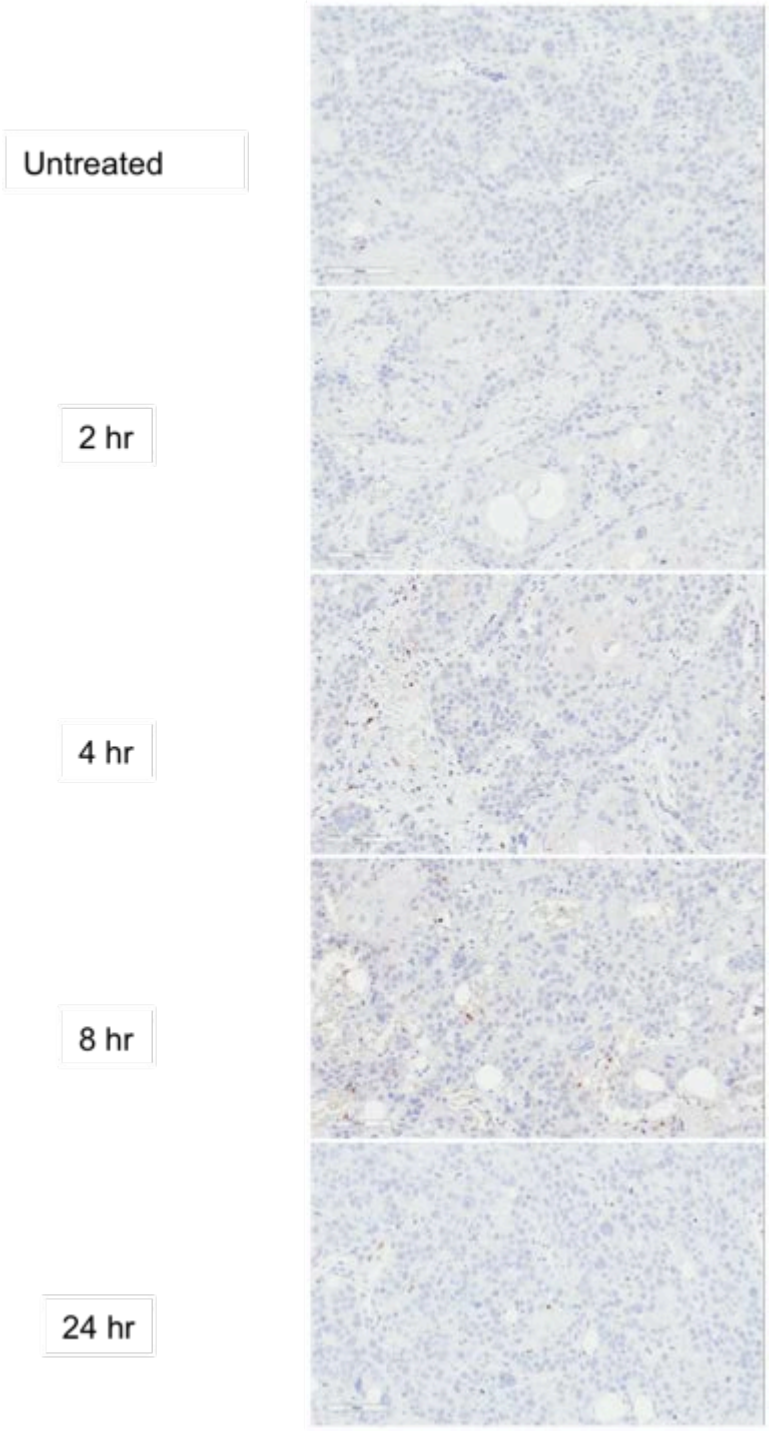

Figure 4.9 Photomicrographs of SCC-15 tumour sections in NOD/SCID mice stained for neutrophils (LyG6) following single intratumoural injection of 30 µg EBC-46 per tumour or 50 µL 40% PG vehicle control from 0 hr to 24 hr. No neutrophil infiltration was demonstrated. Scale bar = 90 µm.

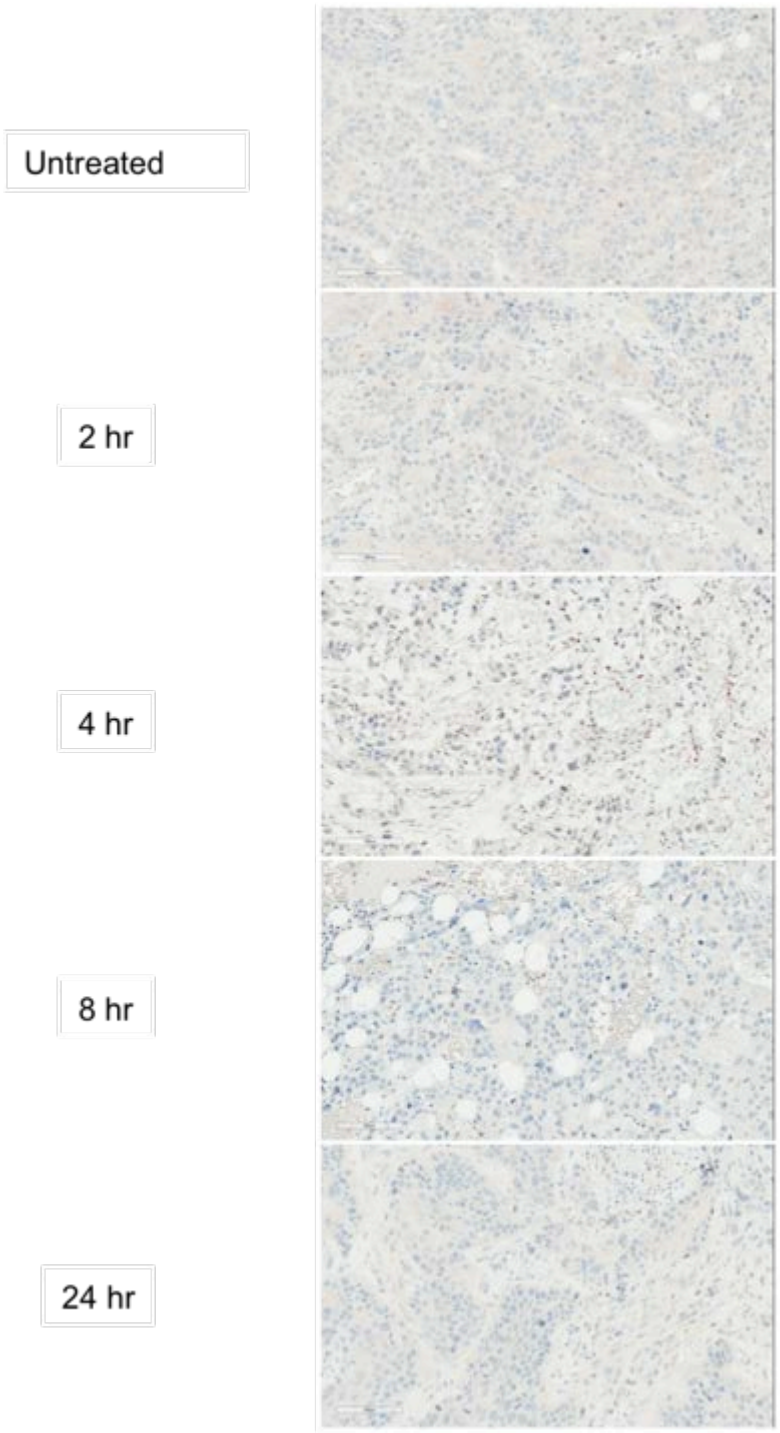

Figure 4.10 Photomicrographs of SCC-15 tumour in NOD/SCID mice sections stained for myeloperoxidase (MPO) following single intratumoural injection of 30 µg EBC-46 per tumour or 50 µL 40% PG vehicle control from 0 hr to 24 hr. No neutrophil infiltration was demonstrated. Scale bar = 90 µm.

4.2.3 Effect of EBC-46 on normal skin of NOD/SCID mice

No significant histological change was noted following the subcutaneous injection of EBC-46 into normal skin from BALB/c *Foxn1*^{nu} mice [10]. To confirm this was also the case with NOD/SCID mice, Section 4.2.1 was replicated again using normal skin from NOD/SCID mice.

As expected, the injection of 40% PG or EBC-46 had minimal effect on the normal NOD/SCID skin morphology within the 24 hours measured. Average counts of endothelial cells, macrophages, and neutrophils did not vary significantly.

4.2.4 Haemoglobin concentration of lysed SCC-15 xenografts

Histology revealed the presence of red cells following treatment with EBC-46. We therefore wished to quantitate the presence of red cells following treatment. Tumours were treated with EBC-46, and then harvested.

Tumours of approximately similar volumes were processed into single cell suspensions, lysed with 1% SDS and the supernatant collected. To estimate the concentration of haemoglobin in each sample, 80 μl duplicate samples were placed into a 96-well plate along with solutions of known haemoglobin concentrations. Samples were read on an ELISA plate reader at 540 nm and haemoglobin concentrations estimated using the constructed standard curve (Figures 4.11 and 4.12).

Tumours excised from the NOD/SCID mice demonstrated a near linear relationship between haemoglobin concentration and time from treatment, with a peak concentration of 1.7 mg at 24 hr. In contrast, the haemoglobin concentration in tumours from BALB/c *Foxn1*^{nu} mice appeared to peak at 8 hours (0.7 mg/ml) post treatment and then decreased to 0.2 mg/ml at 24 hr.

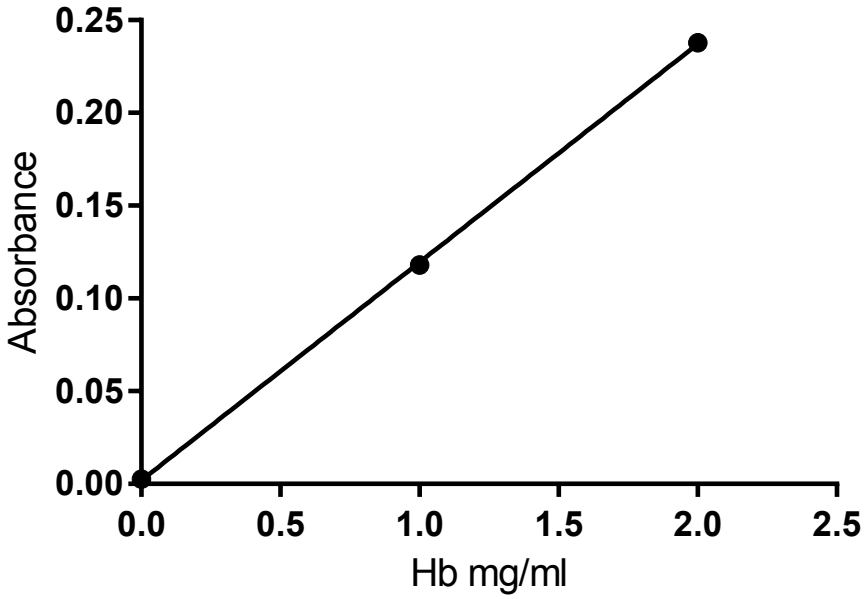

Figure 4.11 Absorbance of samples with a known haemoglobin concentration.

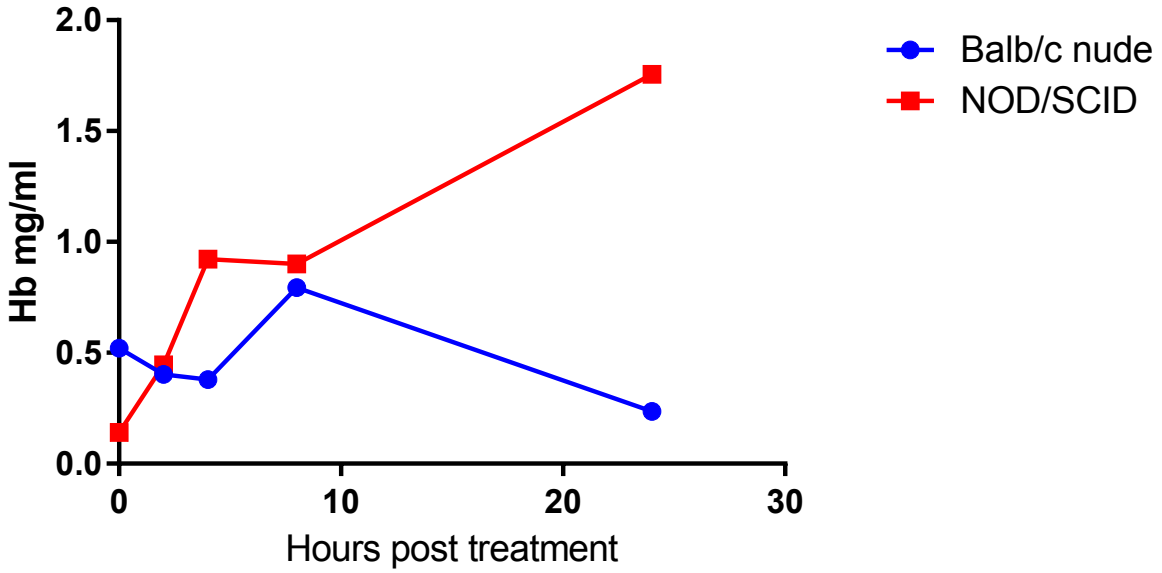

Figure 4.12 Estimated haemoglobin concentrations of supernatant from lysed SCC-15 tumours in BALB/c *Foxn1*^{nu} mice.

4.2.5 Differences between tumour and surrounding skin temperatures following EBC-46 treatment.

Following the findings that endothelial cells lost integrity following EBC-46 and red blood cells extravasated into the tumour tissue, it was hypothesised that an increase in tumour temperature, compared with the surrounding normal skin, may occur as a result of the inflammation.

Using a handheld infrared camera (FLIR Systems, Inc, USA), skin temperatures of tumours and their surrounding normal skin were recorded at the different time points in Section 4.2.1, prior to euthanasia of the BALB/c *Foxn1*^{nu} mice (Figure 4.13). Average surrounding normal skin temperatures were calculated from four peripheral regions and were compared to that of each tumour and the difference calculated (Table 4.1).

Tumour temperatures were 1.7 - 1.8 ºC less than their surrounding skin (Table 4.1). Following EBC-46 treatment, tumour temperature increased at 4 hr and 24 hr. This is in contrast to a rapid decrease in tumour temperature of approximately 5 ºC seen in a dog mast cell tumor (Stewart Lowdon, personal communication).

Table 4.1 Mean skin surface temperature differences (normal skin ºC – tumour ºC) between SCC-15 tumours and surrounding normal skin in BALB/c *Foxn1*^{nu} mice.

Time post treatment (hr)	Temperature difference (normal skin ºC – tumour ºC)	
	40% PG	30 μg EBC-46
0	1.24 ± 0.46	
2	1.7 ± 0.12	1.64 ± 0.68
4	1.73 ± 0.62	0.29 ± 0.30
8	2.07 ± 0.46	1.46 ± 0.39
24	1.76 ± 0.44	0.8 ± 0.33

A

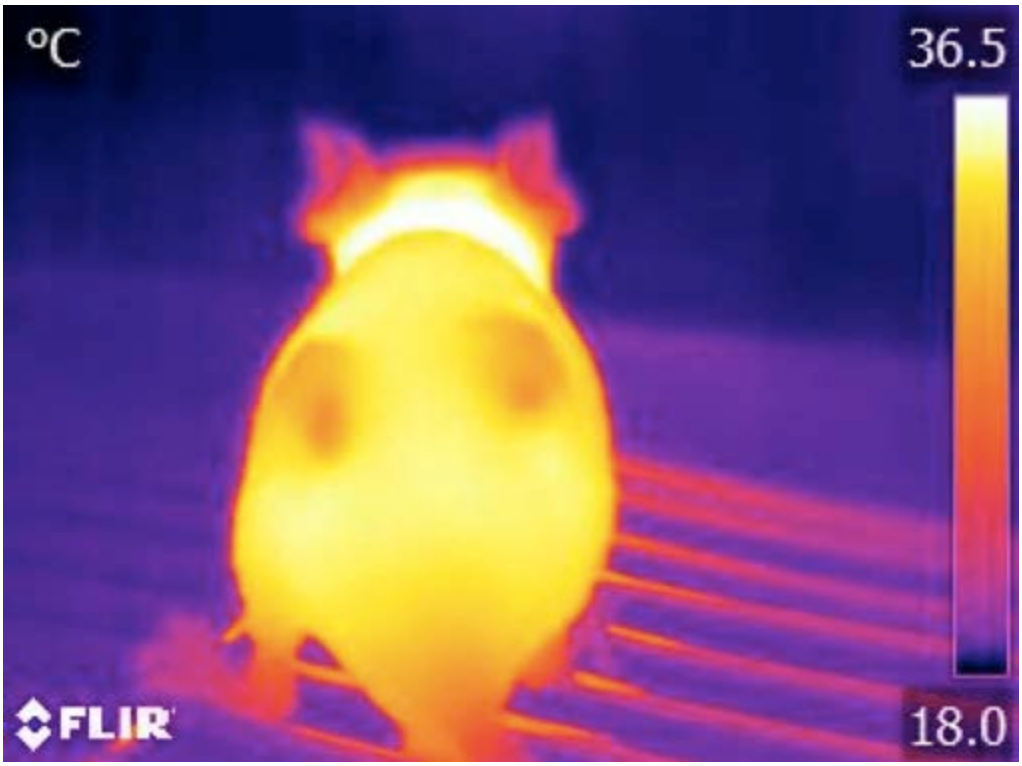

B

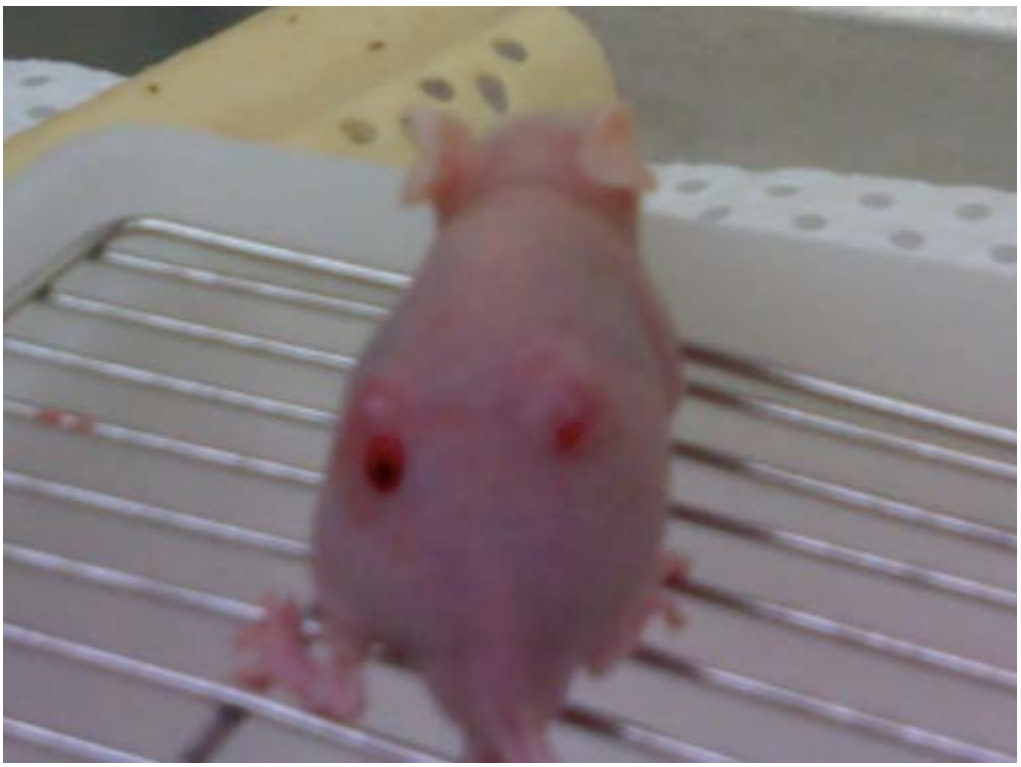

Figure 4.13 Infrared (A) and plain imaging (B) of BALB/c *Foxn1*^{nu} mice with SCC-15 xenografts 2 hours following EBC-46 treatment

4.3 Discussion

The aim of this chapter was to identify histological changes that occurred in SCC-15 tumour tissue following treatment with EBC-46 in both BALB/c *Foxn1*^{nu} and NOD/SCID mouse models. Within two hours following intratumoural treatment with EBC-46, SCC-15 xenografts grown on BALB/c *Foxn1*^{nu} mice and NOD/SCID mice demonstrated blood vessel dilatation, decreased structural integrity of tumour vasculature and subsequent extravasation of red blood cells into the surrounding tissue. The progressive increase in red blood cell extravasation with time was further supported by the increasing concentration of haemoglobin in the supernatant of tumour-derived single cell suspensions from NOD/SCID mice. Despite histological evidence of considerable red blood cell extravasation 24 hr following EBC-46 treatment in BALB/c *Foxn1*^{nu} mice, the corresponding haemoglobin concentration did not correlate. This may have been due to sampling error during the harvesting of tumours for single-cell suspension preparation and may not reflect the actual concentration of haemoglobin from lysed extravasated red blood cells in the tumour tissue.

These histological results further confirmed the findings of Boyle *et al* (2014) where intratumoural treatment of hypopharyngeal SCC (FaDu) xenografts with EBC-46 in BALB/c *Foxn1*^{nu} mice led to a loss of tumour vasculature integrity and red blood cell extravasation within 2 - 4 hr. Furthermore, blood vessel dilatation was noted by the researchers 30 min following treatment. In the same study, cultured monolayers of HUVEC (human umbilical vascular endothelial) cells exposed to 600 µg/ml EBC-46 for 30 min, with or without the addition of BIS-1, showed PKC-dependent increased permeability ($p = 0.0013$). Although there was a reduction in permeability, it was not totally blocked by BIS-1 potentially indicating alternative targets or mechanisms of EBC-46 action.

The disruption of tumour vasculature by EBC-46 may result in an overall decrease in the difference between tumour skin surface temperature and surrounding normal skin as evident by the use of infrared imaging in this study. This pilot temperature data raises the possibility of a biphasic response: temperature increase due to inflammation accompanied by influx of macrophages seen at 4 hr, which subsides to initial tumor temperature by 8 hr and then by 24 hr reverts close to normal skin temperature due to ablation of the tumour mass. However, this technique was performed on a small sample size and would need to be repeated on a larger scale to increase statistical power.

Infiltrations of macrophages and neutrophils were noted in the tumour tissue 4 hr and 24 hr following EBC-46 treatment, respectively, providing evidence of an acute T-cell independent inflammatory response. A comparable reactive neutrophil infiltration was also seen following intratumoural injection of EBC-46 in a melanoma mouse model (D'Souza, 2014) and in BALB/c *Foxn1*^{nu} mice with skin tumours, topically treated with PEP005 (now known at ingenol mebutate or Picato® [90].

The most interesting finding of this chapter was the absence of a comparative infiltration of neutrophils in the NOD/SCID group at 24 hr post treatment. This appears to be first objective evidence for the NOD/SCID strain of having defective homing of pro-inflammatory cells, alluded to in several descriptions of the strain [100 101]. The lack of neutrophil recruitment in the NOD/SCID mice could potentially contribute to the reduced efficacy of EBC-46 seen in this mouse model (Section 3.2.2). With a reduced number of neutrophils present in the tumour tissue following injection with EBC-46, the concentration of NETs and neutrophil-produced cytokines and chemokines in the tumour microenvironment may be substantially lower, thus leading to reduced tumour cell killing.

CHAPTER FIVE: Mechanism of action.

5.1 Introduction

In recent studies, the cytotoxic effects of EBC-46 *in vitro* were found to be inferior to that of the structurally related compound 12-myristate 13-acetate (PMA) in several cell lines particularly sensitive to PKC activators. However, EBC-46 was found to have better efficacy against tumours *in vivo* using the head and neck cancer cell lines FaDu (hypopharyngeal) and CAL 27 (tongue SCC) [10 91].

In conjunction with the finding of neutrophils recruited to the region following EBC-46 treatment (D'Souza, 2014), it was hypothesised that the host's immune response was responsible for the discrepancy in efficacy seen between *in vitro* and *in vivo* experiments. This also aligned with Challacombe and colleagues' [90] finding that the mechanism by which Picato®, a related diterpene ester, worked involved initial tumour ablation followed by a neutrophil-dependent antibody-dependent cell cytotoxicity-mediated eradication of residual disease. In neutrophil-depleted BALB/c *Foxn1*^{nu} mice with LK2 (UV-induced mouse squamous cell carcinoma line) xenografts, a relapse rate to 83% was observed in comparison to only 8.3% in mice with normal neutrophil counts ($p = 0.005$).

Accordingly, this chapter focused on further investigating the mechanism by which EBC-46 caused tumour cell death both *in vitro* and *in vivo*.

5.2 Results

5.2.1 Cytotoxicity of EBC-46 *in vitro*

To determine the effect of EBC-46 on SCC-15 cells *in vitro*, several cytotoxic assays were performed. A 96-well flat-bottomed plate was seeded with 5×10^3 SCC-15 cells per well and left overnight to allow cell adhesion. The following day, media was removed and replaced with media containing 0 – 300 μg/ml EBC-46 diluted from EtOH, a dose range achieveable by intratumoural injection *in vivo*. Cells were exposed to EBC-46 for 0 – 60 min, after which media was replaced to cease the cytotoxic effects of EBC-46. Cells were then incubated for 6 – 7 days in 5% CO_2 at 37 °C (Forma Scientific Water-Jacketed

Incubator). When control wells were approximately 90% confluent, media was removed and a sulforhodamine B (SRB) protein stain was performed as described in Section 2.2.2.1. Assays were performed in triplicate and the average concentration of cell protein was expressed as a percentage of the control wells to estimate cell survival (Figure 5.1). At 300 μg/ml, EBC-46 exposure for 30 min resulted in no detectable tumour cells present 6 days later. Cell survival was impacted even at 50 μg/ml, however, a fairly minimal time response was seen. At all doses, exposure to EBC-46 for as little as 2 min inhibited subsequent cell growth. Importantly, the addition of 2 μl EtOH (0 μg/ml EBC-46) had no appreciable effect on the percentage of tumour cell survival.

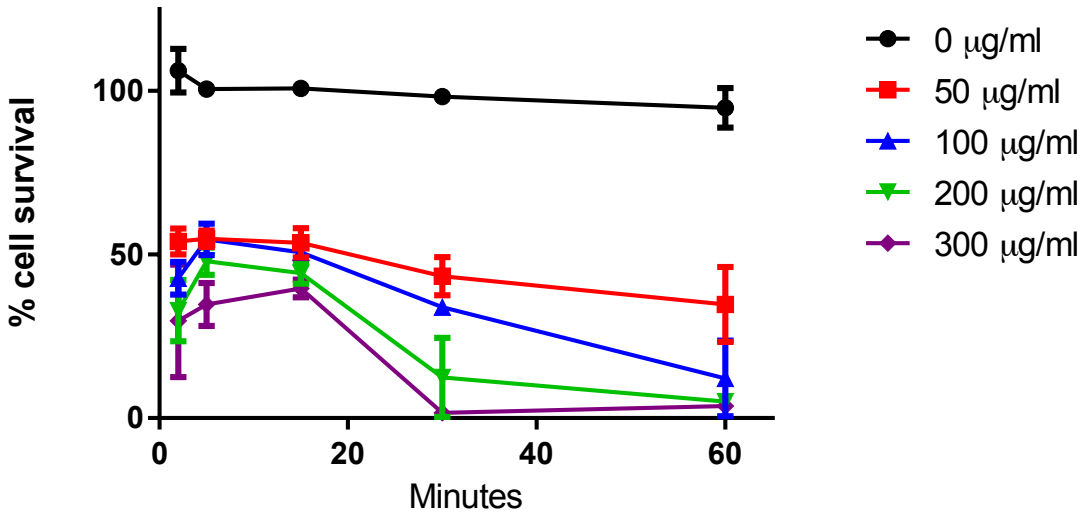

Figure 5.1 Growth inhibition of SCC-15 cells by high doses of EBC-46. Averages of six replicates are shown with ±SD.

5.2.2 Cytotoxicity of propylene glycol *in vitro*

Due to its hydrophobicity, EBC-46 requires an appropriate excipient to solubilise it for intratumoural treatment in an aqueous solution. As discussed in Chapter Three, 40% propylene glycol was found to be the most efficacious excipient. To ensure that propylene glycol itself did not have cytotoxic effects and contribute to EBC-46's action *in vitro*, a 96-well flat-bottomed plate was seeded with 5 x 10^3 SCC-15 cells and exposed to different concentrations of PG. Cells were exposed to PG for 0 – 60 min and then left to grow until

confluent. A SRB assay was performed as previously described and the average percentages of viable cells present are depicted in Figure 5.2.

The addition of 40% PG resulted in the death of nearly all tumour cells. This cytotoxicity was significantly reduced with reducing PG concentrations. PG concentrations less than 6.7% had a minimal effect on tumour cell survival after 60 min exposure.

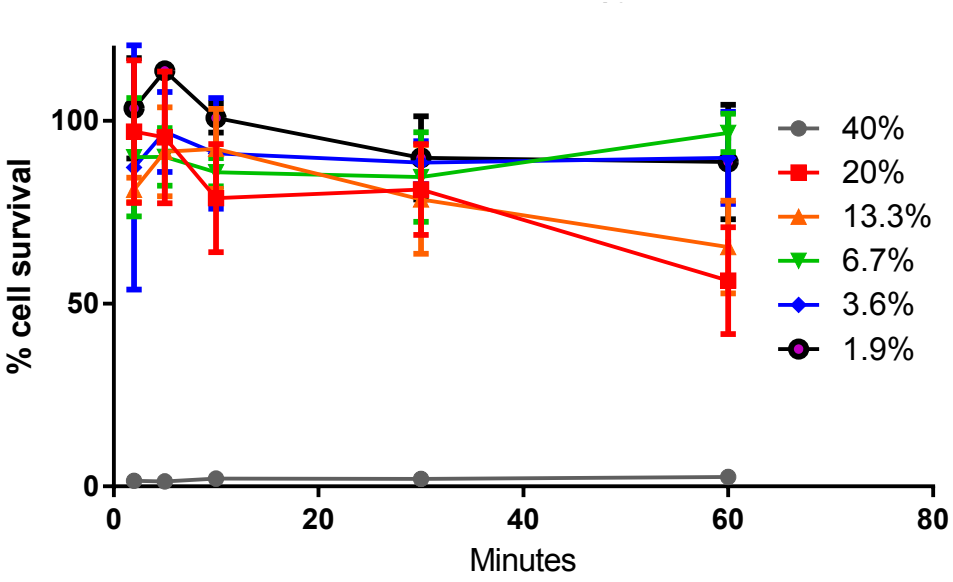

Figure 5.2 Dose response of acute cytotoxicity of propylene glycol in SCC-15 cells.

5.2.3 Propidium iodide uptake in SCC-15 cells following exposure to EBC-46

The main limitation of SRB assays is that cellular protein content in the well is bound by the dye from both viable and dead cells [102], thus many cell doublings are allowed after treatment before staining. The outcome reflects clonogenic survival, an important factor in antitumour therapy, but gives no information about the immediate effects of a compound. To investigate the short-term action of EBC-46 on SCC-15 cells *in vitro* by, a cytotoxic assay was performed with the inclusion of propidium iodide. Propidium iodide is positively charged and cannot enter a cell until the plasma membrane is compromised, upon which propidium iodide intercalates with DNA. It then becomes fluorogenic, and can be used to visually demonstrate cell death over time *in vitro* [103].

A 96-well flat-bottomed plate was seeded with 5 x 10^4 SCC-15 cells per well with RPMI media. The following day, fresh media with 5 μg/ml propidium iodide was added to the wells. Cells were then treated with EBC-46 (50 – 300 μg/ml) for 2 – 60 min alongside negative controls (2 μl of 100% EtOH) and positive controls (10 μl of 1% Triton X-100; rapidly lyses 100% of cells). Cells were imaged using an AMG EvosFl inverted fluorescence microscope (Figure 5.3). Propidium iodide-bound cells were then counted using OpenCFU software [93] and represented as a percentage of the positive controls (Figure 5.4A).

Concentrations of EBC-46 200 μg/ml or less resulted in minimal cell death, as judged by less than 40% of SCC-15 cell nuclei becoming fluorescent after 60 min exposure. Significantly more cell death was demonstrated at 300 μg/ml EBC-46. After 15 - 30 min exposure, approximately 40% of cells had died, however this rose to nearly 75% after 60 min. Nearly all of the fluorescent nuclei were intact, with no evidence for the formation of apoptotic bodies.

Boyle and colleagues [10] recently demonstrated that EBC-46 acted in a PKC-dependent manner. The respiratory burst induced by EBC-46 treatment of purified human polymorphonuclear cells was prevented with prior treatment with 1 μM bisindolylmaleimide-1 (BIS-1) a pan-PKC inhibitor. Furthermore, BALB/c *Foxn1*^{nu} mice xenografted with B16-F0 mouse melanoma cells and treated intratumourally with 10 μg EBC-46 in the presence of 5 μM BIS-1 showed decreased proportion of tumours ablated (17%) compared to no BIS-1 treatment (75%).

To ascertain whether a PKC-dependence would be seen in EBC-46 acute killing of SCC-15 cells, the same propidium iodide assay was performed with the exposure of 4 μM BIS-1 in the media for 5 min (Figure 5.4B). When treated with 300 μg/ml EBC-46 for 60 min, the percentage of cells with propidium iodide uptake appeared to be moderately reduced to approximately 50%. No appreciable difference in uptake was noted at other concentrations or time intervals. These results indicate that PKC may play a significant role in tumour cell killing; however, inhibition of PKC did not completely prevent all cell death caused by EBC-46 therefore suggesting that another mechanism may be involved.

Tumour cells are also known to produce reactive oxygen species (ROS) via membrane-associated NADPH oxidase. The constant presence of ROS is carcinogenic, with the promotion of cellular proliferation and angiogenesis in the tumour microenvironment [104].

ROS also act to attract T-cells, macrophages, and neutrophils to the region. However, excessive ROS are cell damaging and can result in cell death.

Phorbol esters are known to potently increase NADPH oxidase activity in neutrophils and B-lymphocytes [105]. Given the partial inhibition of EBC-46's cytotoxicity with BIS-1 pre-treatment, it was hypothesised that NADPH oxidase activation may also be a pathway through which EBC-46 acts. Therefore, SCC-15 cells were pre-treated for 60 min with 10 μM diphenyleneiodonium chloride (DPI, Invitrogen), an irreversible NADPH oxidase inhibitor, prior to treatment with EBC-46 (Figure 5.4C). Interestingly, the pre-treatment of SCC-15 cells with DPI did not make any appreciable difference to the percentage of cells with propidium iodide uptake.

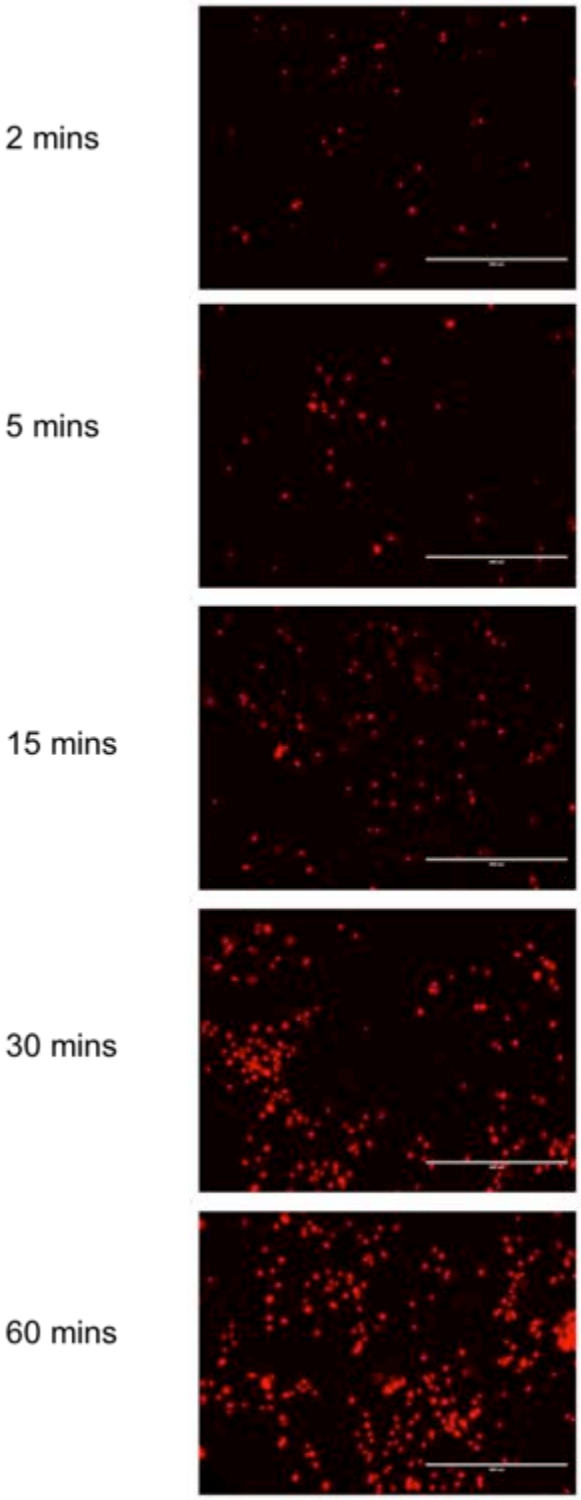

A

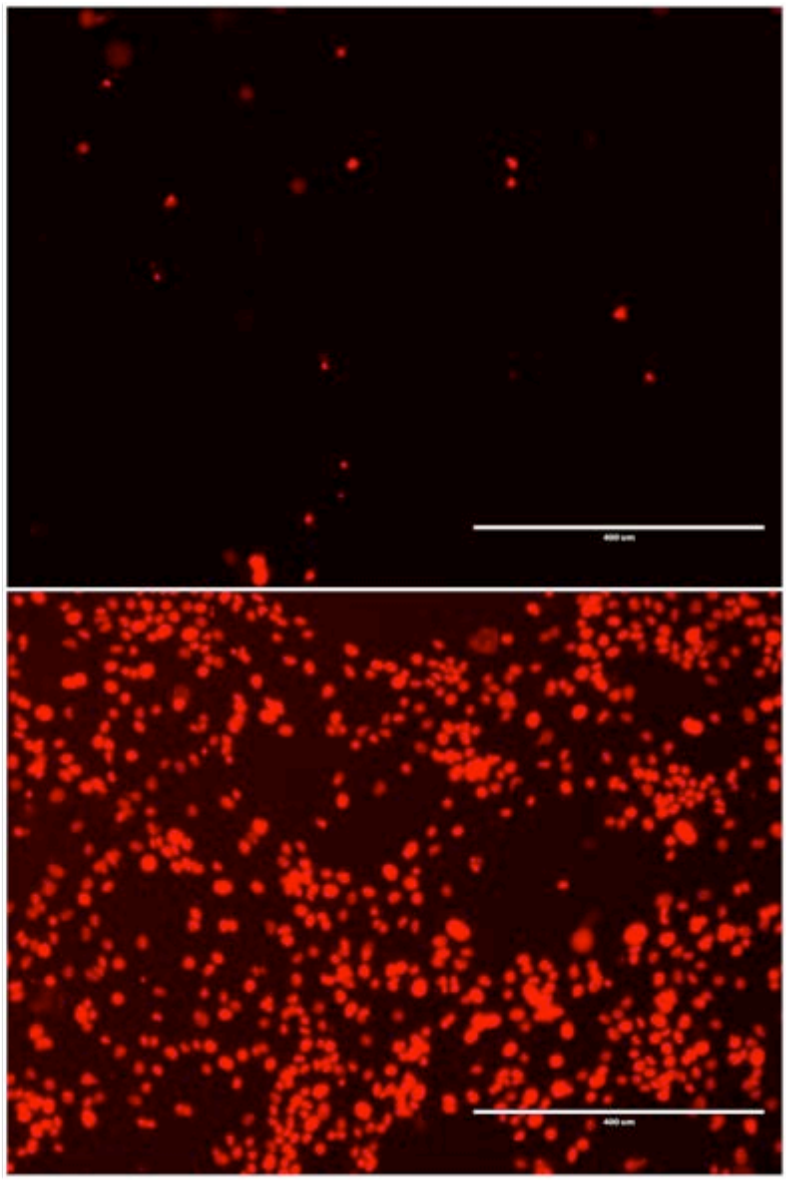

B

Figure 5.3 Serial photomicrographs of SCC-15 cells treated with 300 μg/ml EBC-46 (A) compared to controls (B) *in vitro* and stained with propidium iodide.

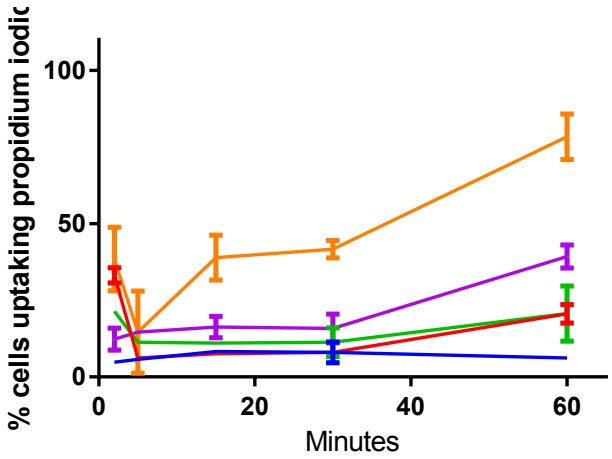

A

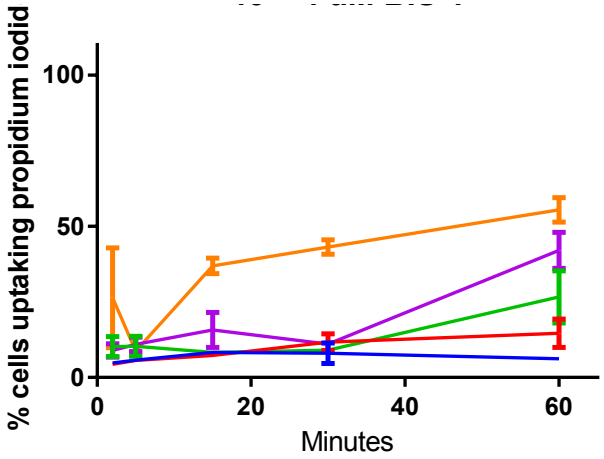

B

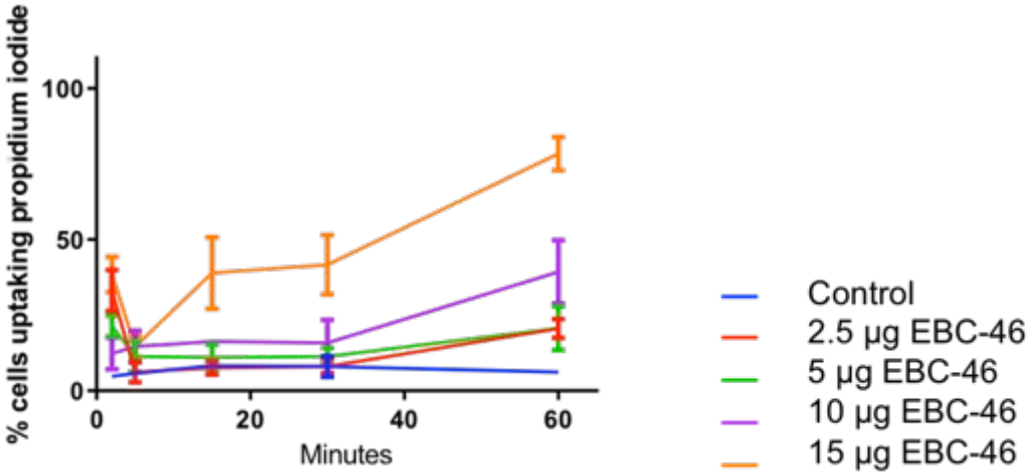

C

Figure 5.4 Uptake of propidium iodide by SCC-15 cells following treatment with EBC-46 alone (A), or with the addition of BIS-1 (B) or DPI (C). Averages from 3 well replicates were used. Error bars are ±SEM.

5.2.4 Time-lapse tumour cell killing by EBC-46

To further characterise *in vitro* tumour cell killing, a time-lapse assay using a Zeiss confocal microscope was performed. A six-well plate seeded with 1 x 10^5 SCC-15 cells were used with the addition of tetramethylrhodamine methyl ester (TMRM) and SYTOX® Green dyes in the RPMI media. TMRM is a red fluorescent probe that is bound by active mitochondria. Mitochondria lose the dye when their membrane potential is lost [106]. In comparison, SYTOX® Green is a nucleic acid stain that is membrane impermeable, therefore, like propidium iodide, can only bind DNA upon cell death [107].

Before and after the addition of high dose EBC-46 (400 μg/ml) to the well, images were taken every 30 sec for 5 min to capture any cellular uptake changes of the two dyes, in addition to differential interference contrast using visible light (Figure 5.5). Approximately 15 -17 min following the addition of EBC-46 to the cells, the SCC-15 cells began to form intracellular vacuoles and lose their TMRM staining, indicating the loss of mitochondrial membrane potential (Figure 5.6). Following this, cells rapidly began to swell and then burst (Figures 5.7 and 5.8). The inclusion of SYTOX® Green at this point indicated the cells were no longer viable. The completion of these changes appeared to occur quite rapidly following EBC-46 treatment, with all cells within the field of view dead within 30 min (Figure 5.9). No appreciable change in mitochondrial membrane potential or cell viability was noted in wells with EBC-46 absent.

The pre-treatment of the cells with 5 μM BIS-1 for 60 min did not prevent cell death, however, it did appear to reduce the rapidity at which it occurred. The addition of 10 μl 1% TX-100 showed a different pattern with loss of cellular adhesion to the well followed by rapid cell swelling and uptake of SYTOX® Green dye.

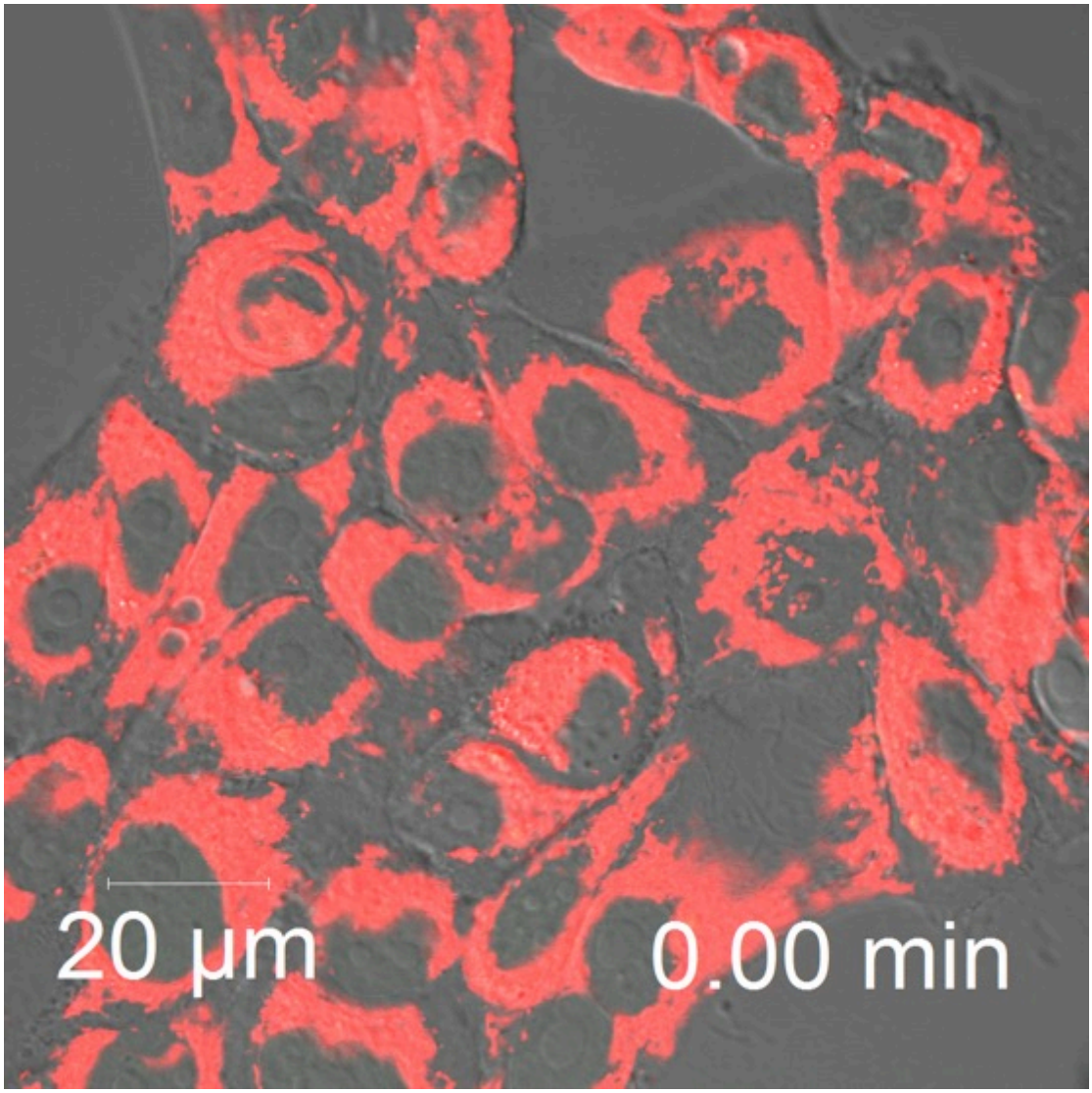

Figure 5.5 Photomicrographs of time-lapse tumour cell killing assay (63x). Prior to treatment of SCC-15 cells with 400 µg/ml EBC-46. Mitochondrial membrane potential was identified with the red fluorescent probe TMRM. Cell viability was determined using SYTOX© (not visible).

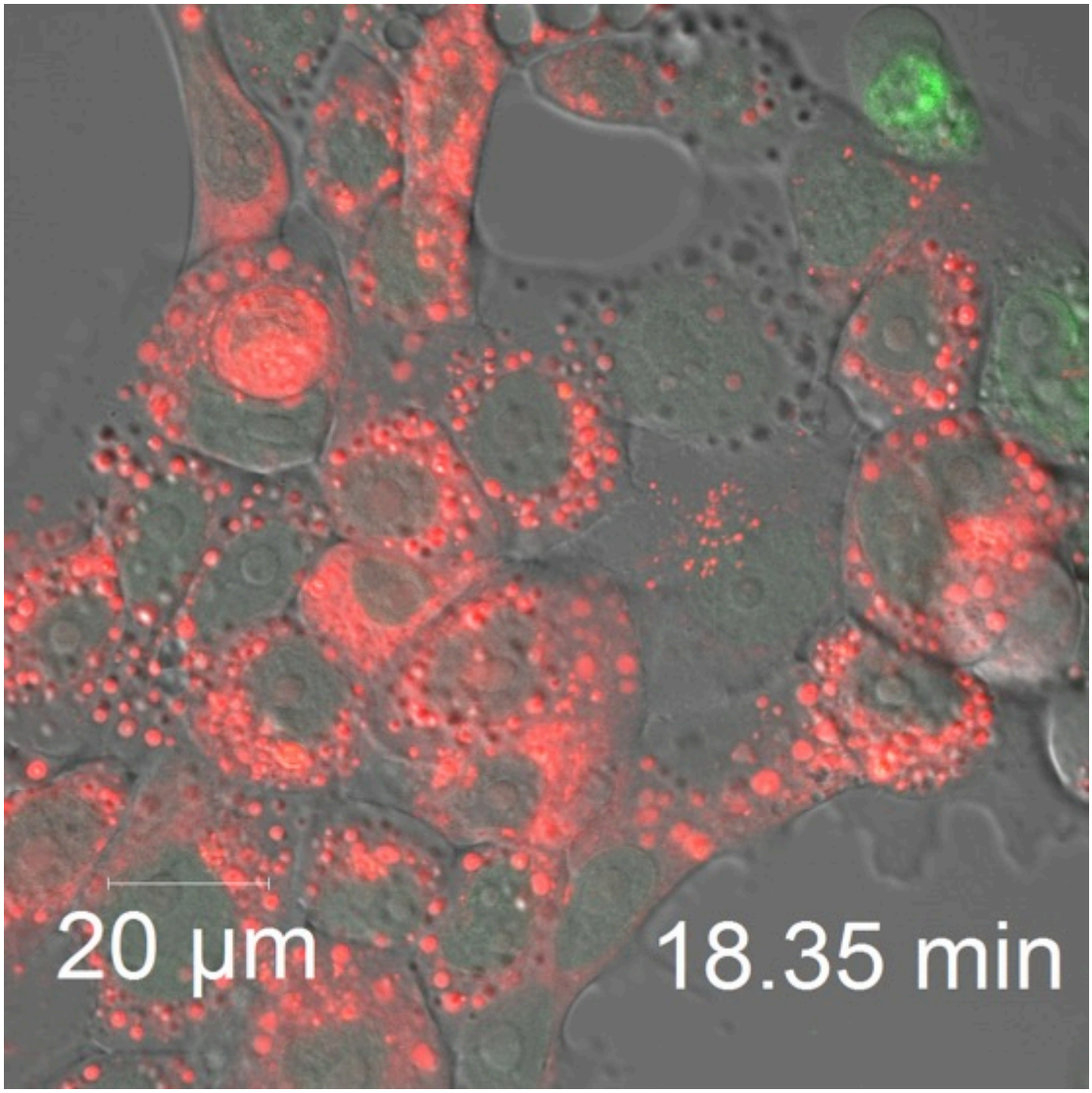

Figure 5.6 Photomicrographs of time-lapse tumour cell killing assay (63x). SCC-15 cells 13 min post treatment with 400 µg/ml EBC-46. Multiple mitochondrial vacuoles containing TMRM are observed.

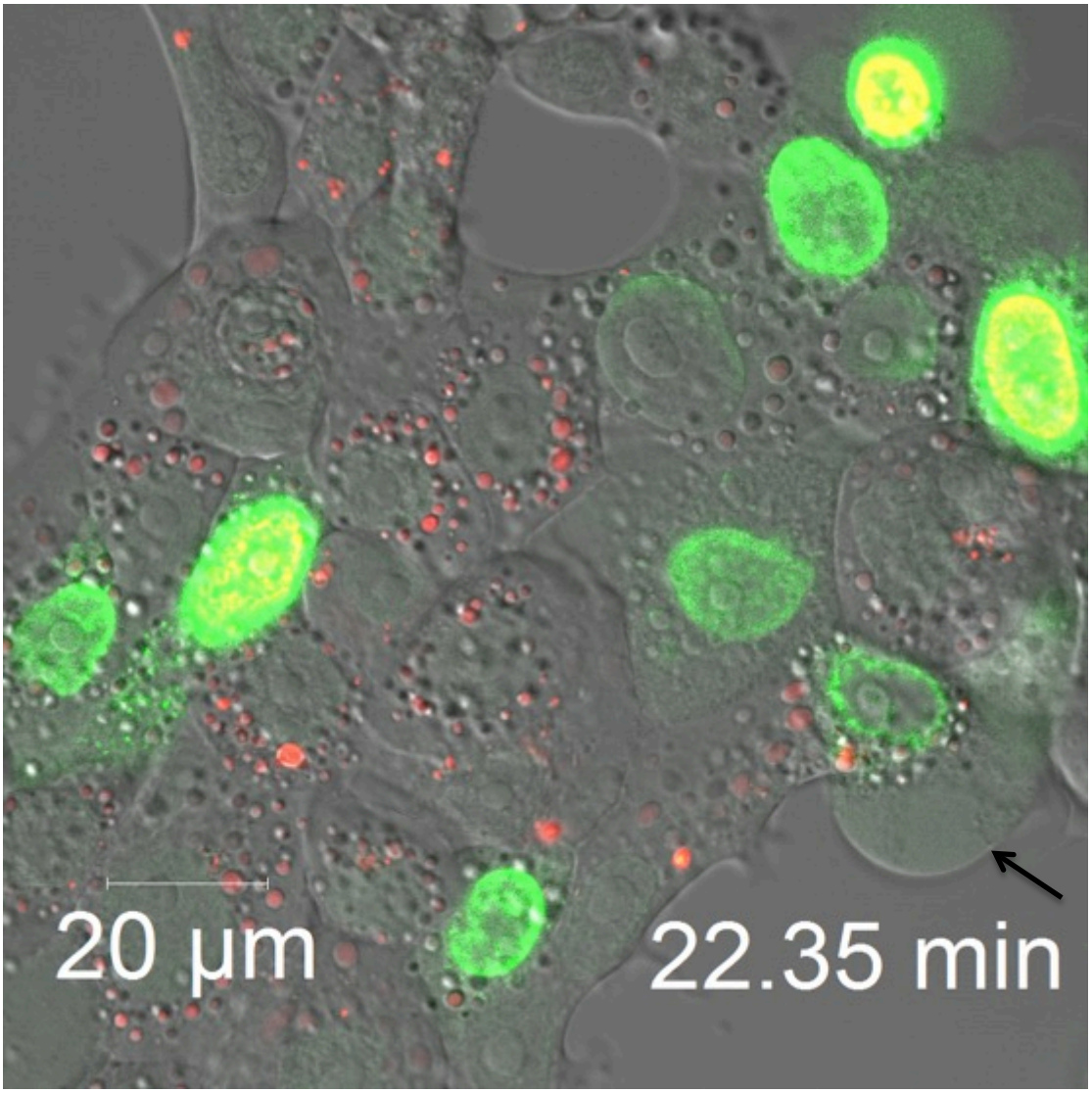

Figure 5.7 Photomicrographs of time-lapse tumour cell killing assay (63x). SCC-15 cells 17 min post treatment with 400 µg/ml EBC-46. Black arrow highlights cellular plasma membrane swelling prior to rupture and subsequent SYTOX® Green uptake by cell nucleus). Mitochondrial membrane potential (red) has largely gone.

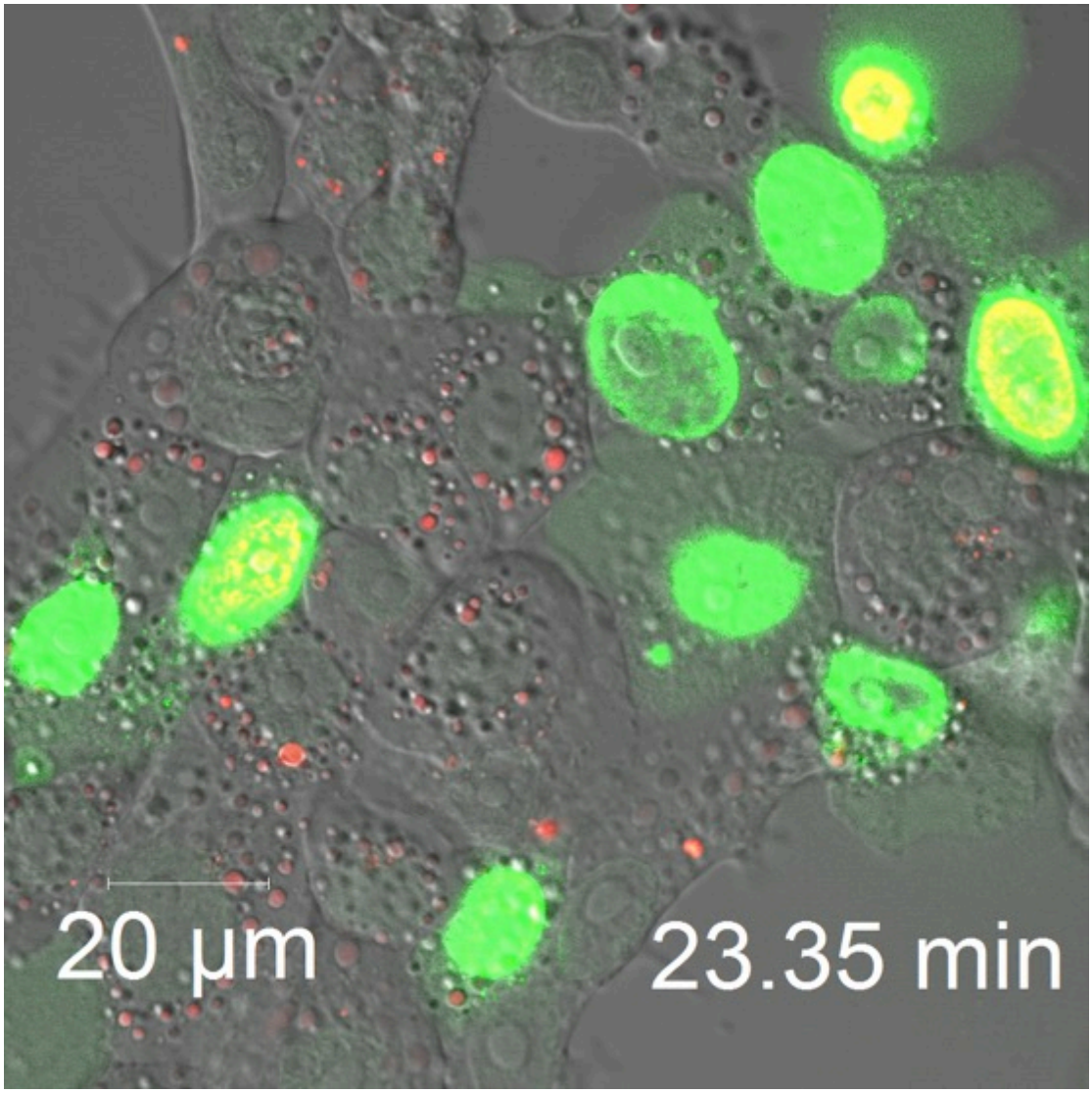

Figure 5.8 Photomicrographs of time-lapse tumour cell killing assay (63x). SCC-15 cells 18 min post treatment with 400 µg/ml EBC-46. Following cell membrane rupture, cell nuclei bind SYTOX® Green indicating the loss of cell viability.

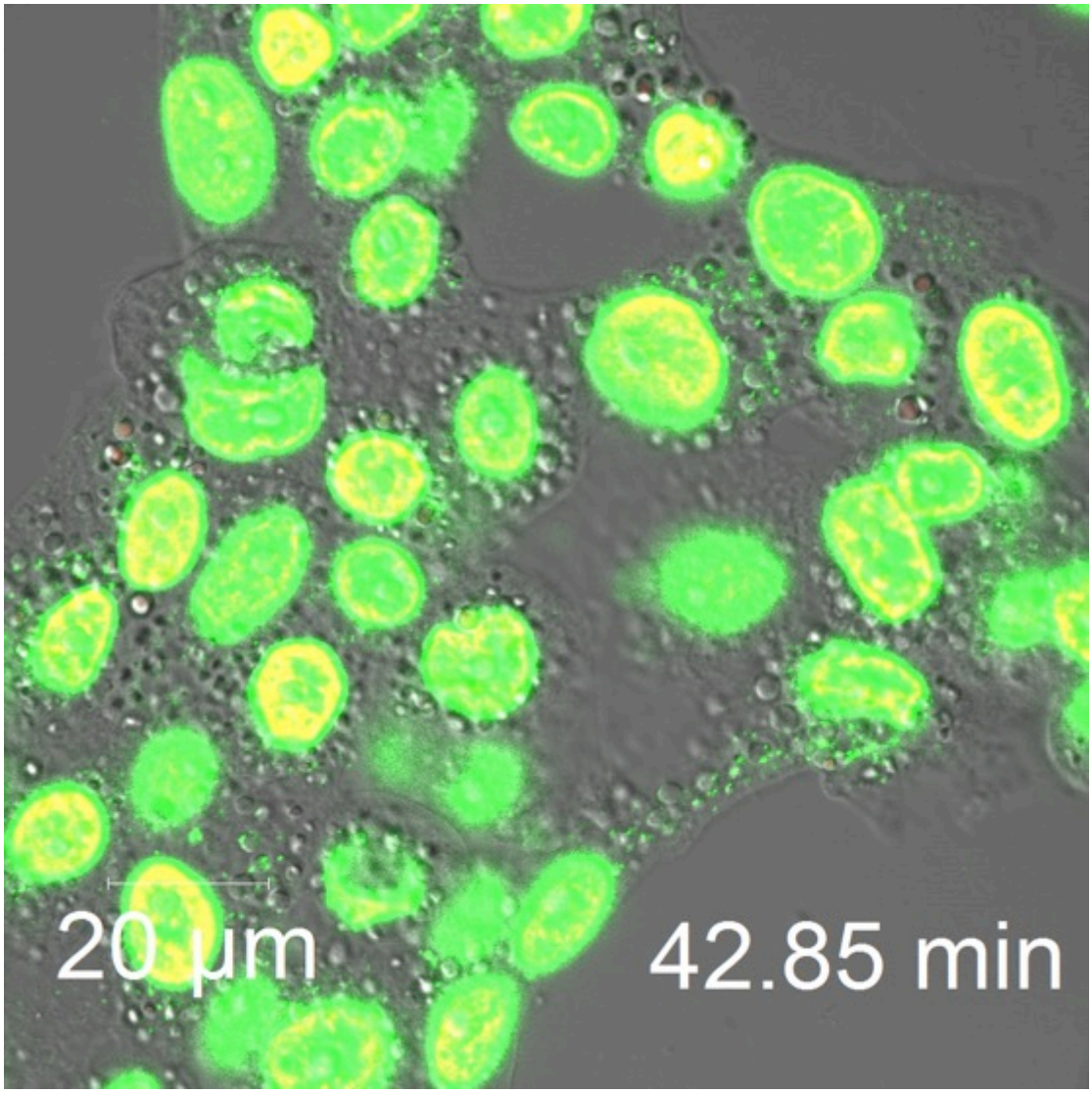

Figure 5.9 Photomicrographs of time-lapse tumour cell killing assay (63x). SCC-15 cells 38 min post treatment with 400 µg/ml EBC-46. All cells demonstrate lack of viability with SYTOX® Green nuclear uptake. As found with propidium iodide uptake, there was no evidence for nuclear fragmentation.

5.2.5 EBC-46 treatment of BALB/c *Foxn1*^{nu} mice xenografted with SCC-15 cells in the presence of BIS-1.

Considering the killing of SCC-15 cells showed some PKC-dependence *in vitro*, the next step was to see if this was also apparent *in vivo*. Twenty BALB/c *Foxn1*^{nu} mice (5 mice per group) xenografted with SCC-15 cells were treated with 30 µg EBC-46 in the presence or

absence of 40 μM BIS-1, co-injected with the EBC-46. Overall, the co-injection with of BIS-1 did not impact tumour growth or survival significantly (Figure 5.10).

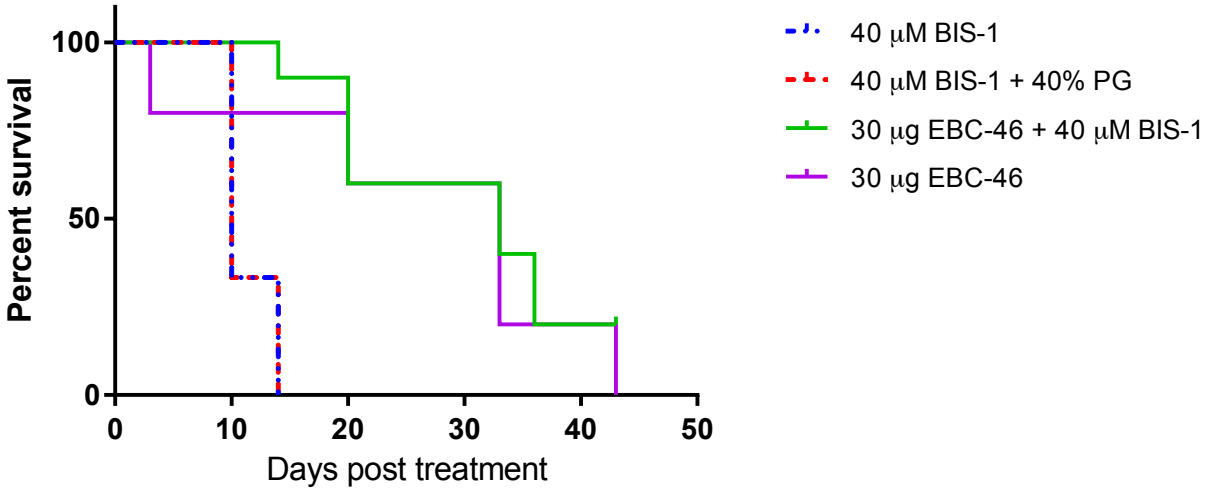

Figure 5.10 Kaplan-Meier plot comparing the differences in survival of BALB/c *Foxn1*^{nu} mice with SCC-15 tumours treated with 30 μg bolus EBC-46 in 50 μL of 40% PG, with or without co-injection of 40 μM BIS-1.

5.2.6 Neutrophil recruitment in NOD/SCID mice

Neutrophil-depleted BALB/c *Foxn1*^{nu} mice bearing LK2 tumours treated with an ingenol-type diterpene ester Picato® showed an increased rate of relapse [90]. A similar experiment used mouse melanoma xenografts and intratumoural treatment with EBC-46, and found no statistically significant difference in relapse rates [10]. An alternative approach was used here, based on the report that an antiangiogenic antibody DC101 enhanced access of proinflammatory leukocytes to tumours in NOD/SCID mice [100].

To determine if neutrophil recruitment would improve tumour ablation efficacy and relapse rates in NOD/SCID SCC-15 xenografts, 25 mice (5 mice/group) were injected intraperitoneally with 600 μg antiangiogenic monoclonal antibody DC101 (or an isotype antibody) -6, -3 days and at the time of EBC-46 treatment [100]. Survival data was recorded and showed that the addition of DC101 antibody did not significantly increase mouse survival when treated with EBC-46 (Figure 5.11)

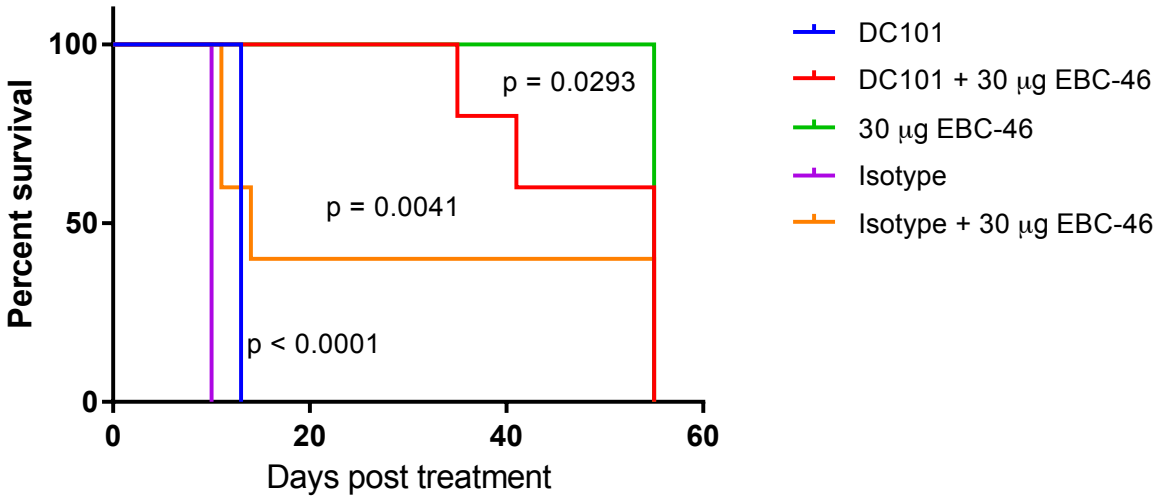

Figure 5.11 Kaplan-Meier plot comparing the differences in survival of NOD/SCID mice with SCC-15 tumours treated with 30 μg bolus EBC-46 in 50 μL of 40% PG, with prior DC101 or isotype control antibody.

5.3 Discussion

The aim of this chapter was to further investigate the mechanism by which EBC-46 causes tumour cell death. In a SRB, clonogenic-type assay, the exposure of EBC-46 at high doses *in vitro* resulted in near total tumour cell death within 30 min. Propylene glycol demonstrated high cytotoxicity at 40%, the level in which EBC-46 is injected into tumors, but showed negligible cytotoxicity at the lower levels assumed to be present in the tumour microenvironment as the injectate rapidly diffuses into the surroundings.

Rapid tumor cell kill was also seen using propidium iodide uptake as a marker for cell death, however, only ~75% of cells showed uptake after 60 minutes of EBC-46 exposure. This discrepancy potentially may be attributed to different analysis methods for each assay, or to detachment and loss from analysis of some of the treated cells. For the SRB assay, triplicate wells were read on an ELISA plate reader and then the absorbance averaged and compared to that of triplicate control wells. In comparison, to measure the propidium iodide uptake, three fields of view at 20x magnification were taken for each triplicate well, counted using OpenCFU software [93] and then averaged. Therefore, it would be possible to underestimate the total number of cells with propidium uptake in each

well, resulting in an overall reduced estimated percentage of cells dead compared to the control wells. Measuring the total fluorescence emitted by each well using a fluorescence plate reader potentially would have gained more accurate readings.

Previously studies have indicated that EBC-46's cytotoxicity was PKC-dependent, however, we were unable to completely prevent cell death by inhibiting PKC activation with BIS-1 *in vitro* with SCC 15 cells. Furthermore, no significant difference in tumour growth or survival was seen in a tongue SCC mouse model treated with EBC-46 in the presence or absence of BIS-1. The lack of PKC-related effects seen *in vivo* in this study, may be due to the relatively large dose of EBC-46 given (30 μg) compared to previous studies (10 μg; Boyle et al. 2014) which showed reduced EBC-46 efficacy with the addition of BIS-1. It is also unclear at the present time as to how quickly and effectively BIS-1 inhibits PKC when co-injected into the tumor with EBC-46. In addition, no difference in EBC-46's cytotoxicity was seen with inhibition of the ROS-producing NADPH oxidase. These results provide evidence that EBC-46 may facilitate some of its cytotoxic effects using a PKC-dependent mechanism, however, there appear to be other pathways involved. The mode of cell death, rapid loss of plasma and mitochondrial membrane function with retention of intact nuclei, resembles a form of necrosis, rather than apoptosis. Further studies using an array of different protein inhibitors in conjunction with EBC-46 both *in vitro* and *in vivo* would provide useful information regarding the pathway(s) EBC-46 utilises to cause tumour cell death.

CHAPTER SIX: FINAL DISCUSSION

6.1 Final discussion

The five-year survival rate for patients with HNSCC has remained at approximately 50% for the past 30 years despite advances in surgical technique, chemotherapy agents and radiation therapy technology. Consequently, there is a great need for the discovery and optimisation of another treatment modality that can be used to improve patient outcome. The novel diterpene ester, EBC-46, can be intratumourally injected and provides an opportunity to treat head and neck cancer patients whom are unable to undergo the traditional multi-modality treatment of surgical resection and/or chemotherapy and/or radiation therapy. A patient's disease burden or co-morbidities may render them unsuitable for the traditional treatment options or they may present with recurrent disease.

The initial aim of this project was to identify a head and neck SCC mouse model that was inherently difficult to treat with EBC-46. Once identified, we attempted to overcome this resistance by adjusting several variables: dose administration, excipient, volume and with/without prior tumour priming.

The most inherently resistant cell line was SCC-15 (ATCC® CRL-1623™), a tongue SCC cell line from a 55 year-old male [108]. In nude mice, a single bolus dose of 30 μg EBC-46 in 50 μl 40% PG to an SCC-15 tumour site led to an 70% long term ablation rate, confirming the potential of EBC-46 for local treatment of HNSCC, but lower than ablation rates obtained with the FaDu and Cal27 xenografts [91]. In NOD/SCID mice, dividing the dose of the compound into multiple injections of the same tumor did not improve survival, nor was further reduction in tumour growth found with the use of 2-hydroxypropyl-β-cyclodextrin as an excipient. Additional use of a priming dose prior to treatment, an attempt to attract pro-inflammatory cells to the site, also gave no additional benefit.

The mechanism of action of EBC-46 was therefore investigated, hoping to find clues to how efficacy could be improved. Immunohistochemical analysis of SCC-15 tumours following EBC-46 treatment in the BALB/c *Foxn1*^{nu} mouse model confirmed the presence of a macrophage and neutrophil infiltration within 24 hr. Blood vessel dilatation, disrupted endothelial cell integrity, and red blood cell extravasation was also demonstrated. A reduction in the temperature difference between the tumour skin and surrounding normal

skin also indicated a disruption to tumours' blood supply. These features were also seen following intratumoural treatment of hypopharyngeal SCC (FaDu) xenografts with EBC-46 in BALB/c *Foxn1*^{nu} mice [10].

Interestingly, a greater degree of tumour resistance was seen in SCC-15 xenografts in a more immunodeficient mouse model. NOD/SCID mice have impaired B-cells and T-cells, similar to BALB/c *Foxn1*^{nu}, however, with an additional dysfunction of their macrophages, natural killer cells and complement components [96]. A reactive macrophage infiltration was seen histologically in the NOD/SCID, however there was a notable absence of a neutrophil infiltration. This difference may allude to the mechanism by which EBC-46 kills tumour cells. Previous researchers have proposed that another PKC activating diterpene ester PEP005/Picato has a biphasic mechanism of action; primary necrosis of tumour cells followed by activation of the host's innate immune system [90]. Furthermore, neutrophil-depleted mice bearing SK-MEL-28 tumours treated with EBC-46 had a 40% tumour recurrence rate compared to no recurrences in mice with normal neutrophil counts [10].

The other focus on mechanism was further investigation into the mechanism by which tumour cells are killed *in vitro* by EBC-46 (12-20 µg) yielded evidence of necrosis with loss of mitochondrial membrane potential, plasma membrane swelling and eventual cell rupture within 30 min. The aim was to reproduce in culture the high local concentration range expected from injection 30 µg EBC-46 into the tumour. Previously studies have indicated that EBC-46's cytotoxicity was PKC-dependent, however, we were unable to prevent cell death by inhibiting PKC activation with BIS-1 *in vitro*. No significant difference in tumour growth or survival was seen in a tongue SCC mouse model treated with EBC-46 in the presence or absence of BIS-1. In the mouse model, BIS-1, a water-soluble compound, was co-injected with EBC-46, which has known hydrophobicity, potentially confounding the findings because of a mis-match in tissue uptake. It is unknown how long BIS-1 was maintained in the tumour microenvironment before diffusing away from the region and whether it's pan-PKC inhibiting action was readily reversed.

Additionally, no difference to EBC-46's cytotoxicity *in vitro* was seen with inhibition of the ROS-producing NADPH oxidase. These results provide evidence that EBC-46 may facilitate some of its cytotoxic effects in a PKC-dependent mechanism, however, there appear to be other pathways involved. The latter may involve other proteins with a C1

region, or disruption of the plasma and/or mitochondrial membranes by insertion of EBC-46 into lipid structures.

6.2 Future directions

Further investigation is required to establish a complete understanding of the mechanism by which EBC-46 works *in vivo*. Strong evidence from previous publications exists to suggest that EBC-46 works at least partly in a PKC-dependent manner. The current body of work was unable to confirm EBC-46's PKC-dependence in tumour cell killing *in vivo*, though this may be attributed to the method of administration of BIS-1. Additional experimentation with BIS-1 and other PKC-inhibitors would be warranted to confirm PKC's role in EBC-46's mechanism of action. Also, the *in vitro* and *in vivo* potencies for cell killing of a range of EBC-46 analogues differing in their levels of PKC isoform activation could be compared.

The involvement of RasGRPs required further validation. These intracellular signalling proteins, containing a C1 sequence, have been shown to be targets of Picato® and induced apoptosis in a human lymphoma cell line [109]. Other potential pathways need to be considered, specifically, those that may be involved in the instigation or maintenance of a reactive neutrophil infiltration into tumour tissue following intratumoural injection. Furthermore, the presence of NETs in the tumour microenvironment and their role in tumour cell killing would be an interesting avenue to pursue.

In this thesis, only 2-hydroxypropyl-β-cyclodextrin was trialled as an alternative to the vehicle propylene glycol. It would be interesting to expand this further and investigate the use of other potential excipients. For example, other types of cyclodextrin as well as EBC-46-loaded nanoparticles could be considered. This type of preparation would ideally maintain the compound's concentration in the tumour microenvironment whilst reducing systemic effects.

At the time of publication, Phase I clinical trials for EBC-46 in a palliative subset of patients with head and neck cancer were underway in Victoria, New South Wales and Queensland. Patients that demonstrate a good response to treatment will be able to apply for further compassionate treatment.

With satisfactory performance in clinical trials, it is hoped that EBC-46 will be approved for the treatment of selected patients with head and neck cancer as an adjunct or stand-alone treatment option.

References

1. Jemal A, Bray F, Center MM, Ferlay J, Ward E, Forman D. Global cancer statistics. CA: A Cancer Journal for Clinicians 2011;**61**(2):69-90.

2. Leemans CR, Braakhuis BJM, Brakenhoff RH. The molecular biology of head and neck cancer. Nat Rev Cancer 2011;**11**(1):9-22.

3. Bose P, Brockton NT, Dort JC. Head and neck cancer: from anatomy to biology. International Journal of Cancer 2013;**133**(9):2013-23.

4. Murdoch D. Standard, and novel cytotoxic and molecular-targeted, therapies for HNSCC: an evidence-based review. Curr Opin Oncol 2007;**19**(3):216-21.

5. Ogbourne SM, Suhrbier A, Jones B, Cozzi S-J, Boyle GM, Morris M, McAlpine D, Johns J, Scott TM, Sutherland KP, Gardner JM, Le TTT, Lenarczyk A, Aylward JH, Parsons PG. Antitumor Activity of 3-Ingenyl Angelate: Plasma Membrane and Mitochondrial Disruption and Necrotic Cell Death. Cancer Research 2004;**64**(8):2833-39.

6. Cozzi S-J, Le T, Ogbourne S, James C, Suhrbier A. Effective treatment of squamous cell carcinomas with ingenol mebutate gel in immunologically intact SKH1 mice. Arch Dermatol Res 2013;**305**(1):79-83.

7. Ersvaer E, Kittang AO, Hampson P, Sand K, Gjertsen BT, Lord JM, Bruserud O. The protein kinase C agonist PEP005 (ingenol 3-angelate) in the treatment of human cancer: a balance between efficacy and toxicity. Toxins (Basel) 2010;**2**(1):174-94.

8. Griner EM, Kazanietz MG. Protein kinase C and other diacylglycerol effectors in cancer. Nat Rev Cancer 2007;**7**(4):281-94.

9. Mason S, Cozzi S-J, Pierce C, Pavey S, Parsons P, Boyle G. The induction of senescence-like growth arrest by protein kinase C-activating diterpene esters in solid tumor cells. Invest New Drugs 2010;**28**(5):575-86.

10. Boyle GM, D'Souza MM, Pierce CJ, Adams RA, Cantor AS, Johns JP, Maslovskaya L, Gordon VA, Reddell PW, Parsons PG. Intra-lesional injection of the novel PKC

activator EBC-46 rapidly ablates tumors in mouse models. PLoS One 2014;**9**(10):e108887.

11. Siegel RMPH, Naishadham DMAMS, Jemal ADVMP. Cancer statistics, 2013. Ca : a Cancer Journal for Clinicians 2013;**63**(1):11.

12. Cooper JS, Porter K, Mallin K, Hoffman HT, Weber RS, Ang KK, Gay EG, Langer CJ. National Cancer Database report on cancer of the head and neck: 10-Year update. Head & Neck 2009;**31**(6):748-58.

13. Cohen SM, Rockefeller N, Mukerji R, et al. EFficacy and toxicity of peritumoral delivery of nanoconjugated cisplatin in an in vivo murine model of head and neck squamous cell carcinoma. JAMA Otolaryngology–Head & Neck Surgery 2013;**139**(4):382-87.

14. Vineis P, Alavanja M, Buffler P, Fontham E, Franceschi S, Gao YT, Gupta PC, Hackshaw A, Matos E, Samet J, Sitas F, Smith J, Stayner L, Straif K, Thun MJ, Wichmann HE, Wu AH, Zaridze D, Peto R, Doll R. Tobacco and Cancer: Recent Epidemiological Evidence. Journal of the National Cancer Institute 2004;**96**(2):99-106.

15. Sharan RN, Mehrotra R, Choudhury Y, Asotra K. Association of betel nut with carcinogenesis: revisit with a clinical perspective. PLoS One 2012;**7**(8):e42759.

16. Trizna Z, Schantz SP. Hereditary and environmental factors associated with risk and progression of head and neck cancer. Otolaryngologic clinics of North America 1992;**25**(5):1089-103.

17. Foulkes WD, Brunet JS, Sieh W, Black MJ, Shenouda G, Narod SA. Familial risks of squamous cell carcinoma of the head and neck: retrospective case-control study. BMJ (Clinical research ed) 1996;**313**(7059):716-21.

18. Herrero R, Castellsagué X, Pawlita M, Lissowska J, Kee F, Balaram P, Rajkumar T, Sridhar H, Rose B, Pintos J, Fernández L, Idris A, Sánchez MJ, Nieto A, Talamini R, Tavani A, Bosch FX, Reidel U, Snijders PJF, Meijer CJLM, Viscidi R, Muñoz N, Franceschi S, Group FtIMOCS. Human Papillomavirus and Oral Cancer: The

International Agency for Research on Cancer Multicenter Study. Journal of the National Cancer Institute 2003;**95**(23):1772-83.

19. Hobbs CGL, Sterne JAC, Bailey M, Heyderman RS, Birchall MA, Thomas SJ. Human papillomavirus and head and neck cancer: a systematic review and meta-analysis. Clinical Otolaryngology 2006;**31**(4):259-66.

20. Ang KKMDP, Harris JMS, Wheeler RMD, Weber RMD, Rosenthal DIMD, Nguyen-Tân PFMD, Westra WHMD, Chung CHMD, Jordan RCDDSP, Lu CMD, Kim HMD, Axelrod RMD, Silverman CCMD, Redmond KPMD, Gillison MLMDP. Human Papillomavirus and Survival of Patients with Oropharyngeal Cancer. The New England journal of medicine 2010;**363**(1):24-35.

21. Miller DL, Puricelli MD, Stack MS. Virology and molecular pathogenesis of HPV (human papillomavirus)-associated oropharyngeal squamous cell carcinoma. Biochemical Journal 2012;**443**(2):339-53.

22. Ariyawardana A, Johnson N. Trends of lip, oral cavity and oropharyngeal cancers in Australia 1982-2008: overall good news but with rising rates in the oropharynx. BMC Cancer 2013;**13**(1):333.

23. AIHW. *2010 National Drug Strategy Household Survey report*. Canberra: AIHW, 2011.

24. Townsend CM, Sabiston DC. Sabiston textbook of surgery : the biological basis of modern surgical practice. Secondary Sabiston textbook of surgery : the biological basis of modern surgical practice 2004.

25. Strobel K, Haerle S, Stoeckli S, Schrank M, Soyka J, Veit-Haibach P, Hany T. Head and neck squamous cell carcinoma (HNSCC) – detection of synchronous primaries with 18F-FDG-PET/CT. Eur J Nucl Med Mol Imaging 2009;**36**(6):919-27.

26. Ng S-H, Yen T-C, Chang JT-C, Chan S-C, Ko S-F, Wang H-M, Lee L-Y, Kang C-J, Wong AM-C, Liao C-T. Prospective Study of [18F]Fluorodeoxyglucose Positron Emission Tomography and Computed Tomography and Magnetic Resonance Imaging in Oral Cavity Squamous Cell Carcinoma With Palpably Negative Neck. Journal of Clinical Oncology 2006;**24**(27):4371-76.

27. Pfister DG. Head and neck cancers, version 2.2013. Featured updates to the NCCN guidelines. Journal of the National Comprehensive Cancer Network 2013;**11**(8):917-23.

28. Edge S, Byrd D, Compton C. *AJCC cancer staging manual*. 7th ed. New York: Springer, 2010.

29. Brandwein-Gensler M, Smith RV. Prognostic indicators in head and neck oncology including the new 7th edition of the AJCC staging system. Head and neck pathology 2010;**4**(1):53-61.

30. Argiris A, Karamouzis MV, Raben D, Ferris RL. Head and neck cancer. The Lancet 2008;**371**(9625):1695-709.

31. Khuri FR, Lee JJ, Lippman SM, Kim ES, Cooper JS, Benner SE, Winn R, Pajak TF, Williams B, Shenouda G, Hodson I, Fu K, Shin DM, Vokes EE, Feng L, Goepfert H, Hong WK. Randomized Phase III Trial of Low-dose Isotretinoin for Prevention of Second Primary Tumors in Stage I and II Head and Neck Cancer Patients. Journal of the National Cancer Institute 2006;**98**(7):441-50.

32. Lui VW, Grandis JR. Primary chemotherapy and radiation as a treatment strategy for HPV-positive oropharyngeal cancer. Head and neck pathology 2012;**6 Suppl 1**:S91-7.

33. Crile G. EXcision of cancer of the head and neck.with special reference to the plan of dissection based on one hundred and thirty-two operations. Journal of the American Medical Association 1906;**XLVII**(22):1780-86.

34. Ganly I, Patel S, Shah J. Early stage squamous cell cancer of the oral tongue—clinicopathologic features affecting outcome. Cancer 2012;**118**(1):101-11.

35. Almangush A, Bello IO, Keski–Säntti H, Mäkinen LK, Kauppila JH, Pukkila M, Hagström J, Laranne J, Tommola S, Nieminen O, Soini Y, Kosma V-M, Koivunen P, Grénman R, Leivo I, Salo T. Depth of invasion, tumor budding, and worst pattern of invasion: Prognostic indicators in early-stage oral tongue cancer. Head & Neck 2013:n/a-n/a.

36. Loree TR, Strong EW. Significance of positive margins in oral cavity squamous carcinoma. The American Journal of Surgery 1990;**160**(4):410-14.

37. Panizza B, Warren T. Perineural Invasion of Head and Neck Skin Cancer: Diagnostic and Therapeutic Implications. Curr Oncol Rep 2013;**15**(2):128-33.

38. Woolgar J, Triantafyllou A, Lewis J, Jr., Hunt J, Williams M, Takes R, Thompson LR, Slootweg P, Devaney K, Ferlito A. Prognostic biological features in neck dissection specimens. Eur Arch Otorhinolaryngol 2013;**270**(5):1581-92.

39. Bourhis J, Overgaard J, Audry H, Ang KK, Saunders M, Bernier J, Horiot J-C, Le Maître A, Pajak TF, Poulsen MG, O'Sullivan B, Dobrowsky W, Hliniak A, Skladowski K, Hay JH, Pinto LHJ, Fallai C, Fu KK, Sylvester R, Pignon J-P. Hyperfractionated or accelerated radiotherapy in head and neck cancer: a meta-analysis. The Lancet 2006;**368**(9538):843-54.

40. Wang X, Hu C, Eisbruch A. Organ-sparing radiation therapy for head and neck cancer. 2011.

41. Pignon JP, le Maitre A, Maillard E, Bourhis J. Meta-analysis of chemotherapy in head and neck cancer (MACH-NC): an update on 93 randomised trials and 17,346 patients. Radiotherapy and oncology : journal of the European Society for Therapeutic Radiology and Oncology 2009;**92**(1):4-14.

42. Gibson MK, Li Y, Murphy B, Hussain MH, DeConti RC, Ensley J, Forastiere AA. Randomized phase III evaluation of cisplatin plus fluorouracil versus cisplatin plus paclitaxel in advanced head and neck cancer (E1395): an intergroup trial of the Eastern Cooperative Oncology Group. Journal of clinical oncology : official journal of the American Society of Clinical Oncology 2005;**23**(15):3562-7.

43. Jacobs C, Lyman G, Velez-Garcia E, Sridhar KS, Knight W, Hochster H, Goodnough LT, Mortimer JE, Einhorn LH, Schacter L, et al. A phase III randomized study comparing cisplatin and fluorouracil as single agents and in combination for advanced squamous cell carcinoma of the head and neck. Journal of clinical oncology : official journal of the American Society of Clinical Oncology 1992;**10**(2):257-63.

44. DVALCSG. The Department of Veterans Affairs Laryngeal Cancer Study Group: Induction Chemotherapy plus Radiation Compared with Surgery plus Radiation in Patients with Advanced Laryngeal Cancer. New England Journal of Medicine 1991;**324**(24):1685-90.

45. Eswaran P, Azmi K. Concurrent chemoradiation with weekly Cisplatin, Docetaxel and Gefitinib: A study to assess feasibility, toxicity and immediate response. Journal of Cancer Research and Therapeutics 2013;**9**(3):392-6.

46. Kundu SK, Nestor M. Targeted therapy in head and neck cancer. Tumor Biology 2012;**33**(3):707-21.

47. Specenier P, Vermorken JB. Cetuximab: its unique place in head and neck cancer treatment. Biologics : targets & therapy 2013;**7**:77-90.

48. Wheeler DL, Dunn EF, Harari PM. Understanding resistance to EGFR inhibitors[mdash]impact on future treatment strategies. Nat Rev Clin Oncol 2010;**7**(9):493-507.

49. Iida M, Brand TM, Starr MM, Li C, Huppert EJ, Luthar N, Pedersen MW, Horak ID, Kragh M, Wheeler DL. Sym004, a novel EGFR antibody mixture, can overcome acquired resistance to cetuximab. Neoplasia (New York, NY) 2013;**15**(10):1196-206.

50. Eke I, Storch K, Krause M, Cordes N. Cetuximab attenuates its cytotoxic and radiosensitizing potential by inducing fibronectin biosynthesis. Cancer Res 2013;**73**(19):5869-79.

51. Napier SS, Speight PM. Natural history of potentially malignant oral lesions and conditions: an overview of the literature. Journal of Oral Pathology & Medicine 2008;**37**(1):1-10.

52. Braakhuis BJM, Tabor MP, Kummer JA, Leemans CR, Brakenhoff RH. A Genetic Explanation of Slaughter's Concept of Field Cancerization: Evidence and Clinical Implications. Cancer Research 2003;**63**(8):1727-30.

53. Slaughter D, Southwick H. "Field cancerization" in oral stratified squamous epithelium. Clinical implications of multicentric origin. Cancer 1953;**6**:963-8.

54. Califano J, van der Riet P, Westra W, Nawroz H, Clayman G, Piantadosi S, Corio R, Lee D, Greenberg B, Koch W, Sidransky D. Genetic Progression Model for Head and Neck Cancer: Implications for Field Cancerization. Cancer Research 1996;**56**(11):2488-92.

55. Perez-Ordoñez B, Beauchemin M, Jordan RCK. Molecular biology of squamous cell carcinoma of the head and neck. Journal of Clinical Pathology 2006;**59**(5):445-53.

56. van Houten VMM, Tabor MP, van den Brekel MWM, Alain Kummer J, Denkers F, Dijkstra J, Leemans R, van der Waal I, Snow GB, Brakenhoff RH. Mutated p53 as a molecular marker for the diagnosis of head and neck cancer. The Journal of Pathology 2002;**198**(4):476-86.

57. Rheinwald JG, Hahn WC, Ramsey MR, Wu JY, Guo Z, Tsao H, De Luca M, Catricalà C, O'Toole KM. A Two-Stage, p16INK4A- and p53-Dependent Keratinocyte Senescence Mechanism That Limits Replicative Potential Independent of Telomere Status. Molecular and Cellular Biology 2002;**22**(19):6930.

58. Ozanne B, Richards CS, Hendler F, Burns D, Gusterson B. Over-expression of the EGF receptor is a hallmark of squamous cell carcinomas. The Journal of Pathology 1986;**149**(1):9-14.

59. Grandis JR, Tweardy DJ. Elevated Levels of Transforming Growth Factor α and Epidermal Growth Factor Receptor Messenger RNA Are Early Markers of Carcinogenesis in Head and Neck Cancer. Cancer Research 1993;**53**(15):3579-84.

60. Wang D, Song H, Evans JA, Lang JC, Schuller DE, Weghorst CM. Mutation and downregulation of the transforming growth factor beta type II receptor gene in primary squamous cell carcinomas of the head and neck. Carcinogenesis 1997;**18**(11):2285-90.

61. Qiu W, Schönleben F, Li X, Su GH. Disruption of transforming growth factor β-Smad signaling pathway in head and neck squamous cell carcinoma as evidenced by mutations of SMAD2 and SMAD4. Cancer Letters 2007;**245**(1–2):163-70.

62. Murugan AK, Munirajan AK, Tsuchida N. Genetic deregulation of the PIK3CA oncogene in oral cancer. Cancer Letters 2013;**338**(2):193-203.

63. Smith A, Teknos TN, Pan Q. Epithelial to mesenchymal transition in head and neck squamous cell carcinoma. Oral Oncology 2013;**49**(4):287-92.

64. Chen C, Zimmermann M, Tinhofer I, Kaufmann AM, Albers AE. Epithelial-to-mesenchymal transition and cancer stem(-like) cells in head and neck squamous cell carcinoma. Cancer Letters 2013;**338**(1):47-56.

65. Balermpas P, Michel Y, Wagenblast J, Seitz O, Sipek F, Rödel F, Rödel C, Fokas E. Nuclear NF-κB Expression Correlates With Outcome Among Patients With Head and Neck Squamous Cell Carcinoma Treated With Primary Chemoradiation Therapy. International journal of radiation oncology, biology, physics 2013;**86**(4):785-90.

66. Kyzas PA, Cunha IW, Ioannidis JPA. Prognostic Significance of Vascular Endothelial Growth Factor Immunohistochemical Expression in Head and Neck Squamous Cell Carcinoma: A Meta-Analysis. Clinical Cancer Research 2005;**11**(4):1434-40.

67. Takai Y, Kishimoto A, Inoue M, Nishizuka Y. Studies on a cyclic nucleotide-independent protein kinase and its proenzyme in mammalian tissues. I. Purification and characterization of an active enzyme from bovine cerebellum. Journal of Biological Chemistry 1977;**252**(21):7603-09.

68. Denning MF. Specifying protein kinase C functions in melanoma. Pigment Cell & Melanoma Research 2012;**25**(4):466-76.

69. Ono Y, Fujii T, Ogita K, Kikkawa U, Igarashi K, Nishizuka Y. The structure, expression, and properties of additional members of the protein kinase C family. Journal of Biological Chemistry 1988;**263**(14):6927-32.

70. Coussens L, Parker PJ, Rhee L, Yang-Feng TL, Chen E, Waterfield MD, Francke U, Ullrich A. Multiple, distinct forms of bovine and human protein kinase C suggest diversity in cellular signaling pathways. Science (New York, NY) 1986;**233**(4766):859-66.

71. Basu A, Pal D. Two faces of protein kinase Cdelta: the contrasting roles of PKCdelta in cell survival and cell death. TheScientificWorldJournal 2010;**10**:2272-84.

72. Chen L, Hahn H, Wu G, Chen CH, Liron T, Schechtman D, Cavallaro G, Banci L, Guo Y, Bolli R, Dorn GW, 2nd, Mochly-Rosen D. Opposing cardioprotective actions and parallel hypertrophic effects of delta PKC and epsilon PKC. Proceedings of the National Academy of Sciences of the United States of America 2001;**98**(20):11114-9.

73. Mochly-Rosen D, Das K, Grimes KV. Protein kinase C, an elusive therapeutic target? Nat Rev Drug Discov 2012;**11**(12):937-57.

74. Simonis G, Braun MU, Kirrstetter M, Schon SP, Strasser RH. Mechanisms of myocardial remodeling: ramiprilat blocks the expressional upregulation of protein kinase C-epsilon in the surviving myocardium early after infarction. Journal of cardiovascular pharmacology 2003;**41**(5):780-7.

75. Palaniyandi SS, Sun L, Ferreira JCB, Mochly-Rosen D. Protein kinase C in heart failure: a therapeutic target? Cardiovascular Research 2009;**82**(2):229-39.

76. Dempsey EC, Cool CD, Littler CM. Lung disease and PKCs. Pharmacological Research 2007;**55**(6):545-59.

77. Koya D, King GL. Protein kinase C activation and the development of diabetic complications. Diabetes 1998;**47**(6):859-66.

78. Li J, Gobe G. Protein kinase C activation and its role in kidney disease (Review Article). Nephrology 2006;**11**(5):428-34.

79. Cozzi S-J, Parsons PG, Ogbourne SM, Pedley J, Boyle GM. Induction of Senescence in Diterpene Ester–Treated Melanoma Cells via Protein Kinase C–Dependent

Hyperactivation of the Mitogen-Activated Protein Kinase Pathway. Cancer Research 2006;**66**(20):10083-91.

80. Schonwasser DC, Marais RM, Marshall CJ, Parker PJ. Activation of the mitogen-activated protein kinase/extracellular signal-regulated kinase pathway by conventional, novel, and atypical protein kinase C isotypes. Mol Cell Biol 1998;**18**(2):790-8.

81. Wilkinson RW, Lee-MacAry AE, Davies D, Snary D, Ross EL. Antibody-dependent cell-mediated cytotoxicity: a flow cytometry-based assay using fluorophores. Journal of Immunological Methods 2001;**258**(1–2):183-91.

82. Nagpala PG, Malik AB, Vuong PT, Lum H. Protein kinase C β1 overexpression augments phorbol ester-induced increase in endothelial permeability. Journal of Cellular Physiology 1996;**166**(2):249-55.

83. Zheng Y, Liu H, Coughlin J, Zheng J, Li L, Stone JC. Phosphorylation of RasGRP3 on threonine 133 provides a mechanistic link between PKC and Ras signaling systems in B cells. Blood 2005;**105**(9):3648-54.

84. Stone JC. Regulation and Function of the RasGRP Family of Ras Activators in Blood Cells. Genes & cancer 2011;**2**(3):320-34.

85. Stang SL, Lopez-Campistrous A, Song X, Dower NA, Blumberg PM, Wender PA, Stone JC. A proapoptotic signaling pathway involving RasGRP, Erk, and Bim in B cells. Experimental Hematology 2009;**37**(1):122-34.e2.

86. Han S, Knoepp SM, Hallman MA, Meier KE. RasGRP1 Confers the Phorbol Ester-Sensitive Phenotype to EL4 Lymphoma Cells. Molecular Pharmacology 2007;**71**(1):314-22.

87. Lebwohl M, Sohn A. Ingenol mebutate (ingenol 3-angelate, PEP005): focus on its uses in the treatment of nonmelanoma skin cancer. Expert Review of Dermatology 2012;**7**(2):121-28.

88. Ramsay JR, Suhrbier A, Aylward JH, Ogbourne S, Cozzi SJ, Poulsen MG, Baumann KC, Welburn P, Redlich GL, Parsons PG. The sap from Euphorbia peplus is effective against human nonmelanoma skin cancers. The British journal of dermatology 2011;**164**(3):633-6.

89. Li L, Shukla S, Lee A, Garfield SH, Maloney DJ, Ambudkar SV, Yuspa SH. The Skin Cancer Chemotherapeutic Agent Ingenol-3-Angelate (PEP005) Is a Substrate for the Epidermal Multidrug Transporter (ABCB1) and Targets Tumor Vasculature. Cancer Research 2010;**70**(11):4509-19.

90. Challacombe JM, Suhrbier A, Parsons PG, Jones B, Hampson P, Kavanagh D, Rainger GE, Morris M, Lord JM, Le TTT, Hoang-Le D, Ogbourne SM. Neutrophils Are a Key Component of the Antitumor Efficacy of Topical Chemotherapy with Ingenol-3-Angelate. The Journal of Immunology 2006;**177**(11):8123-32.

91. Adams R. The Efficacy and Mechanism of Action of EBC-46 in Head and Neck Squamous Cell Carcinoma. The University of Queensland, 2013.

92. Skehan P, Storeng R, Scudiero D, Monks A, McMahon J, Vistica D, Warren JT, Bokesch H, Kenney S, Boyd MR. New colorimetric cytotoxicity assay for anticancer-drug screening. J Natl Cancer Inst 1990;**82**(13):1107-12.

93. Geissmann Q. OpenCFU, a New Free and Open-Source Software to Count Cell Colonies and Other Circular Objects. PLoS ONE 2013;**8**(2):e54072.

94. D'Souza M-AMA. The Antitumor Action of a Novel Diterpene Ester The Universtity of Queensland, 2014.

95. Pelleitier M, Montplaisir S. The nude mouse: a model of deficient T-cell function. Methods and achievements in experimental pathology 1975;**7**:149-66.

96. Shultz LD, Schweitzer PA, Christianson SW, Gott B, Schweitzer IB, Tennent B, McKenna S, Mobraaten L, Rajan TV, Greiner DL, et al. Multiple defects in innate and adaptive immunologic function in NOD/LtSz-scid mice. Journal of immunology (Baltimore, Md : 1950) 1995;**154**(1):180-91.

97. Kurkov SV, Loftsson T. Cyclodextrins. International journal of pharmaceutics 2013;**453**(1):167-80.

98. Cools-Lartigue J, Spicer J, Najmeh S, Ferri L. Neutrophil extracellular traps in cancer progression. Cellular and molecular life sciences : CMLS 2014;**71**(21):4179-94.

99. Sangaletti S, Tripodo C, Vitali C, Portararo P, Guarnotta C, Casalini P, Cappetti B, Miotti S, Pinciroli P, Fuligni F, Fais F, Piccaluga PP, Colombo MP. Defective Stromal Remodeling and Neutrophil Extracellular Traps in Lymphoid Tissues Favor the Transition from Autoimmunity to Lymphoma. Cancer Discovery 2014;**4**(1):110-29.

100. Juan TY, Roffler SR, Hou HS, Huang SM, Chen KC, Leu YL, Prijovich ZM, Yu CP, Wu CC, Sun GH, Cha TL. Antiangiogenesis targeting tumor microenvironment synergizes glucuronide prodrug antitumor activity. Clinical cancer research : an official journal of the American Association for Cancer Research 2009;**15**(14):4600-11.

101. Shultz LD, Schweitzer PA, Christianson SW, Gott B, Schweitzer IB, Tennent B, McKenna S, Mobraaten L, Rajan TV, Greiner DL. Multiple defects in innate and adaptive immunologic function in NOD/LtSz-scid mice. The Journal of Immunology 1995;**154**(1):180-91.

102. Vichai V, Kirtikara K. Sulforhodamine B colorimetric assay for cytotoxicity screening. Nat Protocols 2006;**1**(3):1112-16.

103. Riccardi C, Nicoletti I. Analysis of apoptosis by propidium iodide staining and flow cytometry. Nat Protocols 2006;**1**(3):1458-61.

104. Harrison IP, Selemidis S. Understanding the biology of reactive oxygen species and their link to cancer: NADPH oxidases as novel pharmacological targets. Clinical and experimental pharmacology & physiology 2014;**41**(8):533-42.

105. Inanami O, Johnson JL, McAdara JK, Benna JE, Faust LRP, Newburger PE, Babior BM. Activation of the Leukocyte NADPH Oxidase by Phorbol Ester Requires the

Phosphorylation of p47 PHOX on Serine 303 or 304. Journal of Biological Chemistry 1998;**273**(16):9539-43.

106. Joshi DC, Bakowska JC. Determination of Mitochondrial Membrane Potential and Reactive Oxygen Species in Live Rat Cortical Neurons. Journal of Visualized Experiments : JoVE 2011(51):2704.

107. Unal Cevik I, Dalkara T. Intravenously administered propidium iodide labels necrotic cells in the intact mouse brain after injury. Cell Death Differ 2003;**10**(8):928-29.

108. Rheinwald JG, Beckett MA. Tumorigenic Keratinocyte Lines Requiring Anchorage and Fibroblast Support Cultured from Human Squamous Cell Carcinomas. Cancer Research 1981;**41**(5):1657-63.

109. Song X, Lopez-Campistrous A, Sun L, Dower NA, Kedei N, Yang J, Kelsey JS, Lewin NE, Esch TE, Blumberg PM, Stone JC. RasGRPs Are Targets of the Anti-Cancer Agent Ingenol-3-Angelate. PLoS ONE 2013;**8**(8):e72331.